



UNIVERSITAT
POLITÈCNICA
DE VALÈNCIA



UNIVERSITAT POLITÈCNICA DE VALÈNCIA

School of Industrial Engineering

Development of a hydrogen fuel cell performance
degradation predictive model for road transport applications

Master's Thesis

Master's Degree in Industrial Engineering

AUTHOR: García Rodríguez, Joaquín

Tutor: Novella Rosa, Ricardo

Cotutor: López Juárez, Marcos

ACADEMIC YEAR: 2022/2023

ABSTRACT

Within the framework of the current energy transition towards the decarbonisation of the mobility sector, this study is focused on the development of a hydrogen PEM fuel cell predictive degradation model. Its properties make it a potential large-scale alternative to battery-exclusive electric powertrains, covering some of the shortcomings that these have compared to traditional combustion systems. However, one of the main challenges it faces is durability. Through this study, a model that mimics the electrochemical behaviour of the PEMFC is initially created, which has been calibrated and validated with experimental references to be sensitive to changes in operating conditions. Subsequently, a literature review is carried out to identify the different trends that promote catalyst and membrane degradation as a function of each of the main operating states in which these cells work. Within this trends, three reliable catalyst and membrane degradation indicators are identified and will be used to link overall and specific degradation: the electrochemically active surface area, the ohmic resistance and the hydrogen crossover current. In a next step, the degradation trends found in the literature are incorporated into the PEMFC model to transform it into a model capable of predicting the origin of the degradation depending on the application it serves and through the introduced membrane and catalyst indicators. After analysing the results obtained, applied to the heavy road transport sector, a series of recommendations are made to the industry with the aim of improving the PEMFC lifespan. Among these recommendations, specific measures are proposed to manufacture more durable PEMFCs and to reduce the dynamic states which generate the major part of the performance decay, both focused on extending the durability of the membrane and the catalyst, and thus, of the hydrogen cell.

RESUMEN

En el marco de la actual transición energética hacia la descarbonización del sector de la movilidad, este estudio se centra en el desarrollo de un modelo predictivo de la degradación de la pila de hidrogeno PEM. Sus propiedades la convierten en una potencial alternativa a gran escala frente a los sistemas de propulsión eléctrica basados exclusivamente en baterías, cubriendo algunas de las carencias que éstos presentan frente a los sistemas de combustión tradicionales. Sin embargo, uno de los principales retos a los que se enfrenta es la durabilidad. A través de este estudio, se crea inicialmente un modelo que imita el comportamiento electroquímico de la PEMFC, el cual ha sido calibrado y validado con referencias experimentales para ser sensible a cambios en las condiciones de operación. Posteriormente, se realiza una revisión bibliográfica para identificar las diferentes tendencias que promueven la degradación del catalizador y de la membrana en función de cada uno de los principales estados de operación en los que trabajan estas pilas. Dentro de estas tendencias, se identifican tres indicadores fiables de la degradación del catalizador y la membrana que se utilizarán para relacionar la degradación global y la específica: la superficie electroquímicamente activa, la resistencia óhmica y la corriente de cruce de hidrógeno. En un siguiente paso, las tendencias de degradación encontradas en la literatura se incorporan al modelo PEMFC para transformarlo en un modelo capaz de predecir el origen de la degradación en función de la aplicación a la que sirve y a través de los indicadores de membrana y catalizador introducidos. Tras analizar los resultados obtenidos, aplicados al sector del transporte pesado por carretera, se realizan una serie de recomendaciones a la industria con el objetivo de mejorar la vida útil de la PEMFC. Entre estas recomendaciones, se proponen medidas específicas para fabricar PEMFC más duraderas y para reducir los estados dinámicos que generan la mayor parte de la degradación, ambas enfocadas a alargar la durabilidad de la membrana y el catalizador, y, por tanto, de la pila de hidrógeno.

RESUM

En el marc de l'actual transició energètica cap a la descarbonització del sector de la mobilitat, aquest estudi se centra en el desenvolupament d'un model predictiu de la degradació de la pila d'hidrogen PEM. Les seues propietats la converteixen en una potencial alternativa a gran escala enfront dels sistemes de propulsió elèctrica basats exclusivament en bateries, cobrint algunes de les mancances que aquests presenten enfront dels sistemes de combustió tradicionals. No obstant això, un dels principals reptes als quals s'enfronta és la durabilitat. A través d'aquest estudi, es crea inicialment un model que imita el comportament electroquímic de la PEMFC, el qual ha sigut calibrat i validat amb referències experimentals per a ser sensible a canvis en les condicions d'operació. Posteriorment, es realitza una revisió bibliogràfica per a identificar les diferents tendències que promouen la degradació del catalitzador i de la membrana en funció de cadascun dels principals estats d'operació en els quals treballen aquestes piles. Dins d'aquestes tendències, s'identifiquen tres indicadors fiables de la degradació del catalitzador i la membrana que s'utilitzaran per a relacionar la degradació global i l'específica: la superfície electroquímicament activa, la resistència òhmica i el corrent d'encreuament d'hidrogen. En un següent pas, les tendències de degradació trobades en la literatura s'incorporen al model PEMFC per a transformar-lo en un model capaç de predir l'origen de la degradació en funció de l'aplicació a la qual serveix i a través dels indicadors de membrana i catalitzador introduïts. Després d'analitzar els resultats obtinguts, aplicats al sector del transport pesat per carretera, es realitzen una sèrie de recomanacions a la indústria amb l'objectiu de millorar la vida útil de la PEMFC. Entre aquestes recomanacions, es proposen mesures específiques per a fabricar PEMFC més duradores i per a reduir els estats dinàmics que generen la major part de la degradació, totes dues enfocades a allargar la durabilitat de la membrana i el catalitzador, i, per tant, de la pila d'hidrogen.

INDEX

1.	Introduction.....	1
1.1.	Hydrogen Economy	2
1.2.	FCV.....	4
1.3.	PEMFC: Theoretical foundations.....	7
1.3.1.	PEMFC: Reaction and structure.....	9
1.3.2.	PEMFC: Potential definition and polarization curve	13
1.4.	PEMFC: degradation.....	19
1.4.1.	The origin of PEMFC degradation: Catalyst and membrane	19
1.4.2.	PEMFC degradation by operating conditions.....	22
1.4.3.	Experimental methods for degradation measurement	26
1.4.4.	Influence of degradation in the polarization curve.....	29
1.4.5.	Linkage between overall and specific degradation.....	31
2.	Objectives	32
3.	Methodology	33
3.1.	FC Polarization curve model definition	35
3.2.	FC Polarization curve model calibration and validation.....	37
3.2.1.	Polarization curve parameter classification and definition	37
3.2.2.	Calibration Reference Definition.....	39
3.2.3.	Limitations of manual calibration and curve sensitivity.....	39
3.2.4.	Calibration strategy	40
3.2.5.	Calibration procedure: Genetic algorithm optimization.....	41
3.2.6.	Model validation	43
3.3.	FC Degradation model definition	44
3.3.1.	Literature review.....	44
3.3.2.	Integration of the literature degradation trends into the model	52
3.4.	FC Degradation model setup and calibration.....	53
3.4.1.	Reference data processing: setup of the degradation upper limits.....	53
3.4.2.	Degradation source coefficients	55
3.5.	Full model simulation process.....	58
3.6.	Degradation model limitations	60
4.	Calibration of the predictive degradation model.....	61
4.1.	Degradation Limits identification.....	61

4.2.	Calibration results	64
4.2.1.	FC Polarization curve model calibration.....	64
4.2.2.	FC degradation model calibration.....	66
5.	Analysis of the ECSA, Ohmic Resistance and Hydrogen Crossover degradation for heavy-duty transport applications.....	70
5.1.	Industry recommendations.....	75
5.1.1.	Catalyst durability recommendations	75
5.1.2.	Membrane durability recommendations.....	76
6.	Conclusion and Future Work.....	78
7.	Budget	80

Figure Index

Figure 1. Greenhouse gas emissions distribution in the EU's transport sector [3].....	1
Figure 2. Green hydrogen generation plant [9].	3
Figure 3. Prediction for worldwide electrolyzer capacity and green hydrogen production by region [15].	5
Figure 4. Powetrain balance of plant for a Toyota Mirai [19].	6
Figure 5. Didactic image of the fuel cell working principle [27].	7
Figure 6. PEMFC internal structure and elements [28].	10
Figure 7. Representative image of the membrane, catalyst layer and gas diffusion layer for a PEMFC [30].	10
Figure 8. Representative figure of a PEMFC catalyst structure [33]	11
Figure 9. Fuel cell polarization typical curve shape [13].	13
Figure 10. Theoretical fuel cell voltage losses [13].	14
Figure 11. Kinetic and electrochemical fuel cell losses [13].	16
Figure 12. Platinum catalyst agglomeration and detachment [41].	20
Figure 13. Polymer electrolyte membrane degradation mechanisms [43].	21
Figure 14. Load cycling voltage profile [48].	22
Figure 15. Theoretical and experimental cyclic voltammetry test [51, 61].	26
Figure 16. FC equivalent circuit.	27
Figure 17. Nyquist plot of a theoretical electrochemical impedance spectroscopy [61].	27
Figure 18. Ohmic resistance in a Nyquist plot of a real EIS [55].	28
Figure 19. Evaluating hydrogen crossover current in a linear sweep voltammetry [55].	28
Figure 20. ECSA "location" within the voltage activation losses term.	29
Figure 21. Ohmic resistance "location" within the voltage activation losses term.	29
Figure 22. Hydrogen crossover "location" within the voltage activation losses term.	30
Figure 23. Voltage degradation rate in the FC polarization curve.	31
Figure 24. Master's thesis methodology block diagram.	33
Figure 25. Comparison of different expression representing the voltage concentration losses.	36
Figure 26. Relationship between membrane water content and relative humidity.	38
Figure 27. Reference polarization curves for the model calibration and validation.	39
Figure 28. Influence of "ACT" and "C" on the polarization curve shape.	40
Figure 29. Conceptual representation of a genetic algorithm working mode [88].	41
Figure 30. Progressive optimization of the GA for the fitness value minimization.	42
Figure 31. Example of visual validation of the model calibration.	43
Figure 32. Set of representative voltage patterns accepted as load change AST cycles [52].	45
Figure 33. Typical start-stop voltage response without and with previous dummy load, respectively. [63]	46
Figure 34. OCV voltage decay for four types of Nafion® membranes under a low current AST [71].	46
Figure 35. Representation of the linkage between overall and specific degradation.	51
Figure 36. Example of data processing and identification form a degraded polarization curve plot.	53
Figure 37. Example of literature data processing and weighting as a function of the FC usage at a certain application.	54

Figure 38. Example of high nonlinearities to be fixed in the degradation model.....	55
Figure 39. Distribution of the voltage degradation rate along a full polarization curve [23].	57
Figure 40. Diagram representing schematically the model inputs, processing and outputs.....	59
Figure 41. Temperature and relative humidity distribution for the selected degradation literature references.	63
Figure 42. Comparison between model and experimental data polarization curves after calibration.	65
Figure 43. Three levels of FC to battery dynamics for a FCREx heavy-duty application [23].....	70
Figure 44. Overall degradation distribution by operating source for heavy duty – high dynamics operation.....	71
Figure 45. FC degradation model predictive result for the ECSA loss.....	71
Figure 46. FC degradation model predictive result for the ohmic resistance increase.	72
Figure 47. FC degradation model predictive result for the Hydrogen crossover current.....	73

Table Index

Table 1: Fuel Cells Classification [28]	8
Table 2. PEMFC polarization curve model equations.	35
Table 3. Set of constants in the PEMFC polarization curve model.	37
Table 4. Set of variables in the PEMFC polarization curve model.....	37
Table 5. Set of variables to optimize in the PEMFC polarization curve model calibration.	38
Table 6. Example of a GA output result applied to the calibration of this model.	42
Table 7. Compilation of found load cycling degradation indicators classified by reference.	48
Table 8. Compilation of found start stop degradation indicators classified by reference.....	48
Table 9. Compilation of found low power degradation indicators classified by reference.	48
Table 10. Compilation of found high power degradation indicators classified by reference.....	49
Table 11. Final degradation literature references selection.	51
Table 12. PEMFC polarization curve degradation model equations.	52
Table 13. Example for a degradation result table for a certain operating state.....	56
Table 14. Literature review degradation source coefficients identification for load cycling condition.	61
Table 15. Literature review degradation source coefficients identification for start stop condition.	61
Table 16. Literature review degradation source coefficients identification for low power/ OCV condition.	62
Table 17. Literature review degradation source coefficients identification for high power condition.	62
Table 18. Result for the polarization curve model calibration.....	64
Table 19. Final load change limits for the predictive degradation model.	66
Table 20. Final start stop limits for the predictive degradation model.	67
Table 21. Final low-power/ OCV limits for the predictive degradation model.	68
Table 22. Final high-power limits for the predictive degradation model.	68
Table 23. Catalyst degradation for a 10% overall PEMFC performance loss.	72
Table 24. Membrane ohmic resistance increase for a 10% overall PEMFC performance loss. ..	73
Table 25. Membrane hydrogen crossover increase for a 10% overall PEMFC performance loss.	74
Table 26. Final results from the PEMFC predictive degradation model.	74
Table 27. Time distribution along the master's thesis development.....	80
Table 28. Labour costs.....	80
Table 29. Equipment and software costs.....	81
Table 30. Budget calculation table.....	81

Nomenclature

CO ₂	Carbon Dioxide
BEV	Battery Electric Vehicle
SoC	State Of Charge
ICE	Internal Combustion Engine
H ₂	Hydrogen molecule
FCV	Fuel Cell Vehicle
CO	Carbon monoxide
CCU	Carbon Capture and Utilization
CCS	Carbon Capture and Storage
FC	Fuel Cell
EU	European Union
PEMFC	Proton Exchange Membrane/ Polymer Electrolyte Membrane Fuel Cell
FCREx	Fuel Cell Range Extender
US DOE	United States Department Of Energy
LT-PEMFC	Low Temperature – Proton Exchange Membrane Fuel Cell
HOR	Hydrogen Oxidation Reaction
ORR	Oxygen Reduction Reaction
MEA	Membrane Electrode Assembly
PTFE	Polytetrafluoroethylene
GDL	Gas Diffusion Layer
ACL	Anode Catalyst Layer
CCL	Cathode Catalyst Layer
CL	Catalyst Layer
RH	Relative Humidity
K	Kelvin
OCV	Open Circuit Voltage
°C	Celsius
R&D	Research And Development
Pt/C	Platinum and Carbon catalyst
ECSA	Electrochemically Active Surface Area
Pt	Platinum
AST	Accelerated Stress Test
PEM	Proton Exchange/ Polymer Electrolyte Membrane
V	Volt
EOL	End Of Life
R_{Ω}	Ohmic resistance
H ₂ O ₂	Hydrogen Peroxide
i_{H_2}	Hydrogen Crossover Current
CV	Cyclic Voltammetry
PtO	Platinum Oxide
EIS	Electrochemical Impedance Spectroscopy
δ_{deg}	Voltage Degradation Rate
\overline{RMSD}	Average Root Mean Square Deviation
GA	Genetic Algorithm

t_m	Membrane Thickness
FRR	Fluoride Release Rate
LC	Load - Cycling/ Change
SS	Start - Stop/ Start - up Shutdown
LP	Low - Power/ Idling/ OCV
HP	High - Power
NT	Natural

1. Introduction

In the light of the accelerated race towards the decarbonization of today's society, multiple objectives and policies are being established by administrations and governments, mainly in the most developed countries, to try to reverse the economic model of the last century, where the development has been strongly linked to the growth of a critical climate indicator, the CO_2 emissions. The European Union, up to the date of December 2022, has established the ambitious but necessary objective of reducing the communitarian CO_2 emissions by the 55% to the year 2030 through the set of measures called "Objective 55", with the aim of being totally CO_2 neutral by the year 2050 [1,2].

One of the key roles in this profound change that is taking place belongs to the transport sector. From the last greenhouse gas emissions (CO_2 equivalent) report made by the European Environment Agency (EEA) a quantification of the emissions associated to the transport sector has been made, reporting that this sector is responsible for one quarter of the overall EU's greenhouse gas emissions, from which the road transport accounts for a dramatic 72% of that quarter [3].

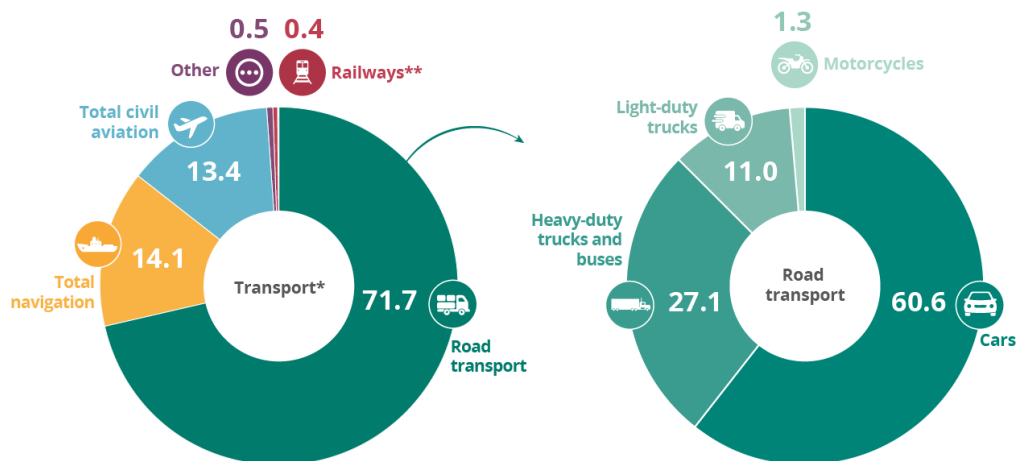


Figure 1. Greenhouse gas emissions distribution in the EU's transport sector [3].

With this situation it is clear that the way to address the climate problem is to seek solutions in the technological field, and more specifically to replace the energy source used to propel these vehicles and the one responsible for CO_2 emissions in the transport sector, hydrocarbons.

The hydrocarbon-free solution that the transport sector has been gradually incorporated over the last decade is battery-powered electric propulsion vehicles. Although the transition is slow and its speed depends highly on the economic level and battery recharging infrastructure of each country, it is undeniable that this is the option that currently leads the change towards transport without hydrocarbons worldwide. However, this new mobility alternative based on lithium-ion batteries faces great challenges and limitations:

- Real emissions. The real emissions associated to the circulation of BEV's depend directly on the energy mix used to generate electricity in the country in which its batteries are recharged. Thus, the use of electric vehicles makes sense only if the origin of the electric current that feeds it comes from a mix with a high share of renewables.
- Necessary materials. An average battery for a BEV has a mass of some hundreds of kilograms. Its composition is based on metals and minerals such as lithium, graphite, cobalt, nickel, copper, iron, manganese or aluminum, among others, for which the demand is rapidly growing up. It is estimated that the available natural resources needed to supply a fully electrified vehicle pool based on large lithium batteries will only be sufficient for a few decades [4].
- Charging time. For security reasons in the electric grid stability, efficiency in the charging process, or accelerated degradation of the battery, the power level when charging the BEV'S is limited to rates that in the best case will allow an 80% state of charge (SoC) in 20 or 30 minutes [5].
- Range. Battery exclusive powertrains are not suitable, with today's technology for long-haul transport applications since the battery pack size and weight increase prohibitively.

In the view of this facts, even though up to date BEV's have been the leading market alternative against internal combustion engine (ICE) vehicles, they face new challenges and limitations which make necessary an increase the number of technological alternatives in order to achieve a successful, viable and sustainable energetic transition from traditional vehicles. It is at this point where hydrogen (H_2) fuel cell vehicles, FCVs, can potentially assume a relevant role among these decarbonized alternatives.

1.1. Hydrogen Economy

Before continuing with a more detailed explanation about FCEVs, it is necessary to understand what hydrogen is and why its use as an energy vector is a high potential solution for a future sustainable mobility.

Hydrogen is the first element on the periodic table, its atom is made up of a proton and an electron, and it is the lightest chemical element that exists. Under normal conditions it is in a gaseous state and is one of the most abundant elements in the universe, although its presence in nature only occurs in combination with other elements, such as oxygen (water) or carbon (organic compounds) (6). As it is not isolated in nature, it is necessary to "manufacture" it, and in the same way that happens with the origin of electricity and BEVs, the origin of hydrogen is fundamental for its use to really be an emission-free solution. There is a wide variety of methods to obtain hydrogen, however, the most relevant according to their origin are the following:

- Steam reforming based on fossil fuels. The 95% of the global hydrogen production is based on natural gas or methane reforming. This process consists of a high temperature and pressure reaction between these hydrocarbons and water stream, obtaining a product gas rich in hydrogen (H_2), carbon monoxide (CO) and carbon dioxide (CO_2). Subsequently through intermediate processes the CO and CO_2 content is eliminated to reach high purity H_2 (99.999%) [7]. Currently, it is the cheapest way to generate hydrogen but at the same time responsible for the emission of 830 million tons of CO_2 per year, so that, fossil-based hydrogen does not meet climate needs [8]. Although

currently there are reforming processes where the CO_2 generated is captured and stored in geological deposits, this makes the process more expensive and means an increase in the production cost, so in practical terms is not a generalized method.

- Water electrolysis could be defined as the opposite process which a fuel cell does. Its basic principle is the separation of elements by supplying energy. In the present case, through an electrolyser by providing electrical energy to a water molecule it is possible to dissociate it into hydrogen and oxygen without additional emissions. The key to create real zero emission hydrogen generated by electrolysis lies on the origin of the electricity. And, if it has a purely renewable origin (wind, photovoltaic, hydroelectric, geothermal ...) the objective of zero total emissions is met

Given the relevance of hydrogen's origin when talking about energy transition, it is essential to distinguish between the use of "clean" and "dirty" hydrogen. With the aim of simplifying this task as much as possible, hydrogen is classified according to several colors based on its generation method, being the electrolysis with renewable electricity (absolute zero CO_2 emissions) and therefore the most important one, the "famous" green H_2 . Even though there is a wide variety of colors depending on the energy source and its category, the most important differentiation is based on whether it emits CO_2 (gray); if it is emitted but captured and reused, CCU, or stored, CCS (blue); or if it does not generate any CO_2 emission (green).



Figure 2. Green hydrogen generation plant [9].

To finish with the contextualization of the current hydrogen's situation in the economy and society, it should be noted that it cannot only play a key role in the future of mobility sector as a direct fuel but also in the energy exchange between countries. Recently the European Union has announced the objective of generating 10 million tons of green hydrogen by 2030 and the immediate investment of € 3 billion for the creation of the European Hydrogen Bank [10]. This demonstrates a firmly intention to promote an international exchange market of this energy carrier, in the same way that is done today with surplus electricity. Furthermore, it is expected that in many cases it will use the current natural gas distribution infrastructure, that can allow up to 20% of hydrogen without modifications, and which could be gradually replaced in the coming years also as an intention of improving the energy independence of the European Union.

To summarize, one of the most important factors for the success of FCV's and the hydrogen "economy", which is the abundance of green hydrogen, seems to be assured in the countries where the installed renewable capacity is high, and through the future interconnection initiatives, it is also expected to be in those where the production of this class of hydrogen is more complex and challenging.

1.2. FCV

After this brief introduction, it is time to talk about hydrogen fuel cell vehicles (FCVs) and what are the reasons which, together with BEVs, make the FCVs serious candidates to lead the energy transition in the mobility sector.

Broadly speaking, an FCV is an electric propulsion vehicle whose current source comes from a hydrogen fuel cell, which is an electrochemical converter whose basic principle consists of the reaction of hydrogen and oxygen, to generate electric current and to form a water molecule as the only by-product. This current will be the one that feeds the electric motor to propel the vehicle, although, as will be explained later, this last statement has certain nuances and in them lies one of the keys to the design of the FCV.

From the climatic point of view, the potential of these vehicles lies in the fact that they can be propelled only with hydrogen, so that they do not emit CO_2 with their circulation as they transfer their only possible emissions (as is the case with BEVs) to the generation method of their fuel, the hydrogen. As introduced above, if this H_2 is green, its production will also be free of greenhouse gases emissions and the total CO_2 emissions associated with the FCV circulation will be zero. Analyzing the advantages of FCVs over BEVs, the following conclusions are reached:

- Greater ease to achieve zero CO_2 emissions due decoupling of the volatility of renewables. In terms of the origin of their energy, BEVs depend on the energy mix with which electricity is generated in each country, therefore, they are subject to the amount of renewable energy installed and its volatility in electricity generation. In times of low renewable shares and/or in countries with a low percentage of installed renewable power, CO_2 emissions associated with electricity generation are far from being null. In the case of FCVs, through electrolysis, green hydrogen can be generated at times of renewable electricity generation surplus and be stored and transported to the distribution points (see subsection 1.1).
- Better charging time to driving range ratio. While BEV's range can be up to 600 km, the needed time for a full recharge suppose in the best case (fast charge) about 2 hours [11]. A *Hyundai Nexo* FCV, with 666 km of range can refill its hydrogen tank in 5 minutes, so the filling time is similar to a traditional ICE vehicle. This reason, together with the high weight of the batteries to achieve great autonomies make FCVs candidates to even lead the heavy-duty transport vehicle sector, ahead of BEVs.
- Less material needed for its construction. BEVs need large amounts of metals and minerals that make the manufacture of their batteries unsustainable in the long term. In the case of FCVs for driving ranges typical of an ICE vehicle, the full FC powertrain and the hydrogen tank offers a considerably lower weight than a battery pack designed for the same autonomy [4, 5,12].

The previously exposed FCV strengths are expected to improve in the coming years, since in the first place the commitment to renewables energies and green hydrogen is receiving tens of billions € of investment in America, Asia and Europe. The relationship between charging time and driving range will probably also improve, although for technical reasons it will be complex to see considerable improvements. Finally, the improvement on the amount and type of materials required for the manufacture of FCs will depend entirely on scientific advances and large-scale feasibility.

However, this technology is not free of facing great challenges, which are summarized below.

- Refueling infrastructure. In 2021, looking at the statistics for Germany, only 125 H_2 charging points were in operation, against 1127 gas stations, and 59400 electric chargers [13]. A great handicap if taking into account that Germany is the country with the biggest number of H_2 refueling points in the EU. However, energy policies in developed countries have a strong tendency towards the hydrogen economy as seen above (subsection 1.1) which also involves strategic plans to improve refueling infrastructure. Recently, an initiative of the European Parliament has emerged to ensure by the end of 2027 the existence of hydrogen refueling points, at least, every 100 km for the entire TEN-T, Trans-European Transport Network [14].
- Hydrogen's color/ production pathway. Currently, green hydrogen is only a small part of the global hydrogen production, and its availability is limited. However, through strong policies and public-private investments for the green H_2 sector, this problem is likely to be solved at a speed analogous to the previous one.

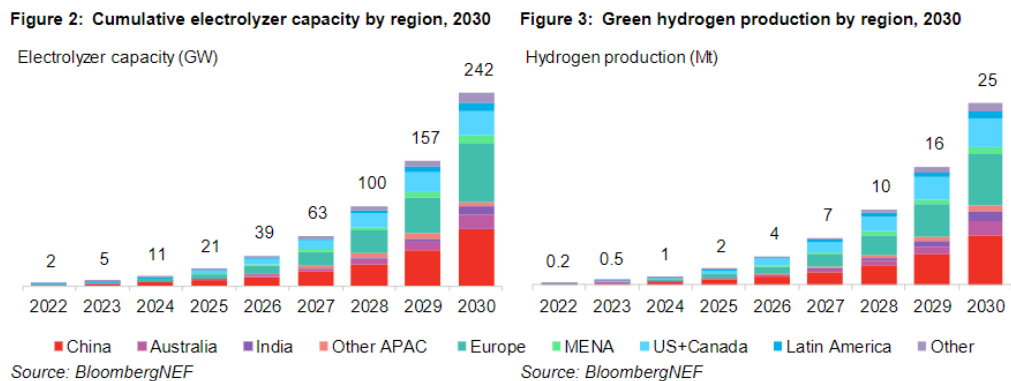


Figure 3. Prediction for worldwide electrolyzer capacity and green hydrogen production by region [15].

- Space on board. A weak point of FCV's is the interior space. Hydrogen is stored in pressurized tanks (between 350 and 700 bar) [16]. However, its specific volumetric energy density (kWh/m^3) is reduced compared to its competitor, the BEV, and therefore requires of a considerable amount of space to be transported in a vehicle.
- Vehicle cost. In the same way that happened with the entry of the BEV into the market, as new technology and economies of scale still low, FCV is not available on the market for less than 60,000€ [16].
- Durability and degradation. The fuel cell types used for road transport application are the proton exchange membrane fuel cells (PEMFC, from now on). These types of FC are the best suited for this application mainly because of their specific power, their rapid response and the temperature and humidity ranges at which they operate. However, under the operating conditions necessary for mobile applications these tend to degrade quickly, usually limiting their lifespan below that of the application it serves.

The present study focuses on this last point, the degradation of the hydrogen PEMFC, and specifically, its origin. However, to finish with the contextualization of this topic (FCV), it is necessary to make a final note so that the reader has all the necessary information to understand, without entering yet into more theoretical concepts, in which modes work, or can work, a FC powertrain in a road vehicle, and how can this influence the degradation of the cell.

Previously, it has been stated that the FC directly feeds the electric motor in FCVs, but this is not entirely true and cannot be generalized, since this system is usually also accompanied by a third protagonist, a lithium-ion battery. This is where different types of FCV arise, since, although the history of the hydrogen fuel cell dates back to the nineteenth century [17], the first hydrogen FCV produced in series dates from 2014 (*Toyota Mirai*). Therefore, it is a technology in full development and research, and its architecture has not yet reached the necessary maturity to define a definitive and unique model [18]. In the case of Toyota, the *Mirai* is based on a direct connection between FC and electric motor, and it is its main work mode, however, depending on the level of power demanded by the user or the driving mode, the battery can work together with the FC, to give, for example, a power boost.

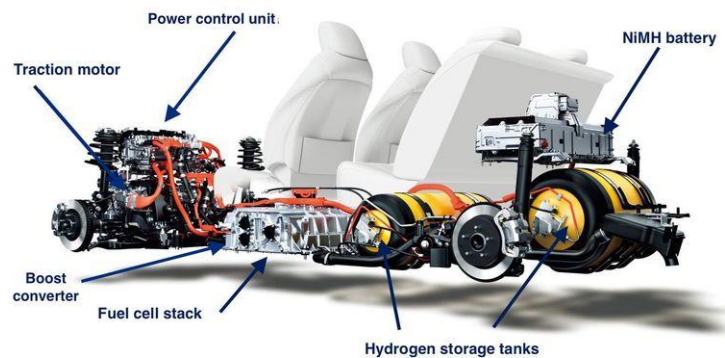


Figure 4. Powetrain balance of plant for a Toyota Mirai [19].

Another architecture with great potential arises from FCReX vehicles where the direct supply of the electric motor is always provided by the battery, and the FC has the role of maintaining the state of charge (SoC) of the latter, which will generally be larger compared to the variant for which Toyota bets, and therefore will not be a vehicle with exclusive refueling option for the hydrogen tank, but also, of its battery through the typical BEV plug.

A research group led by Professor R. Novella in this line of research conclude that the FCReX architecture is really interesting for its potential greater driving range, performance, operational flexibility, cradle-to-grave emissions, and also, its durability. Adjusting the dynamic levels with which the battery is fed by the FC can considerably influence the degradation of the latter, extending its lifespan [20-22]. According to this research project, with a large battery, the dynamics of SoC maintenance requested to the FC can be reduced, and therefore improve its durability. As a recent extension of this project, doctor M. López Juárez has furtherly analyzed the potential of this FCReX technology by comparing different FC-Battery sizes and dynamics applied to the heavy-duty road transport sector. With this, it was solidly proved to be a highly feasible option to electrify heavy-duty transport vehicles which, up to date, have not reached yet a reasonable solution through the battery-exclusive path [23].

The U.S. Department of Energy (DOE) states that FC vehicles must be able to compete with combustion engine cars and corresponding technological alternatives, including, therefore, durability. From its part, the DOE's Fuel Cell Technical Team (FCTT) sets the durability goal for FCs in being able to work at least 8,000 hours (equivalent to 150,000 miles of driving) with a performance loss of less than the 10% [24]. This study, therefore, will be approached according to the maximum degradation objectives established by the DOE, taking as a reference and starting point the corresponding research project led by Professor R. Novella.

1.3. PEMFC: Theoretical foundations

A fuel cell could be defined as “an electrochemical cell which can continuously change the chemical energy of a fuel and oxidant to electrical energy by a process involving an essentially invariant electrode -electrolyte system” [25]. Even though this technology may appear as a recent invention for many, its story goes back to the mid-nineteenth century when the Welsh physicist Sir William Grove wrote about the development of his first fuel cell, laying the foundation of a technology that to this day continues to evolve thanks to the efforts of the scientific community [26].

The elements and basic structure of a FC could be simplified into the following:

- Two reactants, the fuel and the oxidizing agent.
- Two electrodes (anode and cathode), where the partial reaction between fuel and oxidizing agent take place.
- The electrolyte, ion conductor and electron insulator. The negatively charged ions are called anions and move towards the anode, the positively charged ones are called cations and they do it towards the cathode. The type of charge carrier will depend on the type of fuel cell.
- The external electrical circuit which allows the transport of electrons between anode and cathode. In it is integrated the load which will be fed by the electrical current generated by the transport of electrons between the electrodes.

All of them are illustrated in the following figure (figure 5), which schematically shows the operation of the cell on which this study focuses, the PEMFC. But, in turn, is analogously applicable to any fuel cell, with their respective products and reactants.

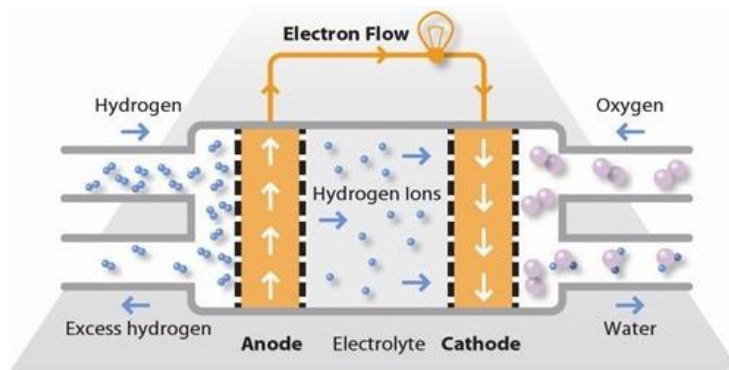


Figure 5. Didactic image of the fuel cell working principle [27].

There are currently several types of fuel cells which vary depending on the electrolyte, charge carrier, temperature, main reaction or catalyst materials among others. However, all of them have in common the ability to combine in a single reaction for each electrode the energy conversion between the fuel and the output electric current, making fuel cells a relatively simple energy converter.

	PEMFC	AFC	PAFC	MCFC	SOFC
Definition	Polymer Electrolyte Membrane Fuel Cell	Alkaline Fuel Cell	Phosphoric Acid Fuel Cell	Molten Carbonate Fuel Cell	Solid Oxide Fuel Cell
Class	Low Temp.	Low Temp.	Mean Temp.	High Temp.	High Temp.
Operating T.	80 - 180° C	80 - 250° C	160 - 220° C	600 - 700° C	800 - 1000° C
Fuel	H_2	H_2	H_2	CH_4, CO, H_2	CH_4, CO, H_2
Charge Carrier	H^+	OH^-	H^+	CO_3^{2-}	O^{2-}
Catalyst	Pt/ Ru	Pt/ Pd	Pt	NiO	Ni
Cell Efficiency	50 - 68%	60 - 70%	55%	65%	65%
Applications	Passenger car Decentralized supply	Space Military	Power Plants	Power Plants	Power Plants Aux. Power Unit

Table 1: Fuel Cells Classification [28]

Through the previous table (Table 1) is intended simply to be an indicative summary of several of the most common types of Fuel Cells, this does not mean that there are not additional ones, or that there are not more relevant properties that differentiate one from another. This work, as already mentioned, will focus on low-temperature PEMFCs. This type of cell is the one that best adapts to the needs and operating conditions of the road transport sector.

1.3.1. PEMFC: Reaction and structure

The Polymer Electrolyte Membrane Fuel Cell, also known as Proton Exchange Membrane Fuel Cell, receives this name because it uses a water-based acidic polymer membrane as electrolyte, and it's also based on the proton transport. As stated before, it is the most suitable fuel cell technology for transport applications, indeed, its most recent development has been carried out mainly around this application. These cells are divided into low temperature range (80°C) and high temperature range (Up to 150 °C), this work will be focused on the first type, the low temperature (LT-PEMFC) [27].

Among others, the properties that make PEMFC the most suitable FC type for the transport sector are their low operating temperature, fast response, high efficiency, power density, compact design, quick start or low noise level in operation.

As introduced in the previous chapter, the basic reaction of a FC is based on the interaction of a fuel and an oxidizing agent. In the case of PEMFCs the fuel is hydrogen (H_2), the oxidizing agent is oxygen (O_2) and the charge carrier through the electrolyte is a positive ion (H^+), more specifically, a proton. The reaction is divided into two partial reactions:

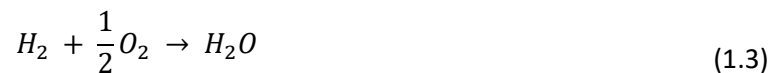
- Anode HOR (Hydrogen oxidation reaction). With this reaction the hydrogen molecule gets oxidated, which means that it donates an electron. The hydrogen molecule gets then dissociated in the anode (positive electrode) into two protons which diffuse through the membrane (electrolyte) and two electrons which flow through the outer electrical circuit to the cathode (negative electrode).



- Cathode ORR (Oxygen reduction reaction). The oxygen molecule gets reduced; thus, it receives the electron donated by the hydrogen molecule. Both, the two protons and the two electrons arrive to the cathode, from the membrane and the outer electrical circuit, respectively. Once the oxygen receives both a water molecule is formed, closing the cycle and the FC reaction.



Therefore, the resulting reaction from the anode and cathode partial reactions which define the PEMFC is the following:



Before continuing with the theoretical principles behind these reactions that combine chemical phenomena with electrical phenomena, it is necessary to pause and analyze with more detail the components of the PEMFC, several of which will be protagonists of this study, due to their involvement in the degradation of these cells, as will be exposed later on 1.4.

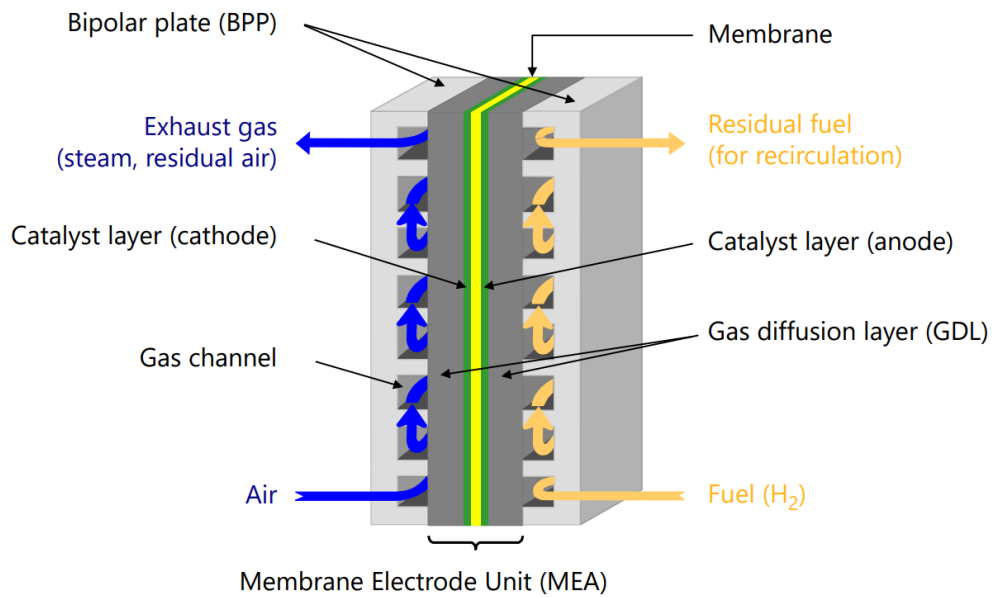


Figure 6. PEMFC internal structure and elements [28].

Bipolar Plates

The external electrodes, also known as bipolar plates (BPP), serve to uniformly distribute both reactants, hydrogen and oxygen to the membrane electrode assembly (MEA) through straight and parallel channels, to remove the produced water and to conduct the electrical current generated with the reaction. They must be structurally tough and resistant to any leakage in case of failure due to vibration or temperature cycling conditions as they are in contact with the MEA catalyst layers and resistant to highly reductive and oxidative environments. As they account for three quarters of the total FC weight, it is essential that these plates are composed of lightweight materials to maximize the power and energy density of the cell [29].

The most critical components of a fuel cell belong to the membrane electrode assembly (MEA), composed symmetrically on the cathode and anode side by a carbon-based gas diffusion layer, a platinum catalyst, and between them, the polymer membrane serving as electrolyte.

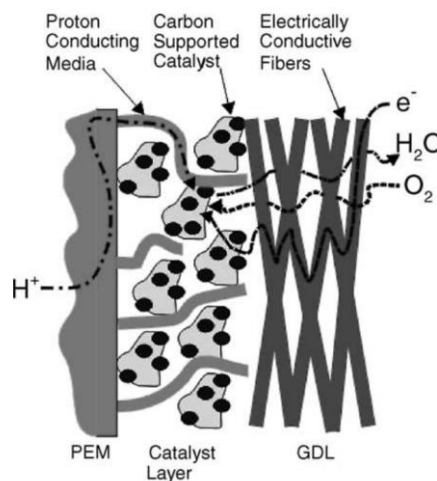


Figure 7. Representative image of the membrane, catalyst layer and gas diffusion layer for a PEMFC [30].

Gas diffusion layer

The GDL is a fibrous porous and conductive medium with three primary functions: to uniformly distribute the reactive gases on the surface of the catalysts, to serve as transport medium for the electrons between these catalyst layers and the current collectors of the external electrical circuit, and to facilitate water evacuation to avoid cell flooding. It is made of porous carbon paper or cloth and is typically coated with PTFE (Teflon) to ensure that the pores of the GDL do not get congested with liquid water thanks to its wet-proof properties. The typical thickness of the GDL is in the range of 100 – 300 μm [31, 32].

Catalyst layer (Electrode)

The anode and cathode catalyst layers (ACL, CCL) are the locations where both half-cell reactions take place, so these catalyst layers are also known as the active layers. As it has been exposed before, on the ACL, the hydrogen oxidation reaction (HOR) takes place, and on the CCL, the oxygen reduction reaction (ORR) occurs. The CL typically consists of a mixture of a carbon support, ionomer and platinum particles. The function of the carbon support is to serve as electrically conductive medium for electrons transport, and to be the “matrix” where the platinum nanoparticles are attached. On the other hand, the ionomer’s presence provides the paths for proton conduction, and it is typically made of Nafion[®], a perfluoro sulfonic acid polymer with key relevance which will be furtherly analysed as it is the membrane’s main material. Finally, the Pt particles are used as the catalyst for the electrochemical reactions, so its function is critical for a good cell performance. As platinum is a costly material, in order to achieve a good compromise between performance and cell cost, its particles are found in the microns (μm) size level, with the objective to reach a high surface to weight ratio and optimize as much as possible the presence of this precious metal. These particles are also very prone to progressively reduce its presence and activity along the lifespan of the cell, thus decreasing its performance with time, as will be analysed with more detail in the PEMFC degradation chapter (1.4). Even though the CL structure is the same on both cell sides (anode and cathode), there may be a difference on the thickness and/ or the platinum loading of each, which depending on the cell design might vary between 0.1 and 0.4 $\text{mg Pt}/\text{cm}^2$.

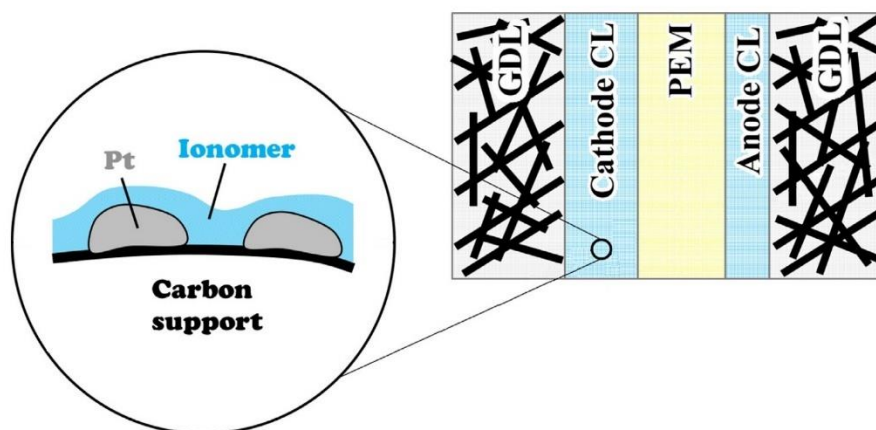


Figure 8. Representative figure of a PEMFC catalyst structure [33]

Polymer Electrolyte Membrane (PEM)

In the following lines, the element which gives the name to the PEMFC is about to be presented, the polymer electrolyte or proton exchange membrane. Its main purpose is to allow a low resistance transport for hydrogen ions (protons) and at the same time to be highly resistive against electrons transport, and thus to avoid an internal short circuit. Besides, the membrane must hinder gas permeation to the opposite electrode, referred as fuel crossover, which would lead to an irreversible performance loss in the fuel cell [34]. Even though there are many types of membrane materials for low temperature hydrogen fuel cells, Nafion[®] is the most widely used material, as it offers a good compromise of the previously exposed properties. It must be noted however, that these membranes are highly sensitive to humidity and temperature changes and are the main responsible for imposing the operating conditions for the LT-PEMFC, which are ideally around 80° Celsius and high relative humidity percentages (50 - 100% RH) always avoiding the cell dehydration, and flooding [35, 36]. The main trade-off with its design is the thickness (typically in the 50 to 250 μm range [31]), as it is inversely proportional to the proton conduction and directly proportional with the durability. Therefore, high thickness membranes ensure a better durability and worse performance, and vice versa. Along with the catalyst, the membrane is the other major source for performance degradation in PEMFC, and it will be furtherly discussed later on (1.4).

1.3.2. PEMFC: Potential definition and polarization curve

The purpose of using a fuel cell as an energy supply or energy converter is to get an electrical current from it, transforming the reactants into a certain output voltage. In this chapter, the purely chemical part of the PEMFC is left aside, to pass on to the definition of the voltage delivered by these cells, the characteristic curve that defines them, and which static and dynamic voltage losses occur in their operation, as the last step before going into the main topic of this master thesis, the PEMFC degradation.

Polarization curve

Independently from its application, a fuel cell is designed to provide electrical power, which is the product of potential and current. In order to characterize the operation of any fuel cell along its own power range the polarization curve is the most generalized representation of both physical magnitudes.

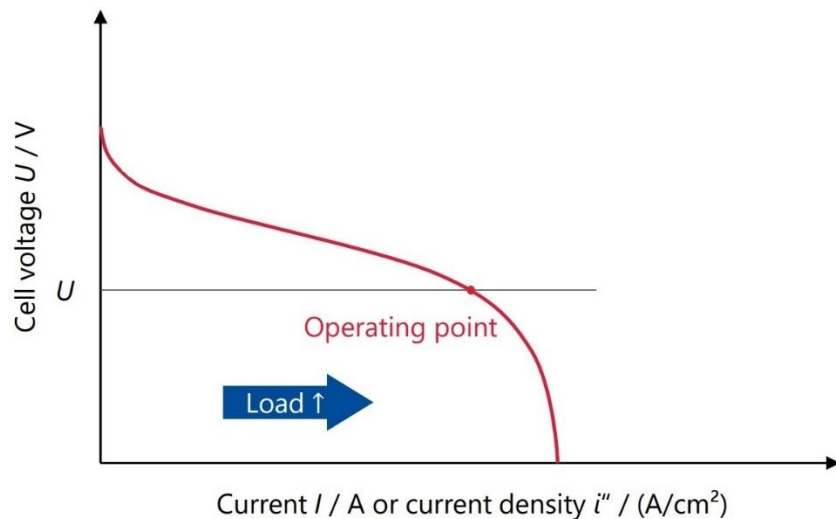


Figure 9. Fuel cell polarization typical curve shape [13].

With the objective of making this curve a representative and generic relation between both magnitudes, the current density is used instead of the absolute current, unlinking the curve from the cell size. As can be observed, the output current density is proportional to the cell load, however, due to the nature of these cells and the different voltage losses that occur along its current density range, the voltage has a more complex tendency, which will be explained further on when reviewing the dynamic voltage losses mechanisms.

Once the polarization curve has already been introduced, it's time to figure out the different voltage losses and the conditions and formulas which define each of them.

Cell Voltage: Thermodynamic losses

These group of voltage losses account for those related to the thermodynamics, going from "ideal to real" conditions. With the aim of providing the reader with the easiest way to understand these phenomena, it is recommended to try to understand these losses as sequential losses, starting with the entropy losses, the deviation from standard conditions, and finally the leakage and short circuit losses, to go from the "ideal" case (Heating value) to the "real" one (Open circuit losses) as it is illustrated in the following figure (figure 10).

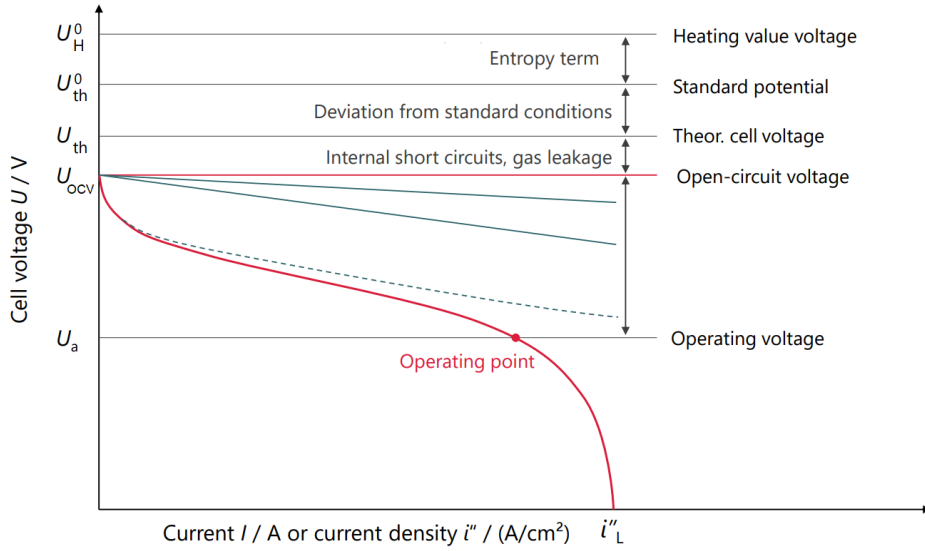


Figure 10. Theoretical fuel cell voltage losses [13].

The theoretical energy released in a hydrogen fuel cell reaction is composed by electrical and thermal energy and it is defined as the heating value. This amount of energy is released due to the exothermic reaction (equation 1.4) that takes place between hydrogen and oxygen to form water, and it can be calculated as the difference between the heat of products and reactants. Depending on the product water state (liquid or gas), the heating value (ΔH) is defined as “higher” or “lower” respectively. By considering the amount of energy carried by a mole of electrons and the number of electrons in the reaction the heating value voltage (U_H^0) is obtained (equation 1.5):

$$\Delta H = H_{H_2O(l)}^{\circ} - H_{H_2}^{\circ} - \frac{1}{2} H_{O_2}^{\circ} \quad (1.4)$$

$$U_H^{\circ} = \frac{\Delta H}{z F} \quad (1.5)$$

Where ΔH is the heating value or enthalpy, z is the number of electrons that a hydrogen molecule host and F is the Faraday constant. Resulting a higher heating value voltage of 1.482 Volts. The standard potential (U_{th}^0) is defined as the theoretical maximum voltage if the entropy term ($T\Delta S$), and therefore the irreversible losses, are subtracted from the enthalpy or the heating value of the reaction, resulting in the Gibbs free enthalpy (ΔG , equation 1.6):

$$\Delta G = \Delta H - T\Delta S \quad (1.6)$$

$$U_{th}^{\circ} = \frac{\Delta G}{z F} \quad (1.7)$$

After applying equation 1.7, the standard potential results to be 1.229 Volts. The theoretical FC efficiency is calculated by dividing the Gibbs free energy by the heating value (equation 1.8), so it is defined as the usable energy portion of the total heat. Which results for the higher heating value of an efficiency of 0.829.

$$\eta_{th} = \frac{\Delta G}{\Delta H} \quad (1.8)$$

Up to this point, even though it was not stated before, standard conditions were assumed, which account for 298 K and 1 Bar of pressure. The voltage which results by considering the deviation from these conditions is defined as the theoretical cell voltage (U_{th}) and its calculation is defined by the Nernst equation (equation 1.9).

$$U_{th} = U_{th}^0 - \frac{R T}{z F} \ln \left(\frac{P_{H_2} \cdot P_{O_2}^{0.5}}{P_{H_2O}} \right) \quad (1.9)$$

Where R is the ideal gas constant, T the cell temperature, and P_Y^x the partial pressure of each element. From this point and ahead, the voltage will depend on the pressure and temperature, which as stated before will be 1.229 Volts at 298 K and 1 Bar and will decrease the further both conditions get from the standard ones.

Finally, there is an additional loss to reach the “real” cell voltage in steady state conditions, which is typically named open circuit voltage (OCV). These last theoretical losses account for different phenomena as: internal short circuits due to electrical conductivity of the electrolyte, internal gas crossover of a reactant through the membrane with subsequent reaction at the counter electrode or gas leakage, among others [37]. These losses are estimated to be from some mV up to 100 mV depending on the cell state [13]. So, this must be taken into account and therefore is not correct to assume an OCV equal to the theoretical cell voltage (U_{th}).

Operating Voltage: Electrochemical and kinetic losses

In the previous section the theoretical cell losses based purely on the thermodynamics laws were presented. Those losses accounted for the heat that the fuel cell is not capable of transforming into usable energy, independently from the load state of the cell, and thus, assuming a null current density. As the following figure illustrates, when the cell starts to operate and therefore, the current density is not null anymore ($i > 0 \text{ A/cm}^2$), a new set of losses surge, which this time depend on the load/ current density range and are now based on various electrochemical kinetics phenomena. The objective of this chapter is to present to the reader the most important losses, in which load range is each of them predominant and, finally, link it to the operating voltage through the general fuel cell equation. Starting from the end, but only at a high level to introduce this chapter, the operating voltage equation is shown below, composed by the OCV as steady state voltage, and subtracting the three main electrochemical losses: activation, ohmic and concentration.

$$U_{FC} = U_{OCV} - U_{act} - U_{ohm} - U_{conc} \quad (1.10)$$

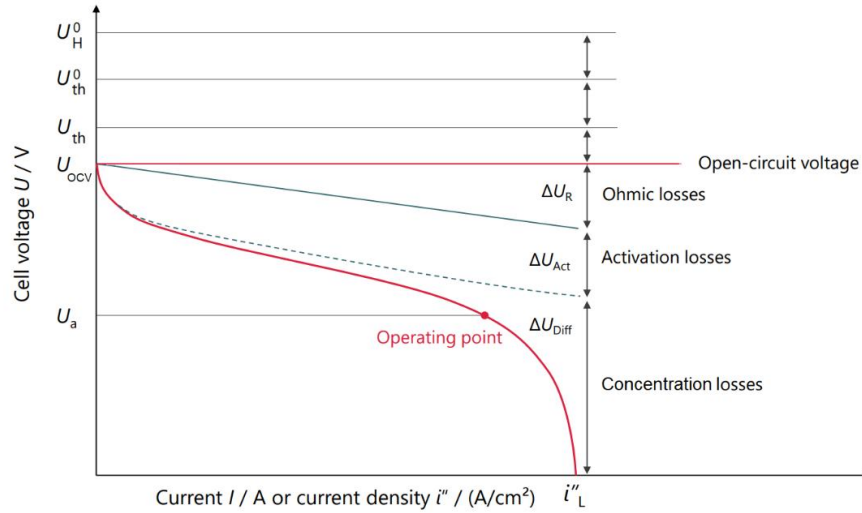


Figure 11. Kinetic and electrochemical fuel cell losses [13].

Activation losses: Predominant at low current density range

The activation losses or overvoltage represent the slowness of the reactions taking place on the surface of each electrode and could be understood as a lost portion of the voltage invested in driving the chemical reaction that transfers the electrons to or from the electrodes. These losses are highly non-linear and are predominant in the low current density range [38].

In 1905, Swiss chemist and electrochemist Julius Tafel discovered that the variation of the potential followed a similar pattern for a wide variety of electrochemical reactions and developed an expression which defined the found tendency, the Tafel Slope [39].

$$U_{act} = A \ln\left(\frac{i}{i_0}\right) \quad (1.11)$$

Through this expression (equation 1.11), a general equation can be used to determine the variation of the activation potential depending on the Tafel slope (A), which is a constant, the current density (i) and the exchange current density (i_0). The exchange current density gathers a large quantity of physical, chemical, and thermal magnitudes behind it, and could be defined as the current density found where the activation loss starts to occur. In order to bring a simplified presentation of those magnitudes which influence the activation term, but at the same time to give the reader all the relevant information about this complex phenomenon which will be necessary to further understand how the degradation affects the operating voltage, the relevant variables are about to be presented. Further, a simplification will be assumed from now on, the reason for this is that this overvoltage is composed by two terms, one for the cathode reaction and one for the anode. The difference in the (i_0) value between the two electrodes reflect the different rates for the reaction at either electrode. The HOR reaction in the anode is fast and simple, while the ORR reaction in the cathode is many times slower due to its complexity, as several reaction steps are involved, whose reason is out of the scope of this study. Therefore, an extended simplification typically assumed when calculating the activation overvoltage is to neglect the anode activation loss, therefore the following expression accounts only for the cathode [38].

The final expression for the activation overvoltage is defined as the following (equation 1.12):

$$U_{act} = \begin{cases} \frac{R_{gas}T}{2F} \left(\frac{i}{i_0} \right) & \text{if } i < \left(\frac{i_0}{1-\alpha} \right) \\ \frac{R_{gas}T}{2\alpha F} \ln \left(\frac{i}{i_0} \right) & \end{cases} \quad (1.12)$$

Where R_{gas} is the universal gas constant, T is the cell temperature, F the Faraday constant, α is the charge transfer coefficient which displays a complex temperature/humidity dependency and is a measure of the FC reaction which may vary depending on the operating conditions (39), i is the current density and i_0 the exchange current density. At the same time the expression for the exchange current density is the following (1.13):

$$i_0 = i_{0,ref} a_c L_c \left(\frac{P_{O_2}}{P_{O_2,ref}} \right)^{\gamma_c} \exp \left[\frac{-E_{act}}{RT} \left(1 - \frac{T}{T_{ref}} \right) \right] \quad (1.13)$$

Where $i_{0,ref}$ is the reference exchange current density, $a_c L_c$ account for the cathode roughness, where a_c is the catalyst specific area and L_c the catalyst platinum loading, P_{O_2} is the oxygen partial pressure in the cell, γ_c is the pressure dependency factor and E_{act} the electrochemical reaction activation energy for O_2 reducing on platinum. All the equations presented above will be of high relevance due to the nature of this study, in which a mathematical predictive FC model will be developed in order to estimate and identify the degradation sources for PEMFC.

To conclude with the activation overpotential, as can be deduced from the presented equations, it is sensitive to the fuel cell temperature or the reactant pressure when looking at the operating conditions of the cell, among others. But, on the other hand, there is also a strong influence of the state of the catalyst, through both electrode roughness coefficients ($a_c L_c$) and as it will be analysed later, the catalyst degradation will play a major role on the evolution of the polarization curve of the fuel cell through its lifespan.

Ohmic resistance losses: Linear with the current density increase

As it was introduced when presenting which is the basic principle of a fuel cell, hydrogen ions must flow through the membrane/ electrolyte, and thus, in the ideal case it should have the lowest ionic resistance possible. Furthermore, at the same time, electrons must flow from one electrode to the other through the current collectors, which are desired to offer a low electronic resistance for this purpose as well. The ohmic resistance loss represents the amount of energy that is lost for this matter when the fuel cell is operating, so, in contrast with the previous one (activation) this is the simplest to understand and to model. The basic expression is the classical one for a voltage loss due to an internal resistance, however, the objective of this study is to try to reach the FC degradation sources, therefore, a further approach into this term is necessary.

$$U_{ohm} = R i \quad (1.14)$$

$$\sigma_{30} = 0.005139w - 0.00326 \quad (w > 1) \quad (1.15)$$

$$\sigma(T_{cell}) = \sigma_{30} \exp \left[1268 \left(\frac{1}{303} - \frac{1}{273 + T_{cell}} \right) \right] \quad (1.16)$$

$$R = \int_0^{t_m} \frac{dx}{\sigma} \quad (1.17)$$

As shown (equations 1.14-1.17), the ohmic resistance (R) depends directly on the conductivity (σ) and the membrane thickness (t_m). At the same time, the conductivity depends on the cell temperature (T_{cell}) and the membrane water content (w). As it was discussed when exposing a first approach about the polymer electrolyte membrane, its performance has a strong dependency of the temperature and humidity which now, translated into equations, can be easily deduced from the equations X, and Y, respectively, for water content (humidity) and cell temperature. However, even though by looking at these expressions it may look that it is just a matter of increasing both magnitudes to improve the membrane conductivity, it must be considered that there are limitations for both. To avoid the membrane flooding or dehydration trough insufficient or excessive water content, respectively, and to avoid temperatures significantly higher than 80°C. All of them would lead, through different paths, to an accelerated degradation of the PEMFC.

Concentration losses: Predominant at high current density range

The concentration or mass transfer overvoltage occur at high current densities, and it is the responsible for the steep slope found in the high-load range of the polarization curve. It is a consequence of insufficient supply of hydrogen to the anode and/or oxygen to the cathode, due to a reduced relation between the partial pressure of the supplied reactants and the conversion speed in the cell reaction. There is not an analytical solution to model the influence of the partial pressure on the voltage as it was for the activation term, however there are various expressions which serve as an accurate enough approach to model the concentration losses, for this study, the following is being used (equation 1.18):

$$U_{conc} = -C \ln \left(1 - \frac{i}{i_l} \right) \quad (1.18)$$

Where C is a parameter that depends on the fuel cell and the operating state, and i_l is the limiting current density, which is also set depending on the fuel cell maximum current density.

1.4. PEMFC: degradation

In order to reach a wide-spread marketing of FC into the transportation sector some technical limitations must first be solved. Being one of the most relevant the improvement of their durability and reliability to make them an economically viable and competitive option for electrified powertrains. PEMFC R&D is deeply focused nowadays in extending its lifespan by reducing degradation, which is a complex and challenging topic due to the high interaction of electrical, chemical, physical and thermal phenomena. However, to enhance this durability is crucial to first understand what makes it to shorten.

There are typically two main stages associated to the fuel cell degradation studies. The first of them is the identification of the degradation sources with respect to the cell materials and the operating conditions. The second one is the development of mathematical degradation predictive models constituted with the aging phenomena and influence to integrate it into fuel cell performance models [40]. There is a considerable number of studies in which the FC degradation is predicted based in both the previous stages, however, this degradation is only given at a high level, which is the reflect on the polarization curve of a voltage loss generated by the cell degradation. Through the present study, a further step is being made, with the aim of developing a mathematical predictive tool capable of identifying which is the origin of this degradation (e.g., membrane resistance, gas crossover, catalyst) and which is the degradation level reached by each of them depending both on the type of operation to which the fuel cell has been subject to. To achieve this complex objective, it is necessary first to review and understand the degradation from its beginning, the present chapter does not pretend to show all the degradation details needed to develop this predictive model, but at least, a proper contextualization.

To facilitate the comprehension of this chapter, a brief overview of the following content is being advanced at this point. Starting with the structural elements of the PEMFC which are more prone to degrade, then the different FC operating modes will be presented together with the effects which each of them cause in the FC structure, after that the methods for estimating this degradation will be exposed, to then give way to analyse how the previously presented voltage equations are affected by this degradation, and thus, the polarization curve as well. And finally, an introduction of the “voltage degradation rate” which will be a useful concept to situate the scope of this degradation study into the maximum acceptable FC performance loss which has been established from the DOE [24].

1.4.1. The origin of PEMFC degradation: Catalyst and membrane

As it has been briefly introduced when presenting the structural elements of a FC, both the catalyst and membrane are critical elements due to its influence in the cell performance. First, the catalyst has the function of being the element on which the hydrogen molecules dissociate into protons and electrons (HOR), on the other hand, when referring to the anode its function in the cathode is to receive those protons and electrons with the presence of the oxygen molecule to close the reaction and form a water molecule (ORR). Taking this into account, the degradation of this active element in the reaction directly means that this process is going to reduce its speed as less active material will be available to keep reducing and oxidizing the

reactants at the desired rate. Secondly, the membrane serves as the low resistance path for the hydrogen protons to flow from one anode to the cathode, and therefore, its degradation implies that again, the efficiency of this process is going to drop. With all, both degradations (catalyst and membrane) are going to produce a reduction in the output voltage of the cell, for the same current density. In other words, for the same “effort” the FC is going to reduce the achievable output voltage, and thus the produced power. To understand better how and why both get degraded, it is necessary to analyse it separately.

Catalyst degradation

PEMFC catalysts are composed, as stated previously, by carbon grains on which Pt particles are attached (Pt/C). The size of these Platinum particles is in nanometre scale, usually in the range 2-8 nm [41]. Nanoparticles intrinsically have the tendency of agglomerating due to their high specific surface energy, therefore when this agglomeration of small Pt particles into bigger ones occur there is a decrease of the electrochemical active surface area (ECSA) of the Pt/C catalyst, thus decreasing the cell performance [42]. Another related tendency which promotes the catalyst loss is the dissolution and migration out of the catalyst layer, so in this case is not only matter of losing active surface due to an increase in the grain size, but also a direct loss of the active material through Pt oxidation/ dissolution [43]. Additionally, there is also indirect degradation which decrease the presence of active Pt, which is the deterioration of the carbon support and the ionomer. There is a large list of mechanisms and conditions which promote the previous types of catalyst degradation which is completely out of the scope of this study, due to the high complexity and extension of the topic, in which, the pH, the humidity, the temperature, the potential, the oxidative and reductive environment, and the materials, among others, constantly interact and progressively degrade the fuel cell catalyst.

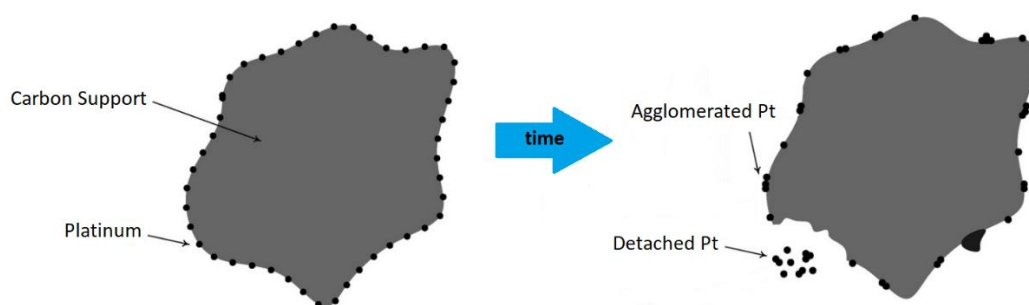


Figure 12. Platinum catalyst agglomeration and detachment [41].

Furthermore, it is important to remember that due to the PEMFC operating conditions there is a constant dynamic state in which all the previous magnitudes, and other not mentioned, are constantly changing, and thus leading to a large number of different interactions difficult to identify separately. To get further information about all the origins of each single degradation mechanism the following read is recommended [33], with more than 400 scientific references at its back. The important message that is intended to transmit here is that the catalyst degradation is induced by a loss of active area, which means, loss of Pt particles or an undesired growth of their size. And, in this study, the identification of the causes that promote this degradation is not going to be done through an approach based on the individual causes, but from the compilation of conditions that each main operating state (high load, low load, idling, load change...) of the FC promotes, as will be seen later on in this chapter.

Membrane degradation

PEMFC membranes are typically made of perfluoro sulfonic acid polymer (Nafion[®] is the most typical one for this application), and its durability is essential for the cell performance. The main consequences of membrane degradation are the increase of hydrogen permeability and the increase of ohmic resistance (R_{Ω}), but again, the causes which promote them are a complex topic due to the number of electrochemical interactions and mechanisms which participate to it. To simplify, it could be assumed that there are two main types of degradation that these membranes must face during its lifetime: chemical and mechanical. Both progress at different rates, through different paths, due to different conditions and also generate different consequences, but both end up shortening the membrane lifespan.

The chemical degradation is mainly caused by hydrogen peroxide (H_2O_2) and oxidative radicals' formation such as hydroxyl ($\bullet OH$) and hydroperoxyl ($\bullet OOH$) which end up unzipping the polymer backbone and cleavage of the side chains [33, 43]. This generates changes in the ionomer morphology reducing the ionic conductivity of the membrane and also promoting membrane thinning. This chemical degradation is mainly promoted by the gas crossover, the potential cycling, the operating temperature, and the dehydration of the membrane, among others [44,45].

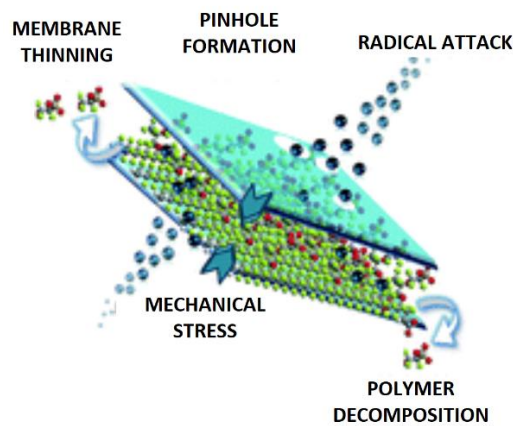


Figure 13. Polymer electrolyte membrane degradation mechanisms [43].

On the other hand, mechanical degradation is mainly caused by humidity cycling, where successive swelling and shrinking cycles due to high and low relative humidity in the cell, respectively, generate a progressive mechanical stress. This mechanical stress coupled with the progressive membrane thinning generated by the chemical degradation facilitate the creation of cracks and pinholes in the membrane, which will generate undesired hydrogen crossover through it, and finally the membrane failure and the destruction of the cell.

1.4.2. PEMFC degradation by operating conditions

A widely accepted method to facilitate the identification of a FC degradation in realistic load conditions is to first segregate the load profile of those real conditions into different operating states. PEMFC's when serving as electrochemical converters for electrified road transport powertrains are mainly subjected to five types of degradation sources, directly related to a specific operating condition: load change, start-stop, low power/ idling, high power and natural degradation [23, 33, 47]. As discussed earlier, and in order to develop a predictive model capable of identifying not only the degradation of the fuel cell performance but also the degradation origin, a realistic approach to successfully achieve this objective is to also segregate the fuel cell operation into these generic conditions. By doing so, an independent evaluation of the degradation can be performed for each of them, as there is a large list of publications which show experimental results of accelerated stress tests (AST's) which only focus on one operating condition, and thus provide degradation results under exclusively one FC load state. A summary of those five operating conditions is given below.

Load change

Load cycling in FC, when referring to transport applications, is a usual operating state and implies, as its name suggests, a dynamic and cyclic operation of the cell. Within the U.S. DOE PEM fuel cell testing protocols, that the scientific community take as reference and standard when performing FC degradation AST's, there is one specific protocol focused for load cycling (Protocol 1) [24]. Even though when looking into the research reports focused on this matter there are usually variations between the DOE protocol and the performed test, a major part of them is strongly based on the conditions that it establishes. A representative load profile for load change AST looks like the following:

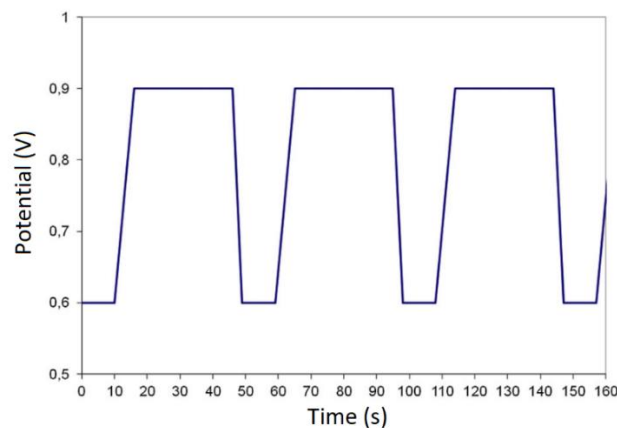


Figure 14. Load cycling voltage profile [48].

The three main causes that promote FC performance decay due to load change are [33, 48-57]:

1. Water production and thermal output. High loads enhance electrode reaction leading to high elevated water content in the membrane and ionomer, conversely a dehydration will occur when the next opposite load happens, generating a shrinking - swelling cycle which produces mechanical degradation of the membrane leading to an ohmic resistance and hydrogen crossover increase. On the other hand, this phenomenon is also harmful for the catalyst. As the catalyst layer (CL) is compressed with the membrane, it is also

sensible to its successive expansion and contraction, thus leading to a progressive delamination between the membrane and the CL, which also gets deformed. This deformation deteriorates the uniformity of the ionomer distribution over the CL leading to uncovered or overcovered Pt particles, which will become partial or totally inactive (ECSA loss). Apart from the ionomer redistribution, the CL deformation induces to a detachment of the Pt particles around the cracks, as they are more likely to be washed away since water tends to flow through these cracks (ECSA loss). Moreover, the delamination between membrane and CL directly affects the transport of protons between them (ionic resistance increase), and additionally, this delamination also harms the “connection” between gas diffusion layer and CL, also affecting the electron transport between both (electronic resistance increase).

2. Dynamic demand of gas supply. The second cause is related to the load-up of the cell, in which, due to the instant change in the current density, the reactant supply (hydrogen and oxygen) lags “behind” it, thus generating the so-called fuel starvation, which gets worse when the faster the load-up is. Each of these starvations (hydrogen and oxygen) have different consequences. The lack of oxygen in the cathode generates an air starvation area, therefore, the protons which arrive from the anode cannot participate in the oxygen reduction reaction (ORR) and tend to generate hydrogen molecules in the cathode which react directly with the oxygen in the starvation area generating hotspots which produce thermal stress to both, the catalyst and membrane, generating predominantly an ECSA loss. On the other hand, the lack of hydrogen in the anode generates air permeation through the membrane to the counter electrode, creating an H_2/O_2 boundary in the anode exacerbating the carbon corrosion in the cathode which, at the same time, leads to Pt agglomeration and again, an ECSA loss.
3. Potential cycling. An intensive potential cycling between 0.6 V and 1 V promote the so-called place-exchange mechanism producing the coupling of different conditions as the formation of Pt oxide at high potentials, its reduction and the cathodic dissolution which generate an intensified Pt catalyst dissolution dominated by the electrochemical Ostwald ripening phenomenon. This phenomenon, promoted by the reduction of the interface energy of the Pt particles leads to the dissolution of the smaller ones and the consecutive redeposition into bigger ones, and thus, an ECSA loss.

It can be concluded that the catalyst of the PEMFC will be seriously deteriorated due to load change operation as there are various mechanisms that decrease the available ECSA, and therefore it will be the most affected element of the cell. On a second level, membrane degradation will also happen under this condition, but at a more reduced rate than for the catalyst.

Start-stop

The start-up and shutdown of the fuel cell is an inevitable step during normal operation, and particularly, for transport applications, in which this procedure is probably happening frequently, and therefore, it is important to analyse which influence does it produce in the cell durability. During normal automotive operation, anode and cathode are filled, respectively with oxygen and hydrogen. When the shutdown occurs both reactants supply is cut off, and the remaining is slowly consumed by ORR. When vehicle is parked and then, the stack is being unused the atmospheric air diffuses through the exhaust vent valve and crosses the membrane

reaching finally the anode side. When the next start-up happens, hydrogen and oxygen will be fed again to anode and cathode. But in this situation, due to the undesired air presence in the anode, a reverse current mechanism will occur due to the formation of a hydrogen-oxygen boundary in the anode while oxygen will be also present in the cathode. This state generates a cathode potential which can be up to twice the OCV potential (remember when introducing the polarization curve, OCV was supposed to be the maximum operating voltage) [63].

Under this conditions, severe cathode degradation occur mainly due to the oxidation of the catalyst carbon and platinum [33, 58-65]. First, by looking on the catalyst side, this high cathode potential corrodes the catalyst carbon support, which, as it has been exposed before in the load cycling part, affects the Pt particles located on this carbon support, leading to detachment and agglomeration of this particles and therefore to an ECSA loss. On the other hand, the carbon framework gets corroded, thus reducing its porosity and increasing the mass transfer resistance. Finally due to the loss of carbon framework the ohmic resistance increase from two sources, first because it is responsible for transferring electrons to the GDL and the current collectors, and secondly because its degradation also affects the ionomer distribution on it, which is responsible for the proton transport, therefore, both the ionic and the electronic resistance increase.

To conclude, the start-stop condition mainly affects the catalyst, consequently the ECSA, and the carbon framework, therefore, the ohmic resistance and the mass transfer resistance.

Low-power

The low power condition could be understood as a steady state operating condition in which the requested current from the cell is in the very low range, or directly, zero, which is, the idling or OCV condition. These could maybe appear as the most innocent condition, as the power demand from the cell is almost null, however, this operating state is the responsible for the most severe part of the PEMFC membrane chemical degradation during its lifetime [33, 66-72]. The degradation mechanisms that dominate in low power condition are:

1. Gas permeation. Under OCV condition due to the absence of reactant consumption there is an increase of its partial pressure of oxygen, which ends up permeating through the membrane to the cathode side. Also, due to the poor generation of water originated by the low reactant consumption both consequences happen, the first one is the dehydration of the membrane, which swells and suffers of an increase of its porosity, secondly, due to the low partial pressure of water in the cathode additional oxygen is accumulated in this area. This whole situation promotes the oxygen permeation to the cathode site, promoting the creation of H_2O_2 and other radicals already introduced in the membrane degradation chapter. Consequently, the membrane suffers of severe chemical degradation losing thickness, increasing its roughness and through the generation of cracks and pinholes. This produces a dramatic hydrogen crossover increase and also a loss in proton conductivity (ohmic resistance increase, R_Ω), but at a minor level.
2. High cathode potential. OCV or low power conditions directly imply high cell potentials, and thus, high cathode potentials. Even though this potential is considerably lower than the previously commented in the start-up process, it is also hazardous for the catalyst promoting the already introduced Pt dissolution, migration, agglomeration or directly, the active Pt loss. Therefore, ECSA loss will also occur at low power mode, but at a more moderated rate than for the membrane chemical degradation.

High-power

In contrast to the previous operating mode, high power accounts for the regime in which the cell current density is extremely high and therefore the demanded reaction rate from the cell. So, when looking again at the polarization curve, this regime would be in the rightest side of the curve, where the current density is very high, and the voltage is in its lowest range. It is usually considered as high power those current densities above $1 A/cm^2$. It is an infrequent operating mode as, normally, when designing a stack for a certain application, it is considered the number of cells which are going to be needed to provide the desired power, therefore, going further than $1 A/cm^2$ is unusual.

However, some studies can be found about this infrequent high-power mode, and its degradation should be also taken into account for any FC application that can reach this current density level [73, 74]. The already commented current overload generates two different scenarios:

1. Gas starvation. As already commented before, reactants starvation generates imbalances that lead to membrane chemical degradation, increasing hydrogen crossover and the ohmic resistance. Also, for the same cause catalyst carbon corrosion occurs producing Pt degradation and ECSA loss.
2. Low humidity. The low humidity state promotes membrane dehydration which leads to pinhole formation and membrane thinning, affecting the membrane stability and conductivity. Furthermore, the low humidity state also promotes carbon corrosion with the subsequent consequences which lead to the degradation of the Pt/C catalyst.

Natural

The final operating mode is, in fact, not an operating mode at all. To classify and quantify the degradation which occurs due to steady-state use of the cell, out of the low and high-power range, and out the high-dynamics operation, where there is also space for low dynamics, the natural or medium-power degradation comes up [23]. It is commonly utilized in the literature to describe the FC natural deterioration during operating conditions out of those already presented.

The objective of this study is to identify degradation sources for certain PEMFC applications, and there is no solid evidence in the literature of how the membrane or the catalyst layer are degraded under this “natural” condition. However, in order to not ignore the portion of cell usage under this regime, a weighted degradation of all the previous presented operating modes will be assigned to the natural degradation, as will be furtherly explained in the methodology chapter.

1.4.3. Experimental methods for degradation measurement

It's now time to briefly present which are the empirical methods to estimate the FC ECSA, ohmic resistance and hydrogen crossover. As a part of every accelerated stress test (AST's) it is necessary to estimate which is the evolution of the cell parameters to register the progression of the cell state under the conditions which are being tested.

As it will be properly explained in the next sub-chapter (1.4.4) the selected degradation indicators which better represent the catalyst and membrane degradation and at the same time are directly related to the fuel cell polarization curve, and therefore make "easy" to evaluate the performance change that they cause are three. The electrochemical active surface area (ECSA), ohmic resistance (R_{Ω}) and hydrogen crossover current (i_{H_2}). The first one represents the catalyst degradation due to loss of active material (Pt). The second and the third one represents the membrane degradation, R through the loss of ionic conductivity and i_{H_2} through the formation of pinholes and cracks which allow the gas permeation.

In the present chapter, the most common methods to estimate each of them will be presented as a relevant part of the literature review made for this study.

Cyclic Voltammetry (CV): ECSA evaluation

Cyclic voltammetry is the most extended method to estimate the electrochemical active surface area for PEMFC electrocatalysts. It involves cycling the electrode over a voltage range to obtain the reactive surface sites by recording the total charge required for hydrogen adsorption/desorption (HAD) [75]. In the following figure (figure 15), a typical CV result is presented, where the different phenomena involved with the platinum catalyst are identified with numbers:

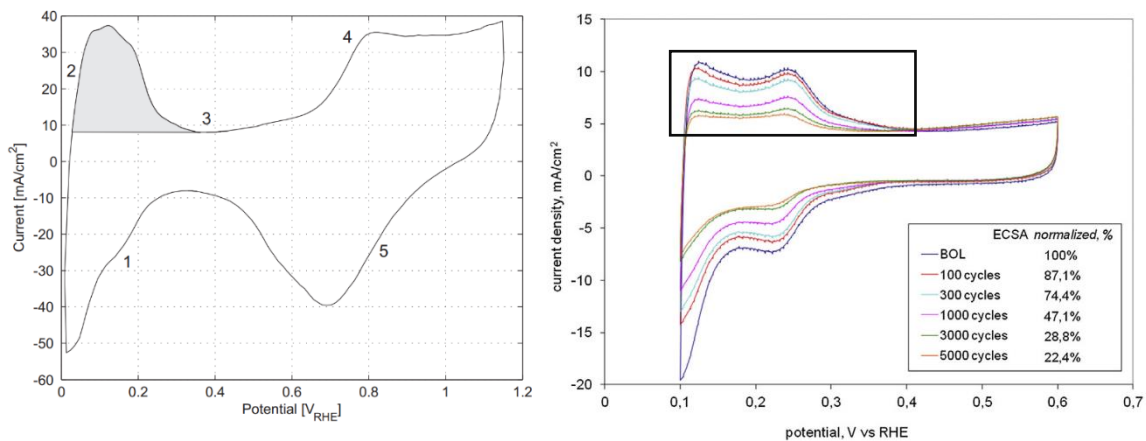


Figure 15. Theoretical and experimental cyclic voltammetry test [51, 61].

1. A monolayer is created due to the proton's absorption to the Pt particles.
2. In the low potential range, the hydrogen desorption from the Pt particles occur.
3. Null specific current from the platinum catalyst, therefore, at this point the current is associated to the double layer capacitance between the membrane and the electrode.
4. Pt particles start oxidizing to PtO due to the oxygen content in the water located in the membrane.
5. PtO is reduced back to Pt.

Finally, the ECSA can be estimated by calculating the shaded area, which corresponds to the hydrogen desorption peak and represents the charge density Q_H ($mC \cdot cm^{-2}$) [76]. Through the following expression (equation 1.19) the charge density is divided by the required charge to reduce a monolayer of protons on Pt ($0.21 mC \cdot cm^{-2}$) and the Pt loading of the cathode L_{Pt} ($g_{Pt} \cdot m^{-2}$), to give the final result of the cathode ECSA.

$$ECSA [m^2 \cdot g_{Pt}^{-1}] = \frac{Q_H}{0.21 \cdot L_{Pt}} \quad (1.19)$$

Electrochemical impedance spectroscopy (EIS): Ohmic resistance evaluation

Fuel cells are usually simplified into an equivalent circuit when studying its electrical properties or modelling the fuel cell electrical behaviour. This equivalent circuit (figure 16) is divided into the ohmic resistance of the cell (R_Ω), the charge transfer resistance (R_{ct}), and the already mentioned double layer capacitance (C_{dl}) [38].

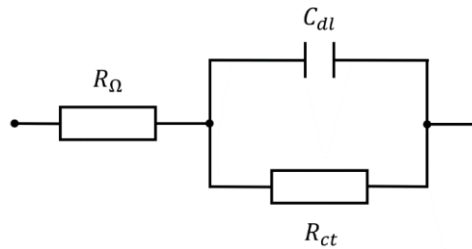


Figure 16. FC equivalent circuit.

The cell internal resistance accounts at the same time for three resistances: the membrane ionic resistance (R_i), the electronic resistance (R_{el}), and the contact resistance (R_c) [77]. As in practice it is very complex to evaluate these parameters separately and the membrane ionic resistance accounts for the biggest part of the cell internal resistance all of the previous are often evaluated together.

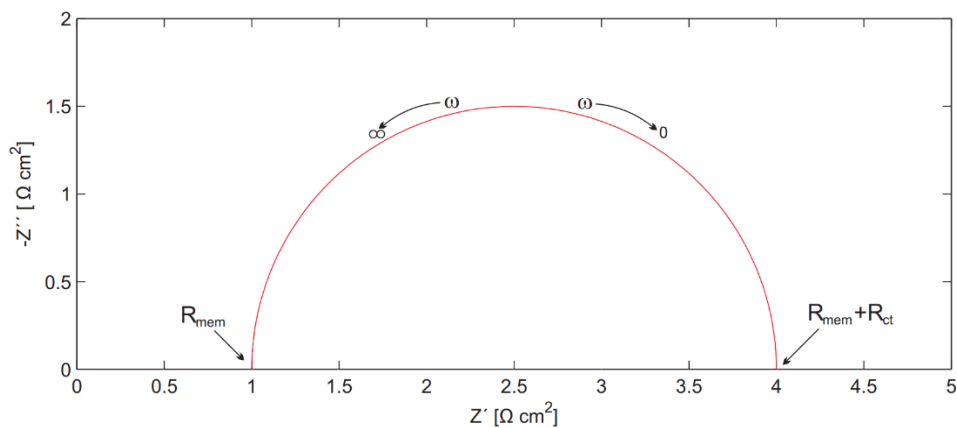


Figure 17. Nyquist plot of a theoretical electrochemical impedance spectroscopy [61].

A widely extended method which serves for this purpose is the electrochemical impedance spectroscopy (EIS). This method consists of applying and alternating current (AC) with different frequencies to the cell measuring the impedance response. The results of the EIS are often

illustrated through the Nyquist plot, representing the real and imaginary part of the impedance (figure 18). Finally, to depict the cell resistance (R_{Ω}) from the charge transfer resistance (R_{ct}) a differentiation in the plot frequencies must be made. On the one hand, in the high frequency range ($\omega \rightarrow \infty$) only the cell resistance is plotted (R_{Ω}), on the other hand, in the low frequency range ($\omega \rightarrow 0$) both resistances are represented (R_{Ω}, R_{ct}). Therefore, to identify the cell internal resistance it will be sufficient by reading the intersection of the Nyquist plot left part (high frequency), with the X-axis.

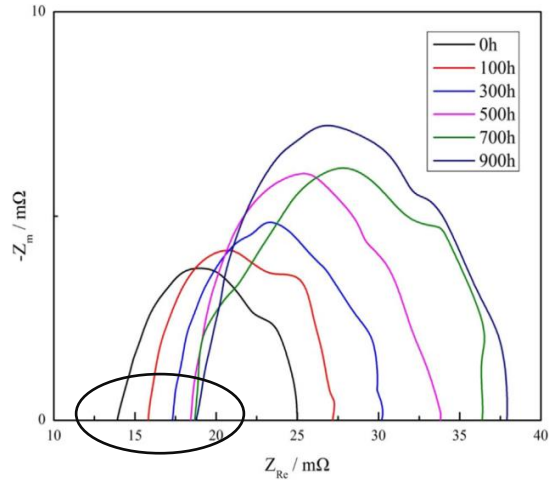


Figure 18. Ohmic resistance in a Nyquist plot of a real EIS [55].

Linear sweep voltammetry (LSV): Hydrogen crossover evaluation

Hydrogen crossover is a direct consequence of membrane degradation and a relatively easy-to-measure indicator. The hydrogen crossover accounts for the fuel which diffuses through the membrane from anode to cathode, reacting directly with the oxygen on the cathode side. As this reaction generates internal currents not useful to feed the load through the external circuit, it is typically classified as an undesired fuel loss. As already stated before, the higher is the membrane mechanical degradation, the higher gets the hydrogen diffusion through the membrane. Therefore, among other indicators, as the fluoride release rate, hydrogen crossover is a common measure which serves as a membrane degradation reference.

Linear sweep voltammetry (LSV) is an easy and extended method for hydrogen crossover measurement. It is similar to the cyclic voltammetry (CV), but instead of a potential cycling in both directions it only involves a single linear sweep from the lowest to the highest voltage limit [79]. By introducing hydrogen and nitrogen through the anode and cathode side, respectively, the cell potential is progressively increased until the current reaches a flat tendency, which means that the hydrogen permeation rate through the membrane is already limiting the hydrogen crossover current to increase and thus the final maximum value has been reached.

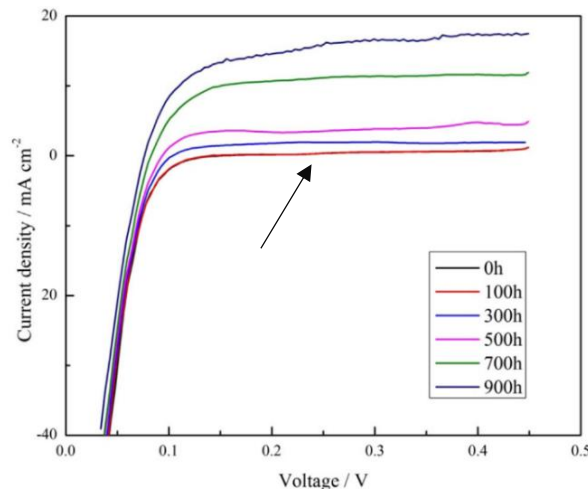


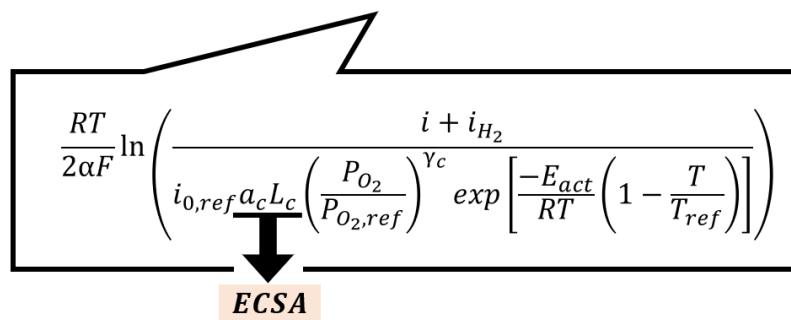
Figure 19. Evaluating hydrogen crossover current in a linear sweep voltammetry [55].

1.4.4. Influence of degradation in the polarization curve

Once a proper contextualization into the PEMFC principles, working mode and degradation has already been given its time to present the integration into the polarization curve of the three main degradation parameters selected for the development of the predictive degradation model: the ECSA, the ohmic resistance and the hydrogen crossover. Each of these parameters have different influence on the FC operating voltage definition and calculation, and thus, different effects and influence on the cell performance along its degradation. As one of the last steps in the introduction of this master thesis, the objective of this chapter is to identify the “location” of these parameters in the already introduced polarization curve equations.

Electrochemical active surface area (ECSA)

At this point it is already known that the ECSA is a measure of catalyst active surface in the PEMFC, but by looking into the given equations (1.3.2) it cannot be directly found. However, there is a variable within the activation losses term, which is directly proportional to it, the electrode roughness. This latter is composed by the product of the catalyst specific area a_c and the cathode catalyst platinum Loading L_c . Therefore, even though the ECSA cannot be directly substituted into the equation, its reduction rate is directly proportional to the reduction of the electrode roughness.

$$U_{FC} = U_{OCV} - U_{act} - U_{ohm} - U_{conc}$$


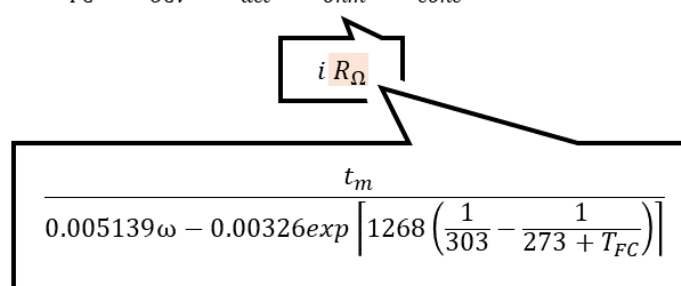
$$\frac{RT}{2\alpha F} \ln \left(\frac{i + i_{H_2}}{i_{0,ref} a_c L_c \left(\frac{P_{O_2}}{P_{O_2,ref}} \right)^{\gamma_c} \exp \left[\frac{-E_{act}}{RT} \left(1 - \frac{T}{T_{ref}} \right) \right]} \right)$$

ECSA

Figure 20. ECSA “location” within the voltage activation losses term.

Cell ohmic resistance (R_Ω)

In contrast with the ECSA, to identify the ohmic resistance within the polarization curve, a zoom out from the equations must be applied, as the resistance is the prime factor by which the current density is multiplied when calculating the ohmic losses term.

$$U_{FC} = U_{OCV} - U_{act} - U_{ohm} - U_{conc}$$


$$\frac{t_m}{0.005139\omega - 0.00326 \exp \left[1268 \left(\frac{1}{303} - \frac{1}{273 + T_{FC}} \right) \right]}$$

Figure 21. Ohmic resistance “location” within the voltage activation losses term.

Hydrogen crossover current (i_{H_2})

Even though the hydrogen crossover current has been defined as a generated current which does not contribute to the cell output voltage, unfortunately it does take place for the cell losses. So, it does not only imply a loss in the available hydrogen to convert into energy, but also increases the voltage losses. In this case, the activation losses term is affected from a second FC degradation source, before it was the catalyst (ECSA) and now the membrane (i_{H_2}).

$$U_{FC} = U_{OCV} - U_{act} - U_{ohm} - U_{conc}$$

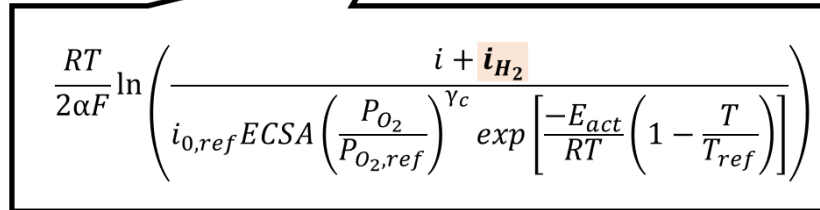

$$\frac{RT}{2\alpha F} \ln \left(\frac{i + i_{H_2}}{i_{0,ref} EC SA \left(\frac{P_{O_2}}{P_{O_2,ref}} \right)^{\gamma_c} \exp \left[\frac{-E_{act}}{RT} \left(1 - \frac{T}{T_{ref}} \right) \right]} \right)$$

Figure 22. Hydrogen crossover "location" within the voltage activation losses term.

1.4.5. Linkage between overall and specific degradation

As stated in the first pages of this work, the Fuel Cell Technical Team from the U.S. DOE establishes, in order to situate the FCV at a competitive level against traditional ICE vehicles, a maximum performance loss of the 10% at 8.000 hours driving as a target that should be reached in the worst case [24]. Consequently, the research project from R. Novella and M. López Juárez developed a 3 – layer (experimental, electrochemical and physical based) PEMFC degradation model in which the limit targeted by the DOE has been considered as end-of-life barrier, in order to follow the international standard up to date [20-23].

The present study, which takes as starting point the mentioned project, aims to achieve the challenge of linking the overall cell degradation with the specific degradation sources (catalyst, membrane), therefore it will also take as reference the 10% performance loss target from the U.S. DOE.

Voltage degradation rate

For this purpose, a new concept is now being introduced, the voltage degradation rate. It is already known at this point that in practice, the FC performance degradation is translated in last instance into a drop in the cell output voltage, hence, via the following expression (equation 1.20) the voltage degradation rate in percentage terms can be calculated [20-24]:

$$\delta_{deg} = \left(1 - \frac{U_{deg}}{U}\right) 100 \quad (1.20)$$

Where δ_{deg} is the voltage degradation rate, U_{deg} is the operating FC voltage at a given current density after degradation, and U is analogous to the latter but before the cell degradation. However, as already noted, the voltage suffers a continuous variation along the current density range, as all the voltage losses equations (activation, ohmic and concentration) depend on the current density. Taking these two factors into account it makes sense to establish a fixed current density point on which the reference voltage degradation is always measured, which will be 1 A/cm^2 . To better illustrate this concept which will be highly relevant for the development of this study, the following figure (figure 23) is given, where the upper curve represents the undegraded cell, and the lower the analogous degraded one.

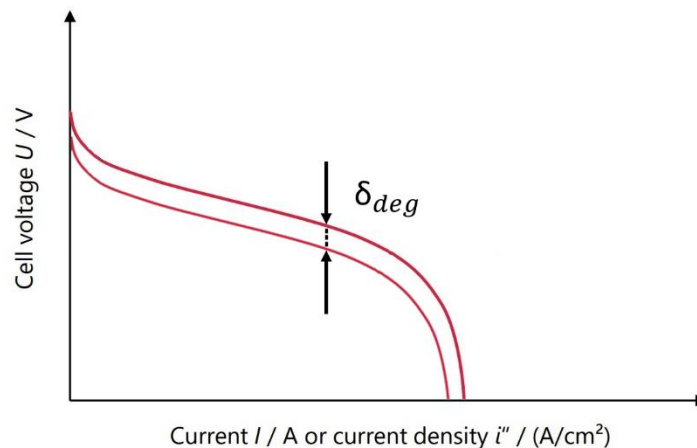


Figure 23. Voltage degradation rate in the FC polarization curve.

2. Objectives

The main purpose of this master's thesis is to develop a literature-based PEMFC predictive degradation model capable of identifying the degradation source within the FC membrane electrode assembly (MEA) applicable to the road transport sector. To achieve this, various sequential objectives must be first successfully accomplished:

- Develop a mathematical polarization curve model, which has good sensitivity within the typical operating conditions range and is open to use for different PEMFC applications.
- Identify the limits in ECSA, Ohmic Resistance and Hydrogen Crossover decay as a function of the voltage degradation rate for calibration
- Analyse the ECSA, Ohmic Resistance and Hydrogen Crossover decay for PEMFC systems in realistic operating conditions
- Determine recommendable countermeasures to maximize durability and high-performance lifespan depending on the degradation trend for each application.

3. Methodology

In order to reach the final objective of developing a PEMFC predictive degradation model capable of identifying the main sources which cause the cell performance decay the followed methodology is represented in the next block diagram (figure 24) which has been completely developed taking MATLAB R2022a as software basis.

The first step is to define a PEMFC polarization curve model which must be based on the electrochemical laws that make up the operating voltage calculation as a function of: the operating conditions (pressure, temperature, relative humidity...), the FC properties (platinum loading, electrode surface area, membrane thickness...) and finally the load range, which is basically based on the current density range in which the FC is expected to be operated.

Secondly, after the initial definition of this first approach of the polarization curve model, it must be calibrated with experimental results at different operating points (pressure, temperature) to ensure the maximum realism of the polarization curve model. As the polarization curve contains various coefficients which may vary depending on all the conditions stated in the first step, which directly affect the operating voltage calculation, a powerful optimization tool is needed to find the best fit to the reference experimental data within all the possible combinations in these coefficients. The selected optimization tool will be the Genetic Algorithm from MATLAB R2022a. Furthermore, it will be essential to precisely define the lower and upper limits for each coefficient to optimize, as the genetic algorithm tool will try to find the best numerical combination to fit as much as possible the polarization curve model with the experimental reference curves, but without taking into account any theoretical consistency. Therefore, the calibration process will first consist of defining a literature-based set of limit windows for each coefficient “free” to be optimised by the algorithm. Then, the optimization can be launched and the iterative process of finding the best fit will start until the best possible approach is found. Once it is, the model will be validated by comparing the output polarization curve with the reference for an identic current density and operating conditions (pressure, temperature) input.

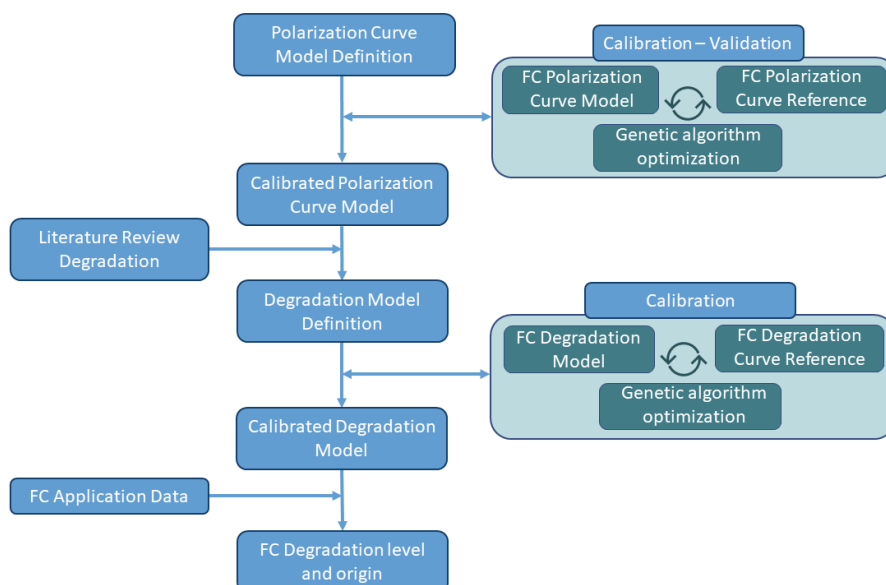


Figure 24. Master's thesis methodology block diagram.

Once the PEMFC polarization curve model is defined, calibrated and validated, the third and most challenging step of the methodology takes place, the PEMFC degradation literature review. Leaving aside the complexity of the PEMFC degradation topic, it must be noted again that the objective of this study is not to develop a PEMFC predictive performance degradation model which “just” reflects the decay of the polarization curve (through the voltage loss) after a certain operation, the objective is to develop a model capable of predicting how and how much the internal components of the PEMFC degrade under this operation. To achieve that, firstly a deep study and comprehension of all the mechanisms behind the internal PEMFC degradation must be made. Secondly, an exhaustive literature review is made to create a database integrating all the relevant degradation data found from each literature reference. Third, a meticulous selection and purge of each reference must be made according to the objective PEMFC properties and operating conditions in order to exclude degradation data which do not fit the scope of this model or are outliers. In fourth place, the degradation source indicators (which finally have been EC_{SA} , R_{Ω} and i_{H_2}) must be selected to be transferred afterwards into the degradation model by considering: its relevance in the PEMFC degradation, its transferability into the polarization curve (there are many degradation indicators which cannot be integrated into de polarization curve), and last but not least, the presence of this indicators into the set of literature references, as not all of them focus on the same indicators and selecting a certain set directly excludes studies which have focused on other degradation parameters. Finally, as fifth and last step, a model adjustment must be made to integrate the selected degradation coefficients in the polarization curve equations (equations 1.10-1.18).

Hereon, after the previous step, the model will not only be representing the PEMFC polarization curve but also will be capable of showing degradation by modifying the previously selected degradation indicators (EC_{SA} , R_{Ω} and i_{H_2}), however, a second calibration following the same procedure as for the first one must be done, but now, it will be without experimental validation. This second calibration, in contrast to the previous will be based on the progression trends found in the literature for each degradation source parameter (EC_{SA} , R_{Ω} and i_{H_2}). Moreover, this calibration will also consist of taking into account the voltage degradation rate found in each literature reference in order to establish a solid link between overall and specific PEMFC degradation.

Finally, after the completion of the previous stage, the model will be ready to receive the degradation data distribution from the desired application, which are those operating states presented in (1.4.2): load cycling, start stop, low power, high power and natural. Through the given distribution of degradation within these operating states, the model will be capable of identifying the degradation origin progress through the percentage variation of the degradation origin indicators (EC_{SA} , R_{Ω} and i_{H_2}) coupling it with the voltage degradation rate (δ_{deg}).

Therefore, to summarize, the model will predict a specific degradation origin ($\%EC_{SA}$, $\%R_{\Omega}$ and $\%i_{H_2}$) for a certain overall performance decay (δ_{deg}) depending on the application which the PEMFC serves ($\%\text{load cycling}$, $\%\text{start stop}$, $\%\text{low power}$, $\%\text{high power}$ and $\%\text{natural}$).

3.1. FC Polarization curve model definition

The first step consists of defining a mathematical model which imitates the PEMFC electrochemical laws in order to obtain the cell operating voltage. This model must contain the already presented (chapter 1.3.2) complete voltage calculation, from the OCV voltage to the final cell voltage, taking into account the activation, ohmic and concentration losses.

$$U_{FC} = U_{OCV} - U_{act} - U_{ohm} - U_{conc} \quad (3.1)$$

Term nomenclature	Abbreviation	Equation	Ref.
Open Circuit Voltage	U_{OCV}	$\frac{\Delta G}{2F} - U_{loss}$	(3.2)
Activation losses	U_{act}	$\frac{RT}{2\alpha F} \ln \left(\frac{i}{i_{0,ref} a_c L_c \left(\frac{P_{O_2}}{P_{O_2,ref}} \right)^{\gamma_c} \exp \left[\frac{-E_{act}}{RT} \left(1 - \frac{T}{T_{ref}} \right) \right]} \right)$	(3.3)
Ohmic losses	U_{ohm}	$\frac{i t_m}{0.005139\omega - 0.00326 \exp \left[1268 \left(\frac{1}{303} - \frac{1}{273 + T_{FC}} \right) \right]}$	(3.4)
Concentration losses	U_{conc}	$-c \ln \left(1 - \frac{i}{i_l} \right)$	(3.5)

Table 2. PEMFC polarization curve model equations.

First, regarding the open circuit voltage, it should be noted that in order to simplify the previously stated deviations between the standard potential and the open circuit voltage (see 1.3.2), which correspond, firstly, to the deviation from the standard conditions, and secondly to the potential losses due to internal short-circuits and/or gas leakage, among others, a term called U_{loss} will be representing both deviations at the same time. With this, the objective is to take into account this voltage losses, but at the same time not giving a certain fixed value for them, as this variable will be part of the parameters to optimize with the model calibration. Also, it must be noted that the activation term equation, as stated in the chapter 1.3.2, will vary depending on the current density value (see equation 1.12). Furthermore, a simplification has been made assuming the cell activation losses equal to the cathode activation losses due to the neglectable influence of those from the anode, as already mentioned in chapter 1.3.2. Finally, regarding the concentration or mass transport losses, the definition of this equation has needed a further analysis as there is not an extended consensus from the scientific community about which expression better represent this phenomenon [38]. This discussion has led to the first sensitivity analysis for the development of this model, where, within the following expressions, the one shown in the previous table has been selected:

$$-c \ln \left(1 - \frac{i}{i_l} \right) \quad (3.6)$$

$$-\frac{RT}{2F} \ln \left(1 - \frac{i}{i_l} \right) \quad (3.7)$$

$$m \exp(ni) \quad (3.8)$$

To compare these three expressions, it is necessary first to define the values of their coefficients. For the first expression (3.6), parameter C depends on the fuel cell state and the operating conditions, according to literature its value is within the range (0.001 to 5). For the second expression (3.7) the value of R (ideal gas constant) and F (Faraday constant) are already known and fixed, on the other hand, the cell temperature will be defined at two different levels (303K, 346K). For the third expression (3.8), again, according to literature the value of m is in the $10^{-5} V$ order of magnitude and the value of n around $10^1 A/cm^2$ (37). Finally, i and i_l represent the current density and the limiting current density, respectively, therefore these variables will be an input when calculating the concentration voltage loss. Finally, a calculation within the $0 - 1.5 A/cm^2$ current density range is made (range of interest for the development of the model), with a limiting current density fixed at $2.4 A/cm^2$. The resulting tendency for each expression is shown below (figure 25):

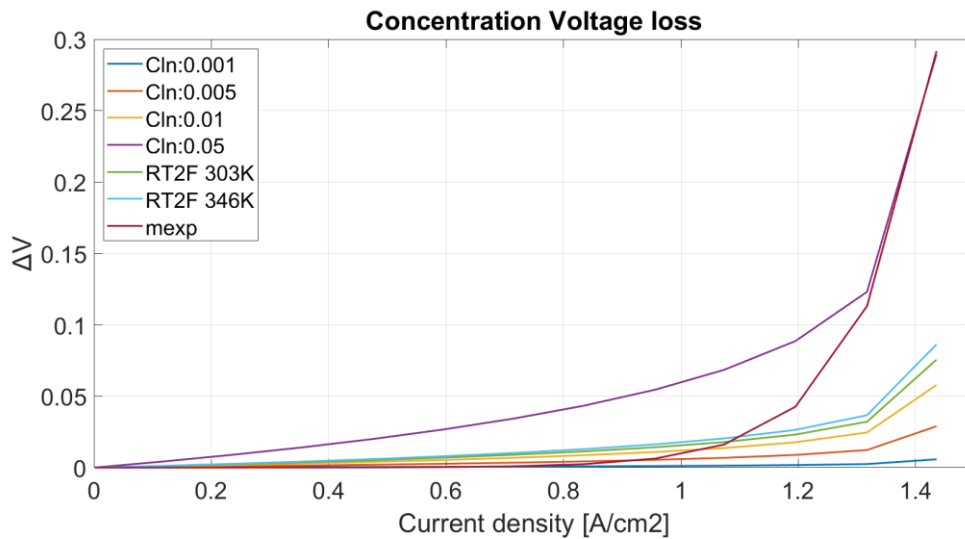


Figure 25. Comparison of different expression representing the voltage concentration losses.

Starting with the expression 3.7, and observing both its results for 303 and 346K, the flexibility which this expression allows for a curve fitting, which will be the objective when calibrating this model, is extremely limited, therefore this expression is discarded for its use. The expression 3.8 follows a pure exponential pattern, and therefore neither does not seem to be a good option for a flexible curve fitting. For the expression 3.6, with changes in C value within its range it is clearly observed how the curve slope is highly flexible and susceptible to change making this expression the best for the present model taking into account that a calibration is to be done as next step. Therefore, expression 3.6 is being selected as the final voltage concentration losses term.

3.2. FC Polarization curve model calibration and validation

The polarization curve model calibration is a relevant step in the methodology of this master's thesis, as, the better is the model fit to the experimental reference values, the more reliable it will be. In order to calibrate it, few steps must be made as part of the methodology.

The first one is to classify each parameter from the whole polarization curve equation into constant, variable or value to optimize in the calibration. Secondly, depending on the previous classification, the value, or possible values for each parameter must be defined. Third, an optimization strategy should be established defining the objective function and calculation procedure for the value or values to optimize. Finally, an optimization tool must be selected depending on its suitability according to all of the previously commented.

3.2.1. Polarization curve parameter classification and definition

Starting with the polarization curve model parameters classification, the first category will be those which are remaining invariant further on, which are physical and chemical constants, reference conditions and FC design properties:

Constant Parameters			
ΔG	Gibbs free energy	237340	J/mol
F	Faraday constant	95485	C/mol
R	Ideal gas constant	8.3144598	$J/mol K$
$P_{O_2,ref}$	Reference anode pressure	101.25	kPa
T_{ref}	Reference temperature	298.15	K
E_{act}	Activation energy	66000	J/mol
t_m	Membrane thickness	183	μm

Table 3. Set of constants in the PEMFC polarization curve model.

The next set of parameters will be the variable ones, which will be directly related to the operating conditions and will always be an input for the model. Note that for the polarization curve model calibration the experimental references will be curves at two stack temperatures (303/ 346 K) and at two levels of anode pressure (130 / 250 kPa), finally, the current density input, in order to obtain a full output voltage curve and not only a single point, will be a set of progressive values within its range.

Variable/ Input Parameters			
T	Cell temperature	305/ 346	K
P_{O_2}	Anode pressure	130/ 250	kPa
i	Input current density (load profile)	(0, 1.44)	A/cm^2

Table 4. Set of variables in the PEMFC polarization curve model.

Finally, the polarization curve parameters which will be optimized in order to calibrate the model will be the following. As previously stated, its value range has been set based on literature references as when using any generic optimization tool, the physical coherence for each parameter to optimize in order to find the best fit won't be contemplated, as this tool will only be looking for a mathematical solution [38,79-84].

Parameters and coefficients to optimize for calibration			
α	Charge transfer coefficient	(0.46, 0.54)	–
ACT	$I_{0,ref} \cdot a_c \cdot l_c$	(1^{-9} , 1^{-3})	–
γ_c	Pressure dependency coefficient	(0.5, 1.45)	–
w	Membrane water content	(4.1, 14.003)	–
i_l	Limiting current density	(1.44, 2.4)	A/cm^2
C	Concentration loss coefficient	(0.001, 5)	–
U_{loss}	Voltage deviation between standard conditions and OCV	(0.1893, 0.2893)	V

Table 5. Set of variables to optimize in the PEMFC polarization curve model calibration.

Two remarks must be made at this point. The first one concerns the parameter “ACT”, which includes the product of the exchange current density $I_{0,ref}$, the catalyst specific area a_c and the cathode platinum loading l_c , where the product of the two latter, as previously commented (chapter 1.4.4), make up the electrochemical active surface area $ECSA$ of the cathode. The reason for unifying all these three parameters into one is just to not increase unnecessarily the number of variables with which the optimization tool must work, so the reason is purely for reducing execution times when calibrating the model, as the three of them are consecutively multiplied in the voltage activation losses term (chapter 1.3.2).

The second point to remark is the membrane water content (w) value range. Through this value, the third critical operating condition of the PEMFC emerges (being the other two temperature and pressure), which is the relative humidity, RH . As introduced in the chapter 1.3.1 the membrane relative humidity must be in the 50% to 100% range in order to ensure a minimum water content in the membrane and therefore a good ionic conductivity. Hence, this critical relative humidity range must be transferred into the membrane water content (w) value range in order to set a model calibration within the required cell conditions. The expression which related both is the following:

$$\omega_{30^\circ} = 0.043 + 17.81RH^3 - 39.85RH^2 + 36RH \text{ for } 0 \leq RH \leq 1 \quad (3.9)$$

Considering the 50% to 100% RH range, the resulting w value range is illustrated below, which corresponds, to the range defined in the table 5.

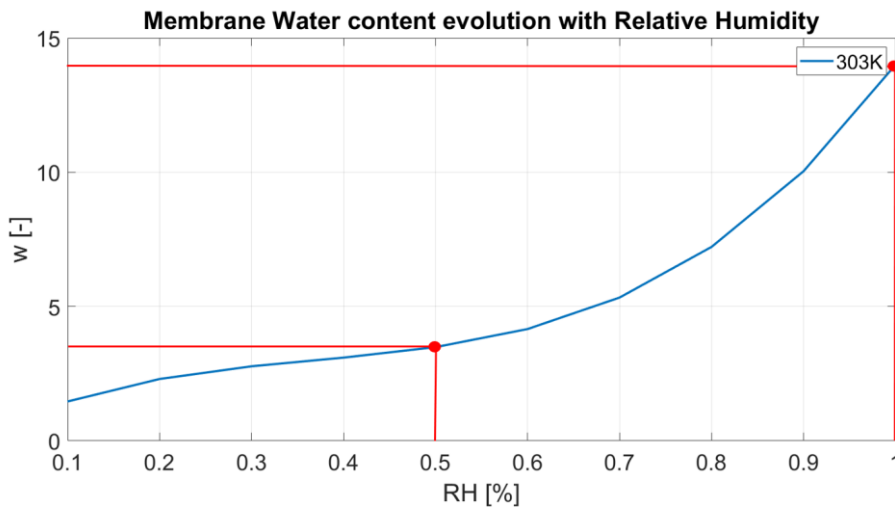


Figure 26. Relationship between membrane water content and relative humidity.

3.2.2. Calibration Reference Definition

Once all the polarization curve parameters are defined, the next step is to determine the optimization strategy followed to fit the modelled curve into the experimental reference ones. The reference curves with which the present model is being calibrated are shown in the following figure (figure 27):

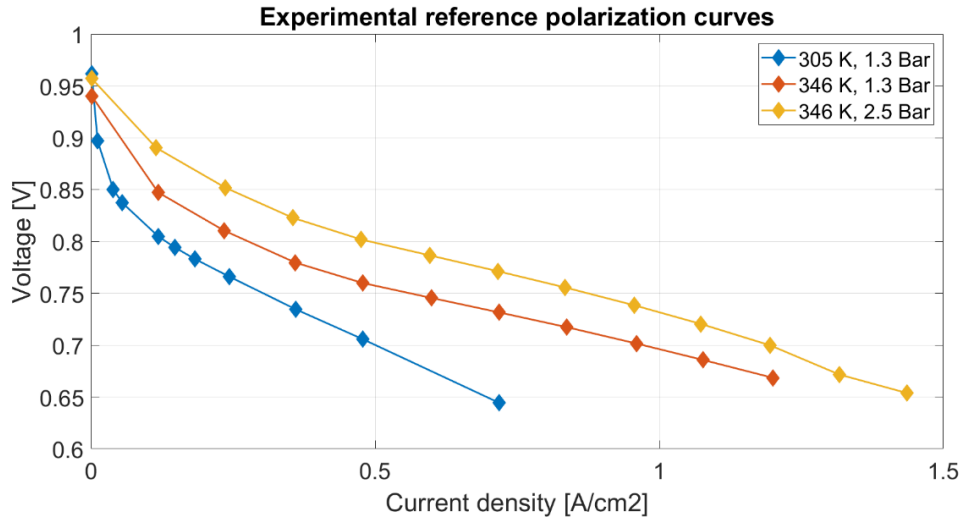


Figure 27. Reference polarization curves for the model calibration and validation.

These three curves, which are experimental results from [85, 86] were already utilized by R. Novella and M. López Juárez in their respective research project [20-23] which has laid the foundations for the development of this master's thesis. These data belong to an 80 – cell 20 kW PEMFC stack with a 250 cm^2 area for each cell and was registered at an experimental facility with temperature, stoichiometry and pressure-controlled conditions, and shows the changes in the polarization curve when varying the stack temperature and the anode pressure. In consequence, this data is selected in order to calibrate and validate the model sensitivity to temperature and pressure variations.

3.2.3. Limitations of manual calibration and curve sensitivity

As already defined in table 5, up to seven degrees of freedom are to be defined in the model calibration, taking with them the representation of each of the four terms in which the operating cell voltage is defined (OCV, activation, ohmic and concentration, or mass transport).

Being U_{loss} part of the OCV term representing the possible deviation between theoretical and real operating voltage. Then, three of them being part of the activation losses term (charge transfer coefficient α ; ACT representing the product of the reference exchange current density, the catalyst specific area and the cathode platinum loading $i_{0,ref} \cdot a_c \cdot l_c$; and the pressure dependency coefficient γ_c). One accounting for the ohmic resistance losses term, which is the membrane water content w representing the influence of the cell relative humidity. And finally, as part of the concentration or mass transport losses the limiting current density i_l along with the concentration loss coefficient C . It must be taken into account that each of these parameters has an individual influence on the polarization curve, which as illustrated below (figure 28), may severely affect the polarization curve shape.

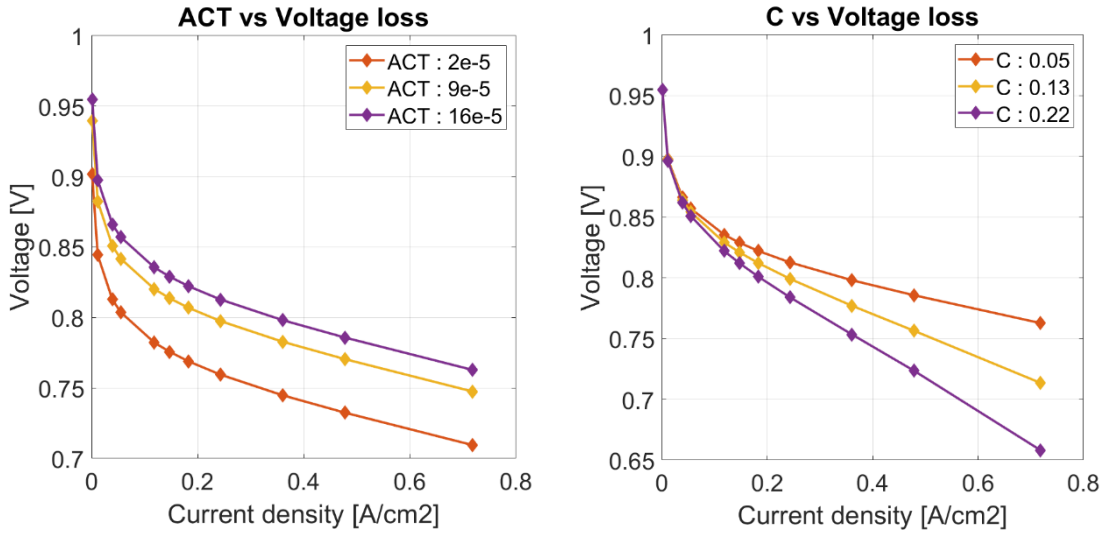


Figure 28. Influence of "ACT" and "C" on the polarization curve shape.

Here, two examples are illustrated accounting from left to right for only one parameter within the activation losses term and the concentration losses term, respectively. It can be observed how small changes (comparing image's ACT and C values with the full ranges found in literature at table 5) have substantial influence on the curve shape. This high sensitivity, along with the fact that, not two, but seven parameters must be adjusted at the same time make essential a numerical evaluation which should be carried out by an optimization tool or algorithm. Furthermore, just not only regarding the factor of finding a multiple solution, but the level of accuracy which the usage of this tools brings with them make it a fundamental step in order to achieve a consistent model calibration over the experimental reference curves.

3.2.4. Calibration strategy

After introducing the reference data for the model calibration and validation and the strong need of establishing a computational procedure to achieve it, is time to introduce the numerical evaluation that will be employed to measure, point by point, the deviation between the polarization curve model, and the reference data for the fitting optimization. To quantify this deviation, the root mean square deviation (RMSD) will be employed, which expression, applied this case where the model voltage is compared to the reference voltage for each current density point is the following:

$$RMSD = \sqrt{\frac{\sum_i^n (U_{ref,i} - U_{model,i})^2}{n}} \quad (3.10)$$

Where i accounts for each datapoint, and n for the sum of all the points forms each polarization curve. However, as the aim of this calibration is to minimize the deviation, not to one reference curve, but to three at the same time, the $RMSD$ of each of these curves will be simultaneously evaluated through the average of each curve's $RMSD$:

$$\overline{RMSD} = \frac{\sum_i^n RMSD_i}{n} \quad (3.11)$$

Where, this time, i represents each polarization curve, and n the number of curves evaluated together.

3.2.5. Calibration procedure: Genetic algorithm optimization

Therefore, another step has been completed defining the objective function, which accounts for the minimization of the average root mean square deviation for each datapoint and versus each reference curve (\overline{RMSD}). The following stage in the calibration procedure is therefore to select an optimization tool suitable for this minimization in which, a nonlinear multivariable evaluation must be feasible and must be also capable of handling a high level of accuracy with a coherent execution time. The selected algorithm taking the previous into account, and the software basis used for the development of this model (MATLAB R2022a) is the genetic algorithm.

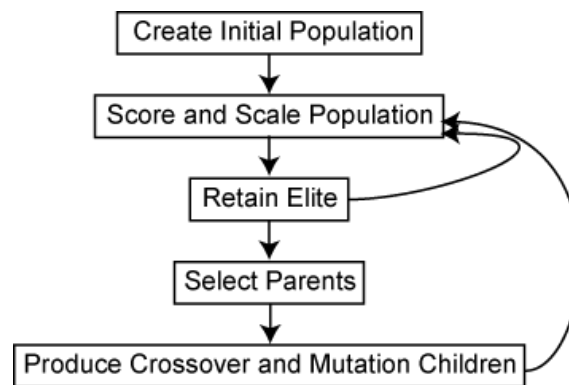


Figure 29. Conceptual representation of a genetic algorithm working mode [88].

The genetic algorithm (GA) is a metaheuristic method for solving optimization (constrained or unconstrained) problems which is based, as its name suggests, on the natural selection process imitating the biological evolution. The GA, as main difference with the classical algorithms, repeatedly selects individuals from the current population of solutions to be “parents” and generate with them the “children” for the next generation, therefore, after successive generations this population evolves to the optimal solution [87-89].

The GA optimization can be found in MATLAB’s *Global Optimization Toolbox* and its application consists of first defining:

- The *fitness or objective function*, which in this case will be a script containing the polarization curve model (table 2) and the three mentioned reference curves (figure 27). The script will compare them using the combination of solutions (coefficients to optimize, table 5) provided from the genetic algorithm at each iteration and will return the average root mean square deviation between model and reference (\overline{RMSD}), which will be the *fitness value* to minimize.
- The *genetic representation or solution domain*, in which all the variables from table 5 will be provided with their respective value range, also the *population size* and the maximum number of *generations* will be defined.

After this definition, the algorithm execution can be launched, and the model calibration starts.

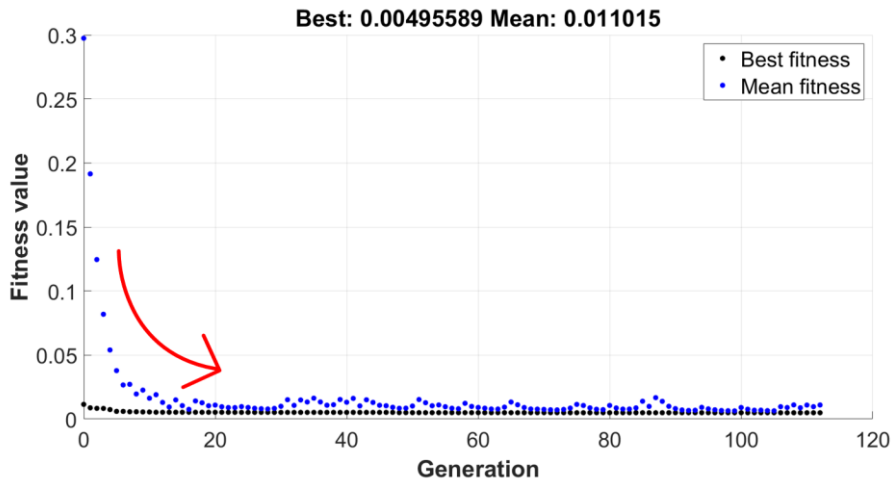


Figure 30. Progressive optimization of the GA for the fitness value minimization.

Once the optimization has finished, the GA returns the minimum \overline{RMSD} found and the set of polarization curve variables which make up the solution found.

Genetic algorithm output				$\overline{RMSD} = X$		
α	ACT	γ_c	w	i_l	C	U_{loss}
X_1	X_2	X_3	X_4	X_5	X_6	X_7

Table 6. Example of a GA output result applied to the calibration of this model.

Up to this point, and regarding the calibration, to find a good model fit against the given references may appear a relatively simple procedure. However, the difficulty of this step (leaving apart the coding and the needed review to define the correct equations) remains, first, in the selection of variables which will be flexible to modify their value during the optimization (inside the defined limits). And, secondly, the limit definition for each variable, since any value found in the literature review has an origin in a certain model or a certain fuel cell, or a certain set of operating conditions, application... and so on, and the key here is to find the best solution, for this specific case, and references.

It must be noted that this calibration strategy has some handicaps, the biggest one among them is the fact that a common solution is being searched by the GA in order to find the best average fitting for the three curves, which implies that an optimal solution can drive a very narrow approximation to one or two curves at the same time, but at the expense of worsening the fitting to other of the reference curves. As the fitness value is an average deviation, the quality of the GA optimization result must be checked, further than just keeping the lowest \overline{RMSD} as the best solution.

Besides, apart from the imbalance that the \overline{RMSD} indicator can “hide” behind it regarding each of the reference curves, an analogous phenomenon can occur with each individual polarization curve point, as the $RMSD$ (equation 3.10) can also “hide” imbalances within the same polarization curve.

So, as stated in previous pages, the optimization tool will be essential to find the best numerical approximation, however, an external supervision and correction is needed in order to find a coherent compromise between quantitative (\overline{RMSD}) and qualitative (best common solution for the three curves) solutions. The best way to evaluate this compromise is through the model validation.

3.2.6. Model validation

The validation process is very simple and just consists of introducing into the model (which has the value of the optimized coefficients updated) the current density points from one of the reference curves along with the definition of the same operating conditions, which in this case are the cell temperature T , and the anode pressure, P_{O_2} . After this, both polarization curves can directly be plotted and compared. If the calibration process has been successful, the voltage difference between the model curve and the reference curve will be similar for the same current density point, and as soon as both curves are plotted together, a rapid visual evaluation will be enough to determine the quality of the calibration.

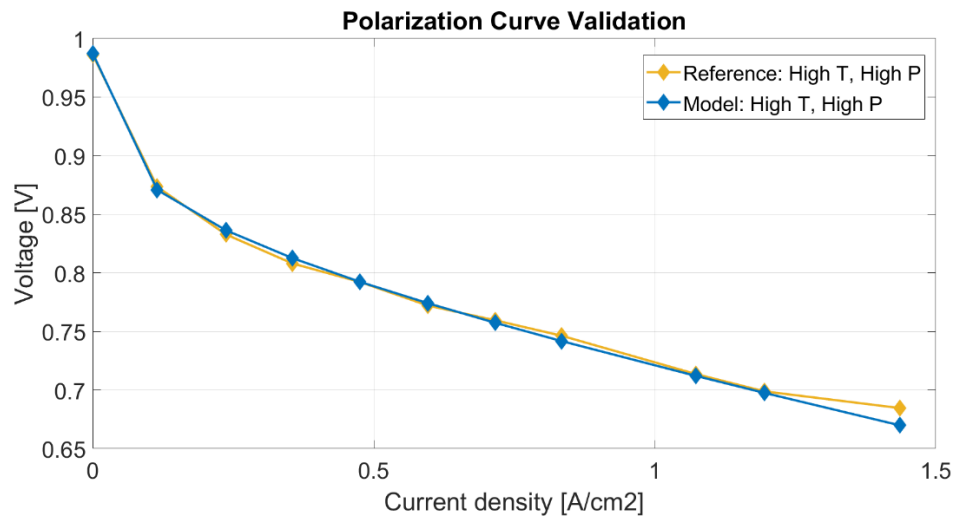


Figure 31. Example of visual validation of the model calibration.

A representative plot of the qualitative validation process is shown above (figure 31), where further than obtaining a low \overline{RMSD} it is also essential to have a homogeneous fit between the model and the reference curve along the complete current density range.

To conclude, it must be taken into account that the main objective of the PEMFC polarization curve model is to develop a mathematical tool which imitates, as precisely as possible, the real electrochemical behaviour of this type of fuel cell being capable of giving, as output, the same voltage response as a real cell for the same operating conditions (input current density, temperature, pressure and relative humidity) and FC properties (membrane, catalyst, size...). Therefore, calibrating the model over an experimental reference, in practical terms, means that the model is able to represent consistently the behaviour of a real fuel cell.

3.3. FC Degradation model definition

Assuming that the model has already been calibrated successfully, the undegraded PEMFC polarization curve model is already “finished” and, therefore, from this point onward, the efforts will be focused on integrating the PEMFC degradation part of the model.

As already discussed above (chapter 1.4.2), the strategy followed for the development of this model which aims to predict the degradation sources ($\%EC_{SA}$, $\%R_{\Omega}$ and $\%i_{H_2}$) in PEMFC's. To achieve this purpose, it is fundamental to develop a model which is sensible to the different operating states in which a PEMFC can run when feeding an electrical machine which propels a fuel cell vehicle (FCV). This prosecuted sensibility to different driving profiles must, somehow, be able to differentiate when the fuel cell is operating at high or low load, at high load changes in time, or when it is started up or switched off. The selected methodology to discern within this states' degradation is to previously analyse them separately, and then integrate each degradation pattern into the model, which will be told, as input, which is the share (%) of each of these operating states within the overall operation that has led the fuel cell to a certain overall degradation (δ_{deg}).

Once this is clarified again, the first step is starting with the literature review, which aims to seek for experimental accelerated stress tests (AST'S) degradation results, which ideally, must be focused on each of the previously commented operating states separately. These operating states, as introduced in 1.4.2, are typically classified into load cycling, start-stop, high power and low power. The last one introduced in 1.4.2, which is the natural degradation, is complex to determine as there is still an absence of scientific publications which study that kind of cell degradation, and as previously stated, it will be pondered in this study as a mix of the rest operating states' degradation.

3.3.1. Literature review

The objective of this stage, as already commented, is to seek for experimental degradation studies focused exclusively on each PEMFC operating condition, however, as a part of this process it is necessary to define other requirements which these studies must comply with.

Degradation references: search and selection

The first indispensable requirement is that the PEMFC tested in the AST must have a Nafion® membrane, which, as introduced in the chapter 1.3.1 and 1.4.1, is the most typical PEMFC membrane and it is made out of perfluoro sulfonic acid polymer. The second requirement is that it must also be a low temperature cell, as there are two types, high temperature and low temperature (HT-PEMFC and LT-PEMFC). The third requirement is having a Pt/C based anode and cathode catalyst, which is, as also presented in the mentioned chapters, a Platinum nanoparticle catalyst based con a Carbon support. Last, but not least, the PEMFC anode and cathode input gasses must be hydrogen and air, respectively. Taking all of the above requirements as indispensable is crucial, as the objective of this chapter is to collect degradation trends from as much experimental tests as possible but without losing homogeneity in the boundary conditions, and thereby creating a reliable degradation data base. The reason for this is that this degradation data will be furtherly used to develop the degradation predictive model.

The second filter for the reference search is regarding the already commented operating states (load cycling, start, stop, low power, high power). The degradation data will be classified and divided into these four classes. However, there is a wide variety of PEMFC experimental AST's studies which, because of their own interest and objectives, may perform the test with different types of cycles within a same operating state and it must also be considered for the reference selection. Furthermore, as in several of these studies thousands or even tenths of thousands of cycles are applied to the cell in order to promote an accelerated degradation, any change in the type of cycle applied, may cause a considerable variation in the degradation result. Therefore, a general criterion for the reference selection must be established for each operating condition.

1. Load cycling. The aim at this operating state is to evaluate how the PEMFC is affected by a continued load change where the current density is being increased and decreased periodically, and as analysed in 1.4.2, it mainly affects the catalyst durability, but also has a relevant influence on the membrane degradation [33, 49-57]. According to the DOE standards [24], the lower and upper voltage limits must be 0.6 V and 0.95 V in order to promote the electrocatalyst degradation, as going further than 1 V will also enhance the catalyst carbon support corrosion which is out of the scope of this kind of tests. Ideally, the cycle shape should be squared, however, in order to include more reference sources and therefore giving more consistency to the load cycling degradation database, which is about to be created, similar cycle patterns within this voltage range are also accepted for this study (figure 31).

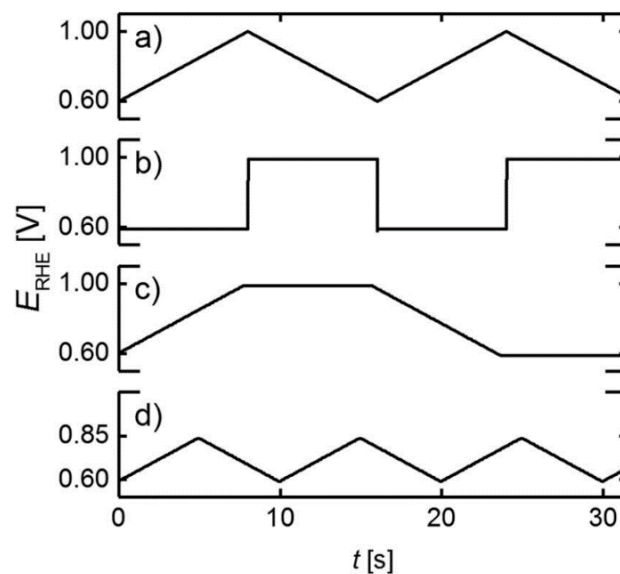


Figure 32. Set of representative voltage patterns accepted as load change AST cycles [52].

2. Start-Stop. In second place comes the start-up and shutdown of the PEMFC. The start-stop AST aims to represent in a relatively short period of time which is going to be the degradation for starting up and switching of a PEMFC during years of usage. As exposed in 1.4.2, this process generates voltages that can overcome the OCV generating serious carbon corrosion which consequently damages the catalyst and also affects the ionic and electronic cell resistance [33, 58-65].

This operating state is often studied comparing the application of a dummy load before the start up with the absence of this dummy load (figure 32) and thanks to this discussion it is relatively easy to find degradation studies focused on the start-up shutdown condition. Therefore, both strategies (dummy on/ dummy off) are being accepted as valid to become part of the degradation data that will be included for the model development.

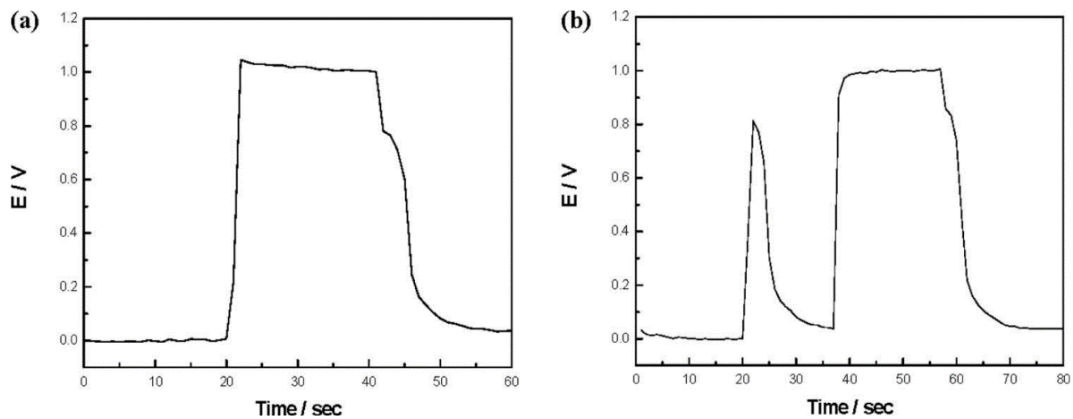


Figure 33. Typical start-stop voltage response without and with previous dummy load, respectively. [63]

3. Low Power/ OCV. Another main operating state for a PEMFC under transport application is the range in which the current density (and therefore the cell power output) is low and steady, or even zero, which accounts for the idling or OCV condition. In this range of operation, the absence of reactant consumption promotes severe membrane degradation, and, in the other hand, high cathode potentials damage the cell catalyst, but at a lower level [33, 66-72]. In order to open the scope and not restrict the collected data to only OCV steady state studies, every steady state AST performed at a current density equal or lower than 0.3 A/cm^2 will be included. It must be remembered that the current density and voltage level are “opposite” in a fuel cell, meaning that at a low or null current density level the fuel cell is giving the highest operating voltage range output. The following image (figure 33) illustrates the OCV decay due to degradation during a low current steady state AST.

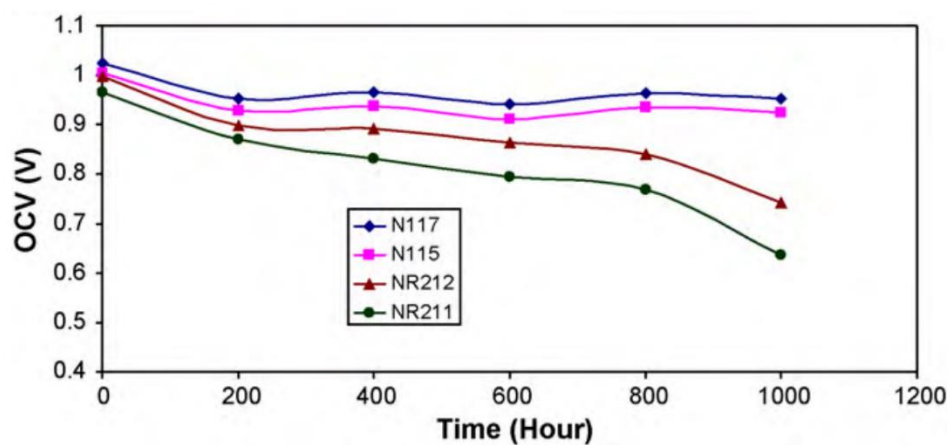


Figure 34. OCV voltage decay for four types of Nafion® membranes under a low current AST [71].

4. High Power. The opposite state to the previous is the high-power operating state, where the FC current density output is maximum, and therefore the power output which it delivers. In contrast to the low power condition, the high current density in this state generates a low voltage output as it is represented in any generic fuel cell polarization curve (see figures 9-11 and/ or 27). The high-power operation is found to deteriorate both the catalyst and the cell membrane, as it was introduced in chapter 1.4.2 [73, 74]. The fact that this regime is infrequent during the PEMFC lifetime complicates the task of finding AST degradation studies about this phenomenon which is located at a second level of priority behind all of the previous. However, some references can be found, and the criteria established for classifying an AST as a high power one is driving the PEMFC into a steady state operation for current densities equal or higher to $1 A/cm^2$.
5. Natural. The natural degradation is understood as the performance decay generated by every FC operation not included in all the previous and also the representation of the “natural” deterioration of the FC due to the pass of time, also leaving apart the previous types of operation. This is the least investigated class of PEMFC degradation and furthermore, taking into account the imposed requisites of: type of cell, membrane, catalyst and provided gasses for the nature of this study, no valid study has been found. Apart, as degradation source it also accounts for a small portion of the overall, therefore, it will be estimated as a ponderation of the degradation found in all the others together.

Registered data

With the selection requisites already defined, it must be also noted that up to this point it is still unknown which are the degradation source indicators that are furtherly being implemented into the degradation predictive model, therefore, the data compilation will include all the parameters considered to be relevant. Once the data compilation is finished, a decision based in various criteria already introduced, will be made in order to select the degradation indicators. The mentioned criteria for this selection are the following:

1. Relevance in the PEMFC degradation. As already seen, the main sources for PEMFC degradation are the membrane and catalyst. Therefore, ideally, the degradation indicators used in the predictive model should be a reliable reflect of the degradation at both structural elements.
2. Transferability into the polarization curve. This model is based on the polarization curve and the operating voltage calculation; therefore, it is essential that these degradation indicators are suitable to be incorporated to the polarization curve equations (table 2).
3. Extended presence in the set of references. Finally, it must be remembered that this model will work simultaneously but separately with each operating state. However, being the basis for all of them the same (table 2), the selected degradation indicators must be also the same for the four operating states and therefore, an extended presence within each operating state set of references will be fundamental.

The set of parameters found in the literature review are listed below (tables 7-10), where it is also indicated if the progression over the cell degradation of a certain parameter is included or not in the respective reference, showing schematically a table for each operating state before giving way to the final parameter's selection, which will be, as commented, the same for the four operating states.

Load cycling literature review						
Evolution during degradation of:		1 [48]	2 [50]	3 [52]	4 [53]	
Pt size	r_{Pt}	No	No	No	No	0
Membrane thickness	t_m	No	No	No	Yes	1
Hydrogen crossover	i_{H_2}	Yes	Yes	Yes	Yes	4
Fluoride release rate	FRR	No	No	No	No	0
Ohmic resistance	R_Ω	Yes	Yes	No	Yes	3
Mass transfer resistance	R_{mt}	No	No	No	No	0
Electronic resistance	R_{el}	Yes	No	No	No	1
ECSA	$ECSA$	Yes	Yes	Yes	No	4
Polarization curve evolution with time	$\delta_{deg}(t)$	Yes	Yes	Yes	Yes	4

Table 7. Compilation of found load cycling degradation indicators classified by reference.

Start-Stop literature review										
Evolution during degradation of:		1 [58]	2 [59]	3 [60]	4 [61]	5 [62]	6 [63]	7 [64]	8 [65]	#
Pt size	r_{Pt}	No	Yes	No	No	Yes	No	No	No	2
Membrane thickness	t_m	No	No	Yes	No	No	No	No	Yes	3
Hydrogen crossover	i_{H_2}	No	No	No	No	Yes	Yes	No	Yes	3
Fluoride release rate	FRR	No	No	No	No	No	No	No	No	0
Ohmic resistance	R_Ω	Yes	No	Yes	No	Yes	Yes	No	Yes	5
Mass transfer resistance	R_{mt}	No	No	No	Yes	No	No	No	No	1
Electronic resistance	R_{el}	Yes	No	Yes	Yes	Yes	Yes	No	Yes	6
ECSA	$ECSA$	Yes	Yes	Yes	Yes	Yes	Yes	Yes	Yes	8
Polarization curve evolution with time	$\delta_{deg}(t)$	Yes	No	Yes	No	Yes	Yes	No	Yes	5

Table 8. Compilation of found start stop degradation indicators classified by reference.

Low power/OCV literature review									
Evolution during degradation of:		1 [66]	2 [67]	3 [68]	4 [69]	5 [70]	6 [71]	7 [72]	#
Pt size	r_{Pt}	No	No	No	Yes	No	No	No	1
Membrane thickness	t_m	No	No	No	Yes	No	No	Yes	2
Hydrogen crossover	i_{H_2}	No	Yes	No	No	Yes	Yes	Yes	3
Fluoride release rate	FRR	No	No	No	No	No	No	Yes	1
Ohmic resistance	R_Ω	Yes	Yes	Yes	No	No	Yes	No	4
Mass transfer resistance	R_{mt}	Yes	No	No	No	No	No	No	1
Electronic resistance	R_{el}	Yes	No	No	No	No	No	No	1
ECSA	$ECSA$	No	Yes	Yes	Yes	Yes	Yes	Yes	6
Polarization curve evolution with time	$\delta_{deg}(t)$	Yes	Yes	Yes	No	No	Yes	Yes	5

Table 9. Compilation of found low power degradation indicators classified by reference.

High power literature review				
Evolution during degradation of:		1 [73]	2 [74]	#
Pt size	r_{Pt}	No	No	0
Membrane thickness	t_m	No	No	0
Hydrogen crossover	i_{H_2}	Yes	No	1
Fluoride release rate	FRR	Yes	Yes	2
Ohmic resistance	R_Ω	Yes	No	1
Mass transfer resistance	R_{mt}	No	No	0
Electronic resistance	R_{el}	No	No	0
ECSA	$ECSA$	Yes	Yes	1
Polarization curve evolution with time	$\delta_{deg}(t)$	Yes	No	1

Table 10. Compilation of found high power degradation indicators classified by reference.

Degradation source parameter selection

As stated before, three different criteria have been established in order to select the degradation indicators that will be furtherly implemented into the PEMFC degradation source predictive model. Based on each of them, the final selection is discussed below:

1. Relevance in the PEMFC's degradation. Regarding this criterion the degradation parameters must reflect consistently the membrane and catalyst degradation, being both the most relevant structural elements to be deteriorated along the FC lifetime.

Starting with the catalyst, the Platinum nanoparticles growth r_{Pt} shows (as explained in 1.4.1) one of the catalyst degradation mechanisms through the agglomeration of these particles into bigger ones, therefore, it accounts only for one part of the catalyst degradation. The other catalyst degradation indicator is the electrochemical active surface area ($ECSA$), which as exposed in 1.4.4. indicates the overall remaining active surface in the catalyst, therefore is an accurate reflect of its overall "health" state.

Going now into the membrane degradation, it is already known at this point that it suffers from chemical and mechanical degradation. The first one can be reflected through the ionic resistance increase (R_{ion}), which is included along with the electronic resistance (R_{el}) within the ohmic resistance R_Ω , which leads consequently to reject the second one in favor of the latter (R_Ω), which includes both. On the other hand, the membrane thinning (t_m) or the fluoride release rate (FRR) also indicate chemical degradation. So, to represent the chemical part, one or more of the last three indicators may be selected. Regarding the mechanical degradation, the hydrogen crossover current i_{H_2} is the only indicator available but also the most important. In an ideal case, two parameters should be selected for their use in the model, representing the membrane mechanical and chemical degradation.

Finally, the mass transfer resistance (R_{mt}), which represents the resistance for the gas concentration or transfer within the cell, cannot be clearly linked neither solely to membrane degradation nor to the catalyst degradation as also other structural elements, such as the carbon support or the gas diffusion layer, influence its decay. Therefore, for identification reasons, it must be rejected its use in the present study.

Therefore, regarding the first “purge”, the candidates according to it are: $ECSA$, R_{Ω} , t_m , FRR and i_{H_2} .

2. Transferability into the polarization curve. This criterion is clear and simple, if one degradation parameter is not transferable into the polarization curve model (table 2) it must be discarded. The $ECSA$ is directly represented in the activation losses term through the product of $a_c \cdot l_c$. The ohmic resistance R_{Ω} is included, at a high level, being the general term, which is multiplied by the current density for the activation losses equation (equation 1.14). The membrane thickness t_m is included in the previous, (equation 3.3) therefore is redundant and the ohmic resistance is selected instead to represent the membrane chemical degradation. Finally, the FRR can't be numerically included in the polarization curve, whereas the i_{H_2} can, (see figure 22), for this reason the latter will be selected to represent the membrane mechanical degradation. Up to this point: $ECSA$, R_{Ω} and i_{H_2} remain.
3. Extended presence in the set of references. This selection wouldn't make any sense if there weren't literature references in which experimental results from the previously selected degradation parameters were available. For this purpose, a meticulous classification of the data available at each literature reference for each operating state has been made. From the set of tables 7-10, it can be observed that $ECSA$, R_{Ω} and i_{H_2} have the most extended presence within all the references making it possible to develop the proposed model, in which all the four operating states will be using the same “platform”, and, therefore, the same degradation indicators. The fact that $ECSA$, R_{Ω} and i_{H_2} have been selected is not a major coincidence as, already introduced in chapter 1.4, these three indicators are highly relevant in the framework of PEMFC degradation, probably for reasons similar to the two previous criteria, among the ease to experimentally evaluate them. However, it must be noted by looking at table 10, that the minimum essential references containing these selected degradation source indicators have been found for the high-power condition, having only one reference for the ohmic resistance and the hydrogen crossover.

So, to summarize, the selected degradation indicators for the development of the PEMFC degradation source predictive model are: $ECSA$, R_{Ω} and i_{H_2} .

Linkage of the degradation parameters to the overall degradation

Once the polarization curve model is defined and calibrated and the degradation indicators already found in the literature and selected, is time to define the methodology which determines how everything is going to be integrated. The objective is giving a degradation source output value (amount of $ECSA$, R_{Ω} and i_{H_2}) for a certain FC performance loss, so, linking them as a progression which is function of the voltage degradation rate δ_{deg} , as stated in 1.4.5, is the best indicator to numerically define the percentage of FC performance loss.

Furthermore, as another relevant characteristic of this model which has not been detailed yet, the output result of the $ECSA$, R_{Ω} and i_{H_2} will be relative, which means that it will be given as a percentage. The reason for this is that this model is predictive, therefore the aim is to give a funded reference of what is being degraded within the cell structure under a certain operation, and in which grade it is happening, therefore, for this purpose, it has been decided that the best option is to give a relative output value of the degradation sources progression.

A representative image of this process is given below, where for a certain voltage degradation rate δ_{deg} , represented now graphically with the polarization curve, the model will be capable (previously given the share of overall degradation from each operating state in this application: %load cycling, %start stop, %low power, %high power and %natural) of giving an output percentage degradation of $ECSA$, R_{Ω} and i_{H_2} as a function of the pre-defined voltage degradation rate δ_{deg} .

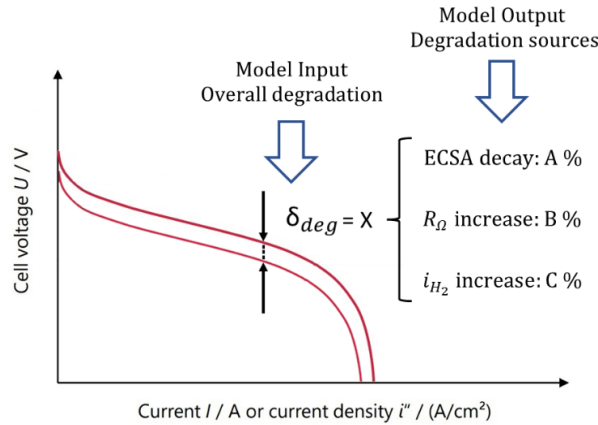


Figure 35. Representation of the linkage between overall and specific degradation.

This underlines the relevance of finding literature references which, apart from all of the previously explained regarding the FC operating states and the specific degradation indicators, also include a report of the polarization curve decay with the progression in time of the degradation experiment. The reader may perhaps be wondering why it is not sufficient with the final polarization curve after the whole degradation test, and there is a crucial reason for this. As the U.S. DOE establishes [24], FCV must pursue, in order to be competitive in the road transportation sector, a maximum of 10% FC performance loss after 8.000 hours which is equivalent to 150.000 miles of driving.

Therefore, to develop a literature reference based predictive degradation model capable of linking a certain overall degradation (δ_{deg}) to a certain specific degradation (% $ECSA$, % R_{Ω} and % i_{H_2}) it is fundamental to have a database which depicts this relation along the evolution of both the overall and the specific degradation at the same time, since this evolution is not linear, hence the final result is not enough to obtain an intermediate result. Giving a counterexample, if a certain reference only tells that for an overall degradation of the 30%, the final decay for $ECSA$, R_{Ω} and i_{H_2} is A%, B% and C%, it is not possible to know these last percentages at a degradation rate of the 10%. However, if the full evolution of the overall degradation from 0% to 30% is given along with the evolution of A, B and C, it will. This model will be focused on estimating the specific degradation at an overall performance loss of the 10%, as the U.S. DOE establishes it as the end of life (EOL) target for any fuel cell propelling a road vehicle.

With this arrives the final “purge” of the literature review, in which, every reference which does not include the overall degradation evolution with time $\delta_{deg}(t)$ will be rejected of being included into the model data. This evaluation is located in the last row of the tables 7 – 10. The remaining literature references after each single selection criteria presented above are resumed in the following table (table 11).

Operating State	Load Cycling	Start Stop	Low Power/ OCV	High power
References	[48, 50, 53]	[58, 61, 62, 63, 65]	[66, 71, 72]	[73]

Table 11. Final degradation literature references selection.

3.3.2. Integration of the literature degradation trends into the model

The subsequent step in the degradation model development is to “add” to the undegraded polarization curve calibrated model the new degradation parameters. As introduced in the chapter 1.4.4, the location of each parameter will be the following (see table 12).

$$U_{FC,deg} = U_{OCV} - U_{act} - U_{ohm} - U_{conc} \quad (3.12)$$

Term	Equation	Ref
Open Circuit Voltage	$U_{OCV} = \frac{\Delta G}{2F} - U_{loss}$	(3.13)
Activation losses	$U_{act} = \frac{RT}{2\alpha F} \ln \left(\frac{i + i_{H_2}}{i_{0,ref} a_c L_c ECSA \left(\frac{P_{O_2}}{P_{O_2,ref}} \right)^{\gamma_c} \exp \left[\frac{-E_{act}}{RT} \left(1 - \frac{T}{T_{ref}} \right) \right]} \right)$	(3.13)
Ohmic losses	$U_{ohm} = \frac{i t_m}{0.005139\omega - 0.00326 \exp \left[1268 \left(\frac{1}{303} - \frac{1}{273 + T_{FC}} \right) \right]} \cdot R_{\Omega}$	(3.13)
Concentration losses	$U_{conc} = c \ln \left(1 - \frac{i}{i_l} \right)$	(3.13)

Table 12. PEMFC polarization curve degradation model equations.

Their usage concept will be the following:

- Independent parameters. Once the model has been updated to the new degradation version, the three added parameters ($ECSA$, R_{Ω} and i_{H_2}) will act independently but contributing together to the voltage decay in the polarization curve through the increase or decrease trend found in the literature review for each of them and for a certain mix of operating states.
- Percentage parameters. They will numerically act as a percentage which, with null degradation will adopt the value of 1, and when progressing through the performance decay will increase as an added (in the case of R_{Ω} and i_{H_2}) or subtracted (in the case of $ECSA$) share which will be function of the degradation rate δ_{deg} .

$$ECSA' = \frac{100 - (ECSA \text{ decay}(\delta_{deg}))\%}{100} \quad (3.14)$$

$$R'_{\Omega} = \frac{100 + (R_{\Omega} \text{ increase}(\delta_{deg}))\%}{100} \quad (3.15)$$

$$i'_{H_2} = \frac{100 + (i_{H_2} \text{ increase}(\delta_{deg}))\%}{100} \quad (3.16)$$

3.4. FC Degradation model setup and calibration

The degradation model has already been defined at this point and also the literature references which will “feed” its database shaping the degradation trends ($ECSA$, R_{Ω} and i_{H_2}) that the model will predict. Hence, this chapter gives way to the degradation model setup and calibration, which will be completely different from the polarization curve model calibration as, this time, there won't be any reference for validation. The procedure will be purely numerical but, always trying to keep the consistency level of each decision and step as high as possible by keeping the results provided by the GA optimizer always within the limits identified from the literature review. Finally, it must be noted that for the simulation process, the genetic algorithm will still be used in the same way that it was when the polarization curve model calibration, but for a different purpose, which will be detailed below.

3.4.1. Reference data processing: setup of the degradation upper limits

Voltage degradation rate (δ_{deg})

One of the objectives within the final simulation process is to predict a certain degradation for a 10% δ_{deg} , which is the target established by the U.S. DOE as maximum acceptable performance decay for a FCV after 8.000h [24]. Even though the final purge applied to the literature references took into account the inclusion among its data of the detailed progression of the degradation rate along the AST development, the data provided in most cases won't coincide with this exact amount of degradation rate (10%). Alongside, it is important at this point to remember that the degradation rate is always being evaluated at $1 A/cm^2$. An example to better illustrate this discussion is given below:

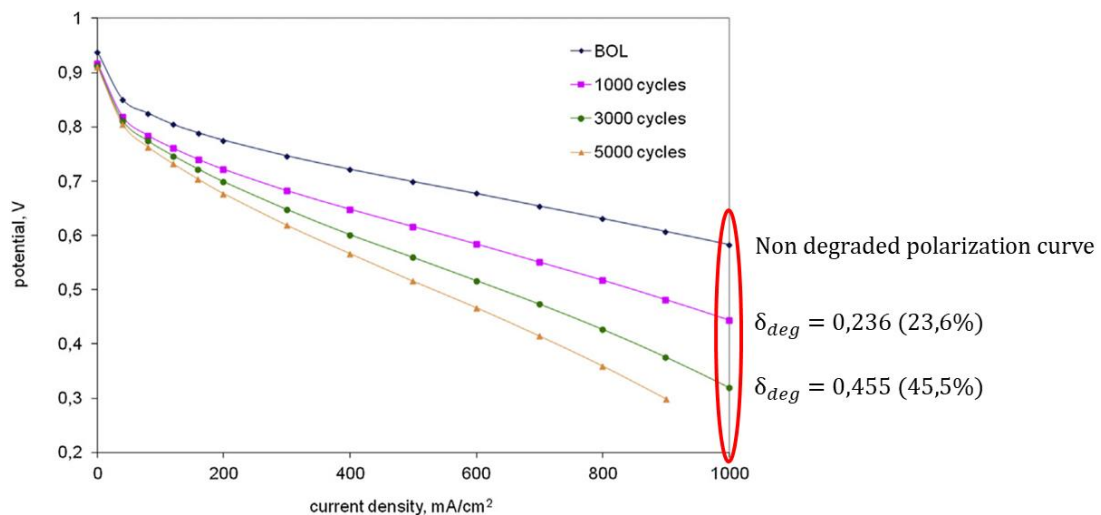


Figure 36. Example of data processing and identification form a degraded polarization curve plot.

The selected literature references, perform, at different points in time of their experimental degradation studies, intermediate cell evaluations analysing which is the new (degraded) polarization curve alongside with the state of the degradation parameters (tables 7-10). Thanks to this, the present study can be focused only on the most proximate level of degradation to the main target, the 10% of cell performance loss and degradation rate δ_{deg} . Logically, the ideal case

would be to have always the degraded cell evaluation at the point of interest (10%). However, the available references have other objectives in their studies and in most cases this level of degradation is not reported. In order to perform the most proximate approach, this study will always focus on the closest point to a δ_{deg} equal to 10%. Serving the previous figure (figure 36), an example of this situation, in which, the point recorded for being the closest to the objective will be 23.6%. Indeed, this is a limitation of this study, however, as will be seen in chapter 5.1, when reporting the final collection of degradation parameters extracted from the selected references, the dispersion of the data is high enough to make the just commented δ_{deg} deviation a minor issue.

It must be also noted, that as part of the methodology, in order to obtain an accurate data reading from the found polarization curves evolution like the shown in figure 36, an online plot digitalizer tool has been used to transform these figures into accurate numerical points [90].

Share of operating states (%LC, %SS, %LP, %HP, %NT)

Conversely, as part of the nature of this model in which each application is evaluated as a disaggregation into the different shares for each cell operating state, a further data treatment has been applied in order to weight it to the respective shares. This is a pure weighting process and directly depends on each FC application. The best way to understand it is through an illustrative representation of the process through a numerical example (figure 37):

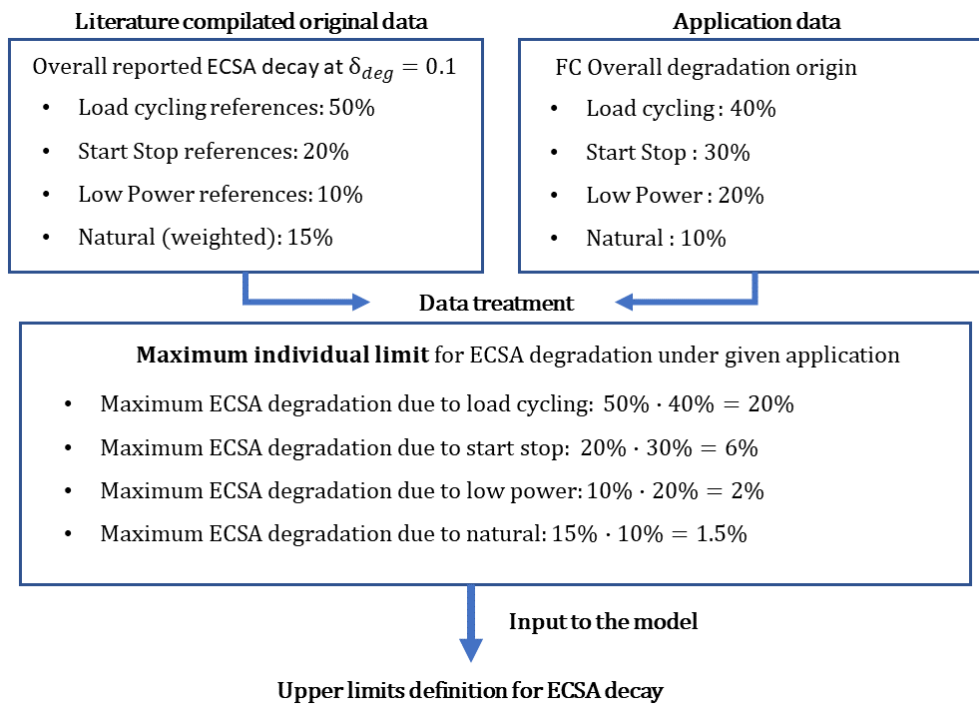


Figure 37. Example of literature data processing and weighting as a function of the FC usage at a certain application.

The previous example shown in figure 37, will be exactly applied for the three degradation source parameters $ECSA$, R_{Ω} and i_{H_2} . After this data adaptation, the model will already have defined the upper limits which will be transferred to the genetic algorithm. This latter, as will be explained in the model calculation process in 3.4.2, will try to find the best numerical solution for the degradation source prediction taking into account the overall voltage decay that has been previously determined along with the share of operating states.

3.4.2. Degradation source coefficients

Degradation source parameters linkage

The next step is part of a necessary procedure to obtain a linear (or at least, close to linear) progression in the degradation model simulations along with the progression of the overall voltage degradation rate δ_{deg} . Even though it was not part of the initial methodology, the nature of the genetic algorithm in its search for the most accurate mathematical solution often leads to a nonlinear progression of the degradation source indicators, which, from the physical point of view is not acceptable. This computation behaviour is not surprising however, as many times in coding, specific rules must be stated in order to avoid solutions that from the mathematical point of view are totally correct, but, conversely, lead to an inconsistent solution from the physical point of view, which is the case (see figure 38).

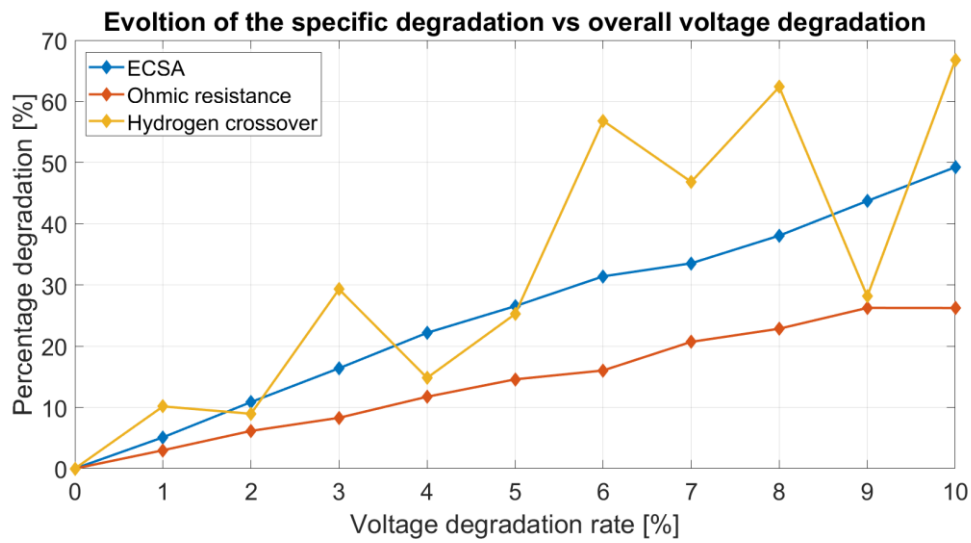


Figure 38. Example of high nonlinearities to be fixed in the degradation model.

In order to avoid these cyclic advance and retreat in some of the degradation source indicators, the progression of the three of them has been linked, always respecting each degradation source particular trend. The linking has been made around the value of the *EC*SA degradation, because of its extended presence at every operating state particular degradation (chapter 1.4.2) and its usual soft increasing trend found during the simulations. Therefore, the previously introduced model degradation parameters (3.14 - 3.16) are being modified in the same way:

$$ECSA'' = ECSA' \quad (3.17)$$

$$R''_{\Omega} = 1 + ECSA' \cdot R'_{\Omega} \quad (3.18)$$

$$i''_{H_2} = 1 + ECSA' \cdot i'_{H_2} \quad (3.19)$$

These change leads to the degradation coefficients definition which define, in turn, the trend of their own evolution in the model and also to the methodology used to define the degradation source parameters lower limits, which will be both conditioned by the just presented linkage between parameters.

Linked degradation source coefficients

According to the presented parameters linkage, a respective modification must be applied to the degradation source coefficient's upper limits with the aim reflecting the R_{Ω} and i_{H_2} degradation trend as they are now linked to *ECSA*, and consequently also to its respective trend. As commented when introducing the data treatment, the degradation coefficients from each FC operating state (load cycling, start stop, high power, low power and natural) must be weighted accordingly with the share of overall degradation that each of these states generate. Therefore, the following introduced procedure, will be applied equally for each of these operating states. This modification consists, as mentioned, of reversing the dependency of R_{Ω} and i_{H_2} to *ECSA*, therefore they will be multiplied by a factor which relates its own trend, with the *ECSA* trend.

After all the previously explained literature studies selection, degradation source parameters selection, data collection according to the degradation rate and weighting the degradation coefficients based on each operating state overall degradation share, a table like the following example remains for each of these states (table 13):

	ECSA decay [%]	Ohmic resistance increase [%]	Hydrogen crossover increase [%]
Reference 1	20	25	90
Reference 2	50	15	50
Reference 3	30	30	80
Reference 4	25	30	80
Minimum	20	15	50
Average	31.25	20	75
Maximum	50	30	90

Table 13. Example for a degradation result table for a certain operating state.

Once this final table is made up, the windows which define the degradation maximum and minimum level at voltage degradation rate of the 10% are already defined. However, due to the parameter linkage made to avoid nonlinearities, these limits are not directly been transferred to the model algorithm without a last conversion. These conversion aims to unlink these parameters and put them (R_{Ω} and i_{H_2}) back into their own trend. To perform this reversing process, a factor relating both maximum values (*ECSA* and R_{Ω} on one side, and *ECSA* and i_{H_2} on the other side) is created. The coefficients remaining after applying this operation will be the upper limit for the resistance and hydrogen crossover degradation. The following equations (3.20 – 3.22) represent this conversion through and example, continuing with the previous shown in table 13.

$$ECSA'' \text{ model upper limit} = \text{Maximum ECSA decay} = 50 \text{ (Example)} \quad (3.20)$$

$$R_{\Omega}'' \text{ model upper limit} = \frac{\text{Maximum } R_{\Omega} \text{ increase}}{\text{Maximum ECSA decay}} = \frac{30}{50} \text{ (Example)} \quad (3.21)$$

$$i_{H_2}'' \text{ model upper limit} = \frac{\text{Maximum } i_{H_2} \text{ increase}}{\text{Maximum ECSA decay}} = \frac{90}{50} \text{ (Example)} \quad (3.22)$$

With all the previously explained measures and adjustments the PEMFC predictive degradation source model calibration concludes. However, the same parameter used for the undegraded model calibration and validation the \overline{RMSD} , will be used in order to compare, point by point, the output degraded polarization curve, with a generic degraded curve provided from [23]. This generic degraded curve segregates the voltage degradation rate at $1 A/cm^2$ to the full current density range creating a full polarization curve with which the present model (or any other) can be numerically compared through the \overline{RMSD} value, which final result will be given in the results section, chapter 4.2.

The distribution along the current density range of a 10% degraded polarization curve, which as stated is, is based on the current density point of $1 A/cm^2$, is spread to the rest of the curve according to the following (figure 39) [23].

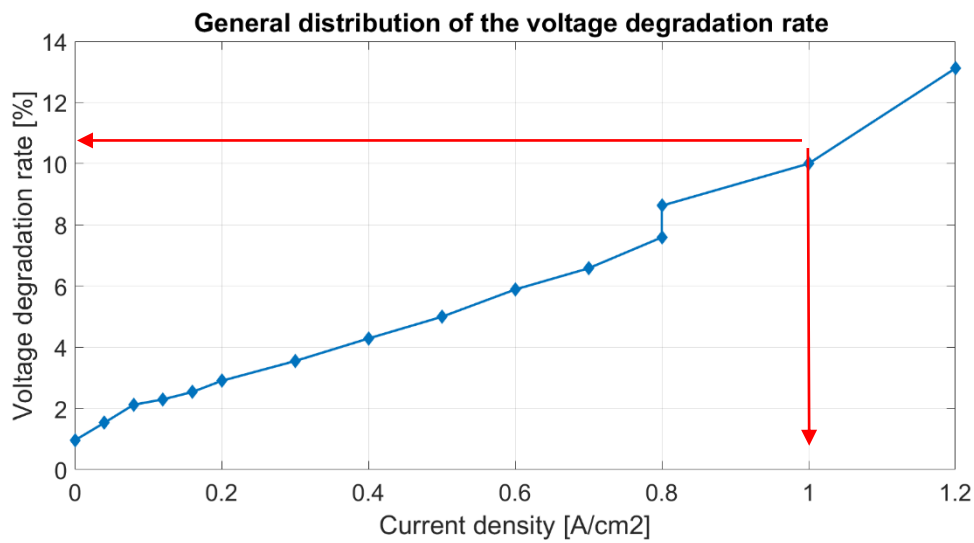


Figure 39. Distribution of the voltage degradation rate along a full polarization curve [23].

3.5. Full model simulation process

The objective of this subchapter is to summarize the full simulation procedure through a simple sequence of all of the previously explained in detail steps to facilitate their comprehension. Starting from the point of having the degradation model defined and calibrated, and the literature reference's degradation data already classified and registered according with the information that has already been given. Up to this point, every relevant part of the methodology has already been presented, except for some limitations which influence the simulation process and will be explained in the next and final chapter of the methodology (chapter 4.6).

The simulation steps are being divided into model inputs (direct and indirect), model processing and model outputs.

Model inputs

The model inputs will be divided in two groups: direct and indirect inputs.

- Direct inputs. FC operating temperature and pressure. Degradation rate level which is desired to reach δ_{deg} . Share of the overall degradation associated to each operating state (load cycling, start stop, low power, high power and natural) for a certain application.
- Indirect inputs. Each operating state has its respective table containing the degradation source data compiled from the literature review, as shown in table 13, which will be modified. Depending on the above commented direct inputs, each of these tables will be weighted according to the share of each operating state in the overall degradation. After this, the degradation source coefficient and limits will be defined as shown in figure 37 and equations 3.20 – 3.22.

Both inputs will be provided to the degradation model which will be ready to be launched.

Model processing

The model will execute the calculation based on the degraded polarization curve equations shown in table 12, and by applying the degradation coefficients for $ECSA$, R_{Ω} and i_{H_2} will search for a certain value for each of them. Through the \overline{RMSD} calculation the genetic algorithm (GA) will compare, point by point, the degraded model curve with a reference degraded polarization curve whose degradation rate distribution has been presented in figure 39. Therefore, the GA will be looking for a set of values for the three degradation indicators which minimize the deviation from the reference curve within the established upper limits and respecting the degradation trends for $ECSA$, R_{Ω} and i_{H_2} . After the whole calculation process performed by the GA, which was shown in figure 29, the model will reach the end of the execution and a final solution for the three degradation indicators.

Model outputs

It must be taken into account that this model will perform sequentially the explained set of steps in "model processing" for each operating state. This means that it will start applying the previous procedure for the most relevant (in overall degradation weight) operating state. The degraded $ECSA$, R_{Ω} and i_{H_2} outputs from the first iteration will be the inputs for the second one, repeating the same procedure for the second most important operating state in the overall degradation.

Subsequently, this process will continue up to the last operating state causing cell degradation, until the 100% of the total share which produces degradation has been calculated.

The final result of the simulation will be the evolution of $ECSA$, R_{Ω} and i_{H_2} from null degradation ($\delta_{deg} = 0$) up to the 10% of performance loss ($\delta_{deg} = 0.1$) under the given share of operating states causing degradation, therefore, the information will be suitable to be plotted in three curves ($ECSA$, R_{Ω} and i_{H_2}) as a continuous progression along de performance decay. These results, together with the \overline{RMSD} value (as a consistency indicator) will be shown for a heavy-duty transport application with high FC to battery dynamics in the results section (chapter 5).

A schematic diagram of the full model simulation process is shown below to better illustrate the most relevant steps that have been here presented (figure 40).

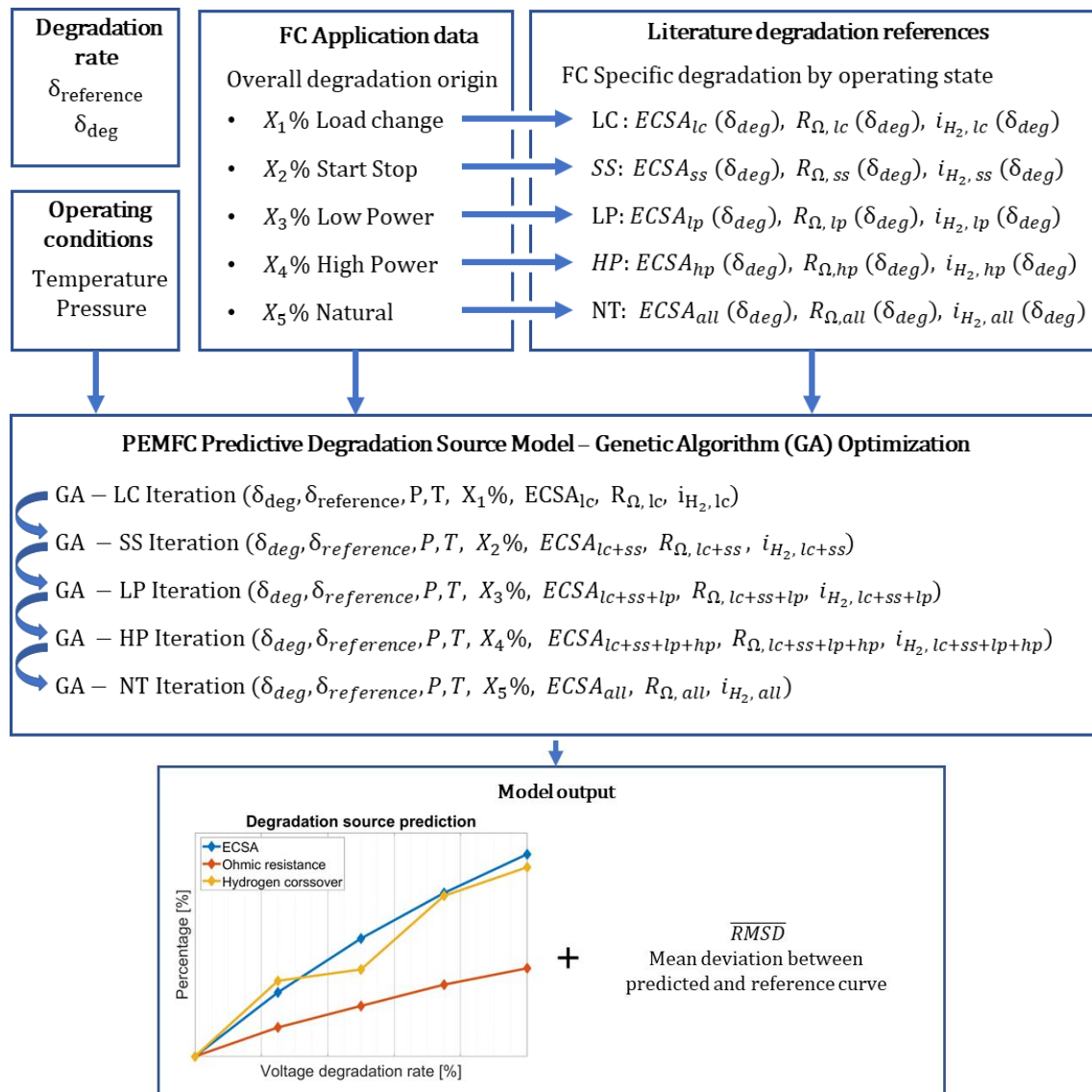


Figure 40. Diagram representing schematically the model inputs, processing and outputs.

3.6. Degradation model limitations

To conclude with the methodology of this master's thesis some of the main limitations of this model are being exposed.

The first and most evident limitation is that there is no possible reference to validate this model, since typically, the major part (if not all of them) of the PEMFC degradation predictive models developed up to date are focused on the overall degradation, instead of the degradation sources, which is the objective of the present. Therefore, the fact of developing a predictive degradation model which aims to go further and deeper in the degradation origin has implicit not having any possible reference (at least, it has not been found despite the deep literature review made in this matter) to validate it to a similar one. However, the developed degradation model is based on experimental trends and each of the methodology steps has been performed within the same framework as the analyzed literature studies. Moreover, it is important to be conscious that this model does not pretend to be precise due to the lack of literature data, but to bring predictive information of which are the most degraded MEA components.

The second limitation is the reference data available. First, starting by the quantity available, even though several studies have been found for the main FC operating states, the more references founded, the more consistent the degradation coefficients and limits would be. Second, the amount of available data at each of them. As the focus of this study is finding out the degradation sources at an overall voltage degradation of the 10%, having more datapoints in the reference's degradation curves would allow to collect more accurate data around this pursued amount of voltage degradation (10%).

Finally, the last limitation is a more specific one, and also more complex to explain. It is related to the nature of the model design and mathematical evaluation, which, as is established as sequential along the progression of the overall degradation, when reaching the last steps, the accuracy of the model is progressively reduced. This fact has led, as will be seen and further explained along with the results in the chapters 4 and 5, to the combination of the two operating states with less weight in the overall voltage degradation distribution.

4. Calibration of the predictive degradation model

Along this chapter the model setup and calibration results are presented. Starting with the identified degradation source limits from the literature review, to give way to both calibration results: the PEMFC polarization curve undegraded model, and the PEMFC degradation predictive model.

4.1. Degradation Limits identification

The following results correspond to the degradation source levels ($\%ECSA$, $\%R_{\Omega}$ and $\%i_{H_2}$) found in the literature review for exclusively one operating state, which means, how the PEMFC would be degraded if its operation state would be each of the following.

Full degradation by load change				
Reference [#]	DV point [%]	ECSA loss [%]	Ohmic resistance increase [%]	Hydrogen crossover increase [%]
1 [48]	23.6	53	20	0
2 [50]	4.6	28.1	3.5	0
3 [53]	7	Unknown	14	Unknown
Maximum	23.6	28.1	3.5	0
Average	11.7	40.6	12.5	0
Minimum	4.6	53	20	0

Table 14. Literature review degradation source coefficients identification for load cycling condition.

As shown in table 14, the decay of the degradation source selected parameters indicates a severe $ECSA$ loss, a moderate R_{Ω} increase and a neglectable i_{H_2} increase. This degradation pattern fits with the stated in 1.4.2, were the theoretical degradation promoted by a pure load cycling operation mainly affects the catalyst, and at a second level the membrane, but for the latter only promoting chemical degradation and not mechanical, therefore affecting R_{Ω} and not i_{H_2} .

Full degradation by start-stop				
Reference [#]	DV point [%]	ECSA loss [%]	Ohmic resistance increase [%]	Hydrogen crossover increase [%]
4 [58]	19.7	30	35	Unknown
5 [61]	21.5	79	26	Unknown
6 [62]	15.6	25.6	3	Unknown
7 [63]	15	50	0	0
8 [65]	15.5	64	0	0.36
Maximum	21.5	25.6	35	0.36
Average	17.46	49.72	12.8	0.18
Minimum	15	79	0	0

Table 15. Literature review degradation source coefficients identification for start stop condition.

The start-stop specific degradation reported in the literature references has a similar pattern to the reported for the load cycling degradation source, however, as stated in 1.4.2, the mechanisms which promote it are different, being the main cause in this case the high cathode potential generating high carbon support corrosion.

Full degradation by low power/ OCV				
Reference [#]	DV point* [$\mu V/h$]	ECSA loss [%]	Ohmic resistance increase [%]	Hydrogen crossover increase [%]
9 [66]	547	Unknown	59	Unknown
10 [71].1	260	0	32	Unknown
11 [71].2	180	0	32.1	1068
12 [71].3	90	0	41	Unknown
13 [71].4	90	0	22.2	Unknown
14 [72]	491	5	Unknown	500
Maximum	547	5	59	1068
Average	276.33	1	37.26	784
Minimum	90	0	22.2	500

Table 16. Literature review degradation source coefficients identification for low power/ OCV condition.

The degradation trend for low power or idling condition is completely different to the two previous, being neglectable for the catalyst and extremely severe for the membrane. Again, the reported results from the literature references fit with the theoretical degradation discussed in 1.4.2. As can be observed, i_{H_2} increases bigger than 1000% have been reported, which have its origin in the membrane mechanical degradation, on the other hand, serious mechanical degradation also occurs as can be seen with the R_{Ω} increase. *It must be noted that for this operating condition the voltage degradation is usually measured as voltage loss per time, therefore, the availability of the voltage degradation rate typically used for the rest of operating states is not reported for this type of steady state AST's.

Full degradation by high power				
Reference [#]	DV point [%]	ECSA loss [%]	Ohmic resistance increase [%]	Hydrogen crossover increase [%]
15 [73].1	6	30	0	0
16 [73].1	15.3	42	0	0
Maximum	15.3	42	0	0
Average	10.8	36	0	0
Minimum	6	30	0	0

Table 17. Literature review degradation source coefficients identification for high power condition.

Regarding the high-power condition few references can be found in the literature, as this type of FC operation is infrequent as has been already discussed. However, fortunately, at least one was found giving the voltage degradation rate, and therefore, it has been possible to incorporate it into the degradation source "data base". Again, as expected, the experimental reported degradation matches the theoretical one, with a relevant degradation in the FC catalyst and the subsequent ECSA loss.

Degradation references' operating conditions

As repeatedly commented along this text, the temperature and humidity state are fundamental for a good membrane performance and therefore durability during the PEMFC lifetime. This study is focused on the low temperature variant of the PEMFC, which typically operate at temperatures (T) in the range of 70°C to 80°C for an ideal membrane water content and therefore proton conductivity. This model has been calibrated and validated for having good sensitivity in this temperature range, therefore, it is fundamental that also the literature references employed to develop the degradation model have made their experimental studies under similar conditions. Analogously, the relative humidity (RH) is also a relevant parameter in PEMFC operation ensuring an optimal ionic transport and the durability of the membrane, and ideally should be in the upper percentage range.

Through the following figures, both the RH and T operating conditions are shown for each of the selected degradation literature references for the model development. The average for each of these magnitudes are $RH = 86\%$ and $T = 72^\circ\text{C}$ (345 K) as shown with the black lines.

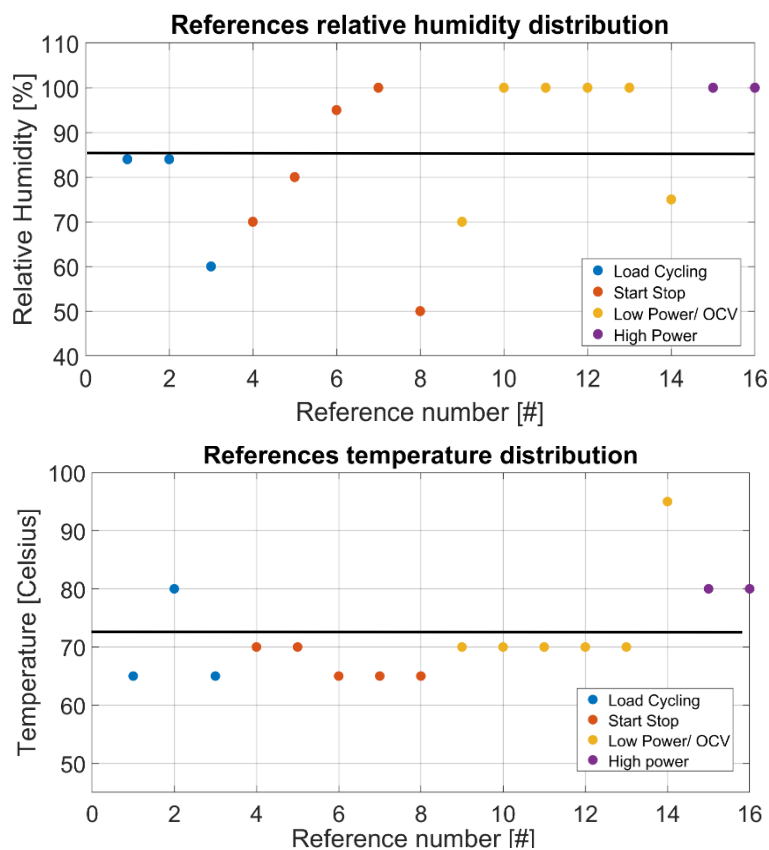


Figure 41. Temperature and relative humidity distribution for the selected degradation literature references.

4.2. Calibration results

In this chapter both model calibration results will be presented, along with the validation (in the case of the FC polarization curve model) to the experimental references. A good model calibration is fundamental for a good consistency, as this model mathematically imitates a real physical and electrochemical behaviour, therefore, even though the employed equations (table 2 and 12) are well theoretically funded, a further adjustment is necessary to reach a better approach to the real phenomenon which drives the FC operating voltage definition.

4.2.1. FC Polarization curve model calibration and validation

As detailed in section 3.2, the polarization curve model calibration consists of the mathematical evaluation of a genetic algorithm (GA) optimization tool, which through the \overline{RMSD} calculation numerically compares the model against experimental curves (figure 27, [23, 85, 86]) at different pressures (1.3/ 2.5 bar) and at the LT-PEMFC operating temperature (346 K), to optimize the value of different parameters and reach the best fit between model and reference. The GA will have seven degrees of freedom through the variable parameters shown in the table below (table 18), which limits have previously been defined based in a literature review to ensure the physical consistency of the values within the defined limits [38, 79-84].

After all, the final values for these seven parameters which allow the best fit between the model and the experimental references are the following:

Parameters and coefficients to optimize for calibration			
	Nomenclature	Limits	Final value (GA)
α	Charge transfer coefficient	(0.46, 0.54)	0.46107
ACT	$I_{0,ref} \cdot a_c \cdot l_c$	(1^{-9} , 1^{-3})	$2.916 \cdot 10^{-5}$
γ_c	Pressure dependency coefficient	(0.5, 1.45)	1.45
w	Membrane water content	(4.1, 14.003)	12.29
i_l	Limiting current density	(1.44, 2.4)	2.4
C	Concentration loss coefficient	(0.0001, 5)	$1.381 \cdot 10^{-4}$
U_{loss}	Voltage deviation between standard conditions and OCV	(0.1893, 0.2893)	0.243
\overline{RMSD}			$4.96 \cdot 10^{-3}$

Table 18. Result for the polarization curve model calibration.

As can be observed, the \overline{RMSD} value accounts for $4.9559 \cdot 10^{-3} V$, which is, less than 5 mV. This means that the average root mean squared deviation between the model and the two experimental references at high and low-pressure polarization curves, point by point, is 5 mV. This low deviation proves the quality of the model calibration being properly sensitive to pressure changes (1.3/ 2.5 Bar) at an operating temperature of 346 K. It must be also noted that this latter, is practically the same as the average experimental temperature found in the degradation source references (figure 41), which is 345 K (72°C), thus facilitating the model match with the degradation source experimental data found in the literature.

To validate the presented calibration, the model will be updated with the seven values shown in table 18. After that, the double-validation can be performed by defining the same temperature, pressure and current density points for the model and each experimental curve. The result is plotted in the following figure (figure 42). The model and the experimental polarization curves at both P -T states share the same tendency, as can be observed, and as the \overline{RMSD} value from the calibration already advanced (5 mV).

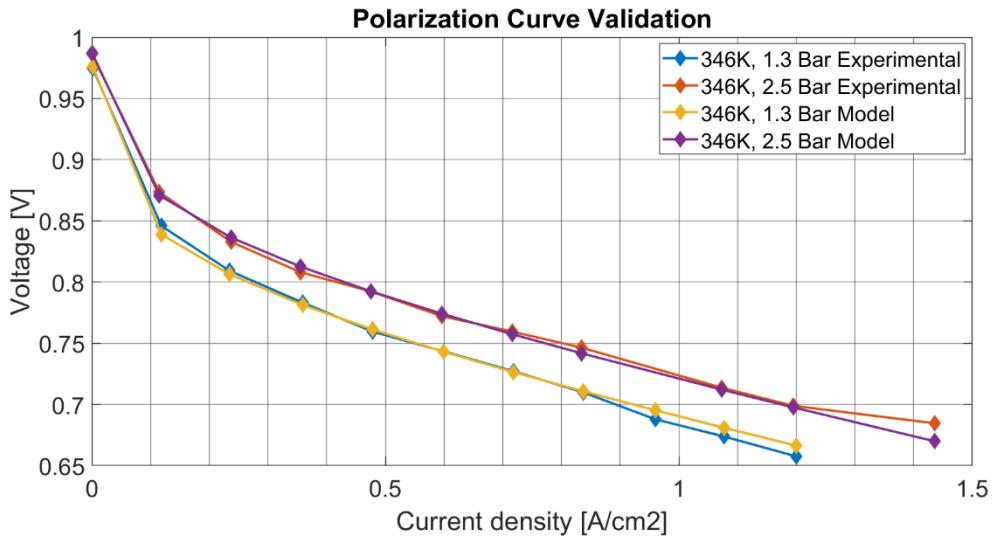


Figure 42. Comparison between model and experimental data polarization curves after calibration.

4.2.2. FC degradation model calibration

As detailed in 3.4, the FC degradation model calibration consists mainly of eliminating nonlinearities along with the degradation prediction progress as the overall voltage degradation increases. Furthermore, on processing the data trends found in the literature according to the shares of overall degradation caused by each operating state, which depend on the application. Finally, after the data processing according to the mentioned shares of these operating states, the degradation limits and coefficients are being defined according to the equations 3.17 – 3.22. As a further step, the integration of the natural degradation trend will also be part of the results presented in this chapter as it is part of the FC degradation model calibration.

The following tables present the final degradation limits and coefficients that are transferred into the model. As shown in figure 40, the model will evaluate sequentially each degradation source according to its weight in the overall degradation, therefore the genetic algorithm will evaluate progressively each of them, being the input for a certain operating state, the output from the previous.

In the following tables, the calibrated coefficients of a given share of operating states will be presented along with some applied measures to improve the model performance. The share of operating states overall degradation corresponds to the application analyzed in this master’s thesis, which is a heavy-duty transport vehicle with a FCReX powertrain, which will be further detailed in chapter 6. The distribution of its overall degradation, provided by [23] is the following: 67.64 % from load change, 21.08 % from start stop, 5.39 % from low power, 5.86 % from natural degradation and 0.016 % from high power. For simplicity reasons, in the following tables, they will be assumed to be 68%, 21%, 5%, 6% and 0%, respectively, however it must be taken into account that in the model these shares have been considered with its total accuracy (10^{-15}).

68% Degradation by load change				
Reference [#]	DV point [%]	ECSA loss [%]	Ohmic resistance increase [%]	Hydrogen crossover increase [%]
1 [50]	4.6	28.1	3.5	0
2 [51]	23.6	53	20	0
3 [53]	7	Unknown	14	Unknown
Maximum	23.6	28.1	3.5	0
Minimum	4.6	53	20	0

Table 19. Final load change limits for the predictive degradation model.

Even though weighting the literature references’ degradation is the methodology which drives its application and integration into the model an important remark must be made regarding it. The intention with this is to transfer into to the model the operating state distribution in the overall degradation for a certain application, however, the model itself has the last word. What is meant to explain with this is that exact weightings from each operating state are being introduced in the model, however, it must be considered that the dispersion in the degradation data found for each operating state and then transferred into the model is considerably high. This high dispersion implies that defining now very exact shares and limits may not drive to the solution that the model aims to predict, and therefore, weighting the degradation data strictly

is not supposed to be an exact matter, but just an approximation of the degradation trends for each operating state. Finally, it must be also taken into account that what really drives the model predicted trend is the relation between $ECSA$, R_{Ω} and i_{H_2} through the equations that are being shown down below. These relations and coefficients will remain the same no matter any percentage change is applied, as it will affect all the three degradation sources in the same way and therefore the ratios between them will remain constant.

After this brief, but essential discussion, the final results from load cycling can be commented. For the given application, the load change degradation source limits were all reduced by a 30% (resulting the 68% of their original value). However, it was found that the model, for the correspondent overall voltage degradation of this 68% was trying to go further than the established degradation source limits, saturating its values to the limits before even reaching the final overall degradation level. For this reason, and according to which has been discussed in the previous paragraph, the load change weighting (only from the degradation source part, not from the overall part) was left to be the 100% of the data found in literature, therefore table 19 has been unaltered.

The relation between the degradation source coefficients, which must be remembered that is independent from any weighting as they preserve their ratios, is the following. These are the coefficients that will be transferred to the genetic algorithm for the degradation source prediction.

$$R_{\Omega,LC} \text{ coefficient} = \frac{Max R_{\Omega,LC}}{Max ECSA_{LC}} = \frac{20}{53} = 0.377 \quad (3.21)$$

$$i_{H_2,LC} \text{ coefficient} = \frac{Max i_{H_2,LC}}{Max ECSA_{LC}} = \frac{0}{53} = 0 \quad (3.22)$$

21% Degradation by start stop				
Reference [#]	DV point [%]	ECSA loss [%]	Ohmic resistance increase [%]	Hydrogen crossover increase [%]
4 [58]	19.7	5.76	6.72	Unknown
5 [61]	21.5	15.17	4.99	Unknown
6 [62]	15.6	4.91	0.57	Unknown
7 [63]	15	9.6	0	0
8 [65]	15.5	12.28	0	0.07
Maximum	21.5	23.07*	10.22*	0.11*
Minimum	15	5.76	0	0

Table 20. Final start-stop limits for the predictive degradation model.

The next operating state producing overall degradation for the given application is the start stop condition. The weight was defined by [23] to be a 21%, however, in a similar way that for load change, the model was asking for higher upper limits, therefore it was finally increased by an extra 10%. This increase is reflected in the set of maximum* values for ECSA loss, ohmic resistance increase and hydrogen crossover increase.

Again, it is remembered that this change does not affect the degradation distribution among the three sources ($ECSA$, R_{Ω} and i_{H_2}) because this adjustment is applied equally to all of them, therefore the degradation coefficients transferred into the GA do not change, and the model predicted degradation trend will remain unaltered, only its upper limits are being modified to avoid premature saturation.

$$R_{\Omega,SS} \text{ coefficient} = \frac{Max R_{\Omega,SS}}{Max ECSA_{SS}} = \frac{10.22}{23.07} = 0.443 \quad (3.21)$$

$$i_{H_2,SS} \text{ coefficient} = \frac{Max i_{H_2,SS}}{Max ECSA_{SS}} = \frac{0.11}{23.07} = 0.00476 \quad (3.22)$$

5% Degradation by low power/ OCV				
Reference [#]	DV point* [$\mu V/h$]	ECSA loss [%]	Ohmic resistance increase [%]	Hydrogen crossover increase [%]
9 [66]	547	Unknown	2.95	Unknown
10 [71].1	260	0	1.6	Unknown
11 [71].2	180	0	1.61	53.4
12 [71].3	90	0	2.1	Unknown
13 [71].4	90	0	2.95	Unknown
14 [72]	491	0.25	Unknown	25
Maximum	547	0.5*	5.9*	106.8*
Minimum	90	0	1.6	25

Table 21. Final low-power/ OCV limits for the predictive degradation model.

The application weight for the low power/ OCV overall degradation is a 5%, and, analogously to the two priors, the model “claims” for a higher degradation limit, it is increased by an additional 5%, reaching therefore the 10% of weight if comparing to a full low power degradation (table 16). This correction is again applied only to the degradation sources maximums*.

$$R_{\Omega,LP} \text{ coefficient} = \frac{Max R_{\Omega,LP}}{Max ECSA_{LP}} = \frac{5.9}{0.5} = 11.8 \quad (3.21)$$

$$i_{H_2,LP} \text{ coefficient} = \frac{Max i_{H_2,LP}}{Max ECSA_{LP}} = \frac{106.8}{0.5} = 213.6 \quad (3.22)$$

0.0158% Degradation by high power				
Reference [#]	DV point [%]	ECSA loss [%]	Ohmic resistance increase [%]	Hydrogen crossover increase [%]
15 [73].1	6	0.0008	0	0
16 [73].1	15.3	0.0067	0	0
Maximum	15.3	0.0067	0	0
Minimum	6	0.0008	0	0

Table 22. Final high-power limits for the predictive degradation model.

Finally, even though it has been neglected due to its negligible impact on the overall voltage degradation; the high-power degradation shares and final values are presented in table 22. This extremely low percentage summed up to the reason that the model simulates progressively each operating state by overall weight, leads to the situation of having a neglectable amount of degradation source remaining to be incorporated, with the fact that the model losses accuracy as it reaches the final portions of degradation. Therefore, it is not suitable with this model to consider such low values.

Also, for the commented reason, regarding that the model losses accuracy when reaching the final percentages of degradation, which is no more than completing the full overall degradation (10 %) with the increase of the degradation sources EC_{SA} , R_{Ω} and i_{H_2} according to their trends and weights for each operating state (LC, SS, LP, HP, NT), a further adaptation is made to integrate the natural and low power degradation. Both of these operating states generate together, as introduced, the last 11% of degradation for this application (from 89% to 100%), therefore, to avoid nonlinearities due to accuracy loss of GA at this last stage both have been combined into one. This means that instead of simulating the 5% for low power and then the 6% for natural, both degradation tendencies have been combined and has been simulated as an 11% combining both weights.

To perform this adaptation, the results of the first 89% of degradation are needed, since, as already discussed in this text, the natural degradation trend is composed of a mix of the previous ones, which in this case, from 0% to 68% will be load cycling, and from 68% to 89% will be load cycling + start stop. Therefore, the previously presented methodology will remain the same, with the difference that the natural degradation data instead of coming from literature references will come from the 89% of the predicted degradation. After this, the new natural degradation trends will be reduced to the 6% (according to its weight for this application) and will be added to the 5% from low power, shown in table 21. With this, the last 11% (from 89% to 100%) of the degradation prediction is simulated as the last calibration step of the model.

The following chapter (chapter 5) will present the final degradation source prediction results for a road transport heavy-duty application with the subsequent analysis.

5. Analysis of the ECSA, Ohmic Resistance and Hydrogen Crossover degradation for heavy-duty transport applications

The final degradation source results given by the PEMFC degradation predictive model are presented and analysed in the present chapter. As stated at the end of the FCV introduction (chapter 1.2) the aim of this master's thesis is to develop a predictive tool capable of identifying the degradation source trends at the overall performance decay of 10% (established by the U.S. DOE [24] as a target) applied to the FCREx technology proposed and investigated by R. Novella and M. López Juárez [20-23].

The FCREx architecture consists of a battery electric vehicle with a fuel cell system integrated acting as a range extender, which has the objective of maintaining stable the battery state of charge (SoC) and therefore extending the vehicle range before a recharging stop is needed. This interaction between FC and battery has different dynamic levels which are referred to the FC response to the battery SoC loss during operation. High FC-battery dynamics implies a rapid FC response to feed back in the "lost" electric energy from the battery, therefore, the FC usage tends to be more aggressive and dependent in time of the energy extracted from the battery, which, at the same time is dependent of the vehicle type of driving. Conversely, a low dynamic relation between both leads to a slower energy transfer from the FC to the battery, leading to higher share of time under high load due to the slower energy transfer.

In the following figure (figure 43) the current density shape of a FCREx under three levels of FC-battery dynamics is represented for a heavy-duty diesel truck driving cycle. As has been briefly discussed, high dynamics ($0.1 A/cm^2s$ in this case) drive the FC to fast and aggressive responses, and as this dynamic level gets lower ($0.01 A/cm^2s$ and $0.001 A/cm^2s$), this response gets smoother and slower, leading to a load delay if comparing with high dynamics.

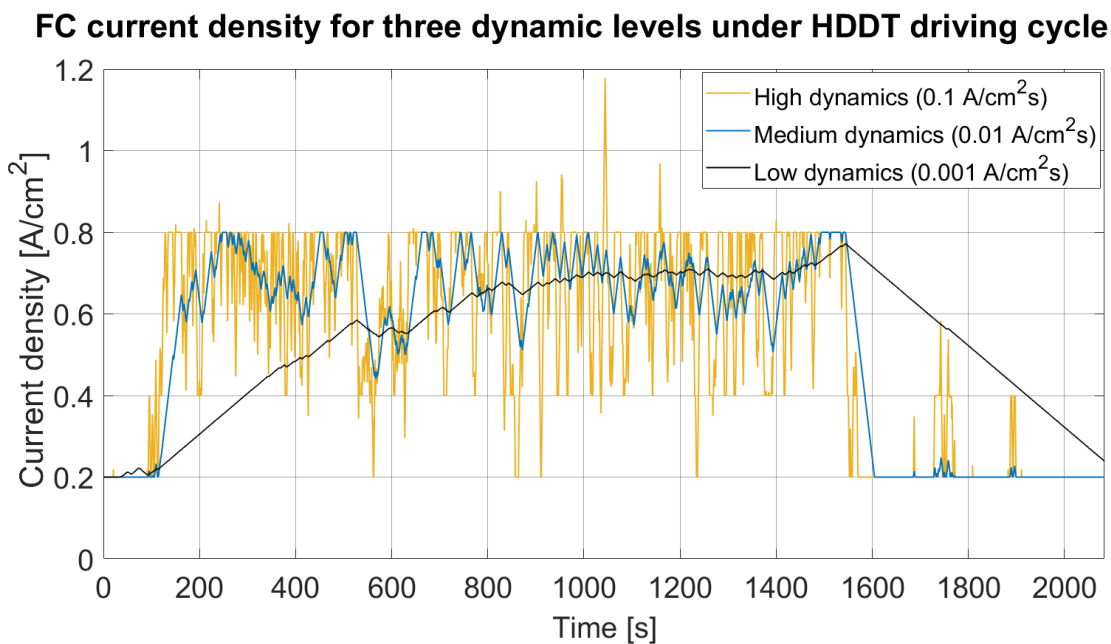


Figure 43. Three levels of FC to battery dynamics for a FCREx heavy-duty application [23].

The application considered in this master's thesis corresponds to the highest dynamics profile ($0.1 A/cm^2 s$) of the three shown above (figure 43). As can be observed, changes in these dynamics severely affect the FC degradation source distribution along the cycle, being for example very easy to identify that the main degradation source under the high dynamics' operation is load cycling. This operating state distribution gives way to introduce the degradation source distribution shown in the following figure (figure 44).

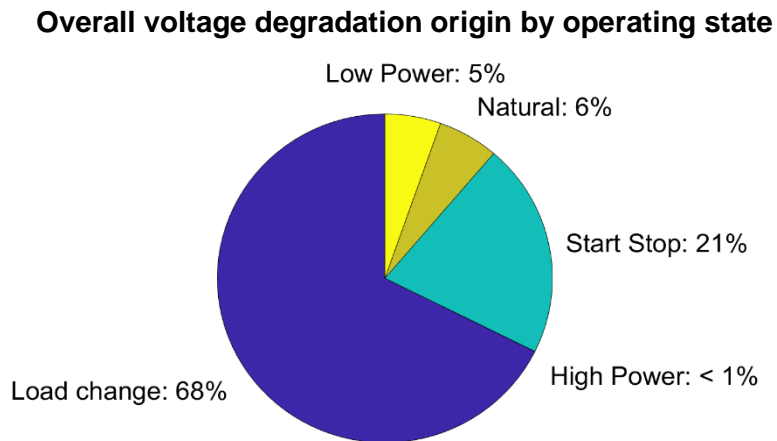


Figure 44. Overall degradation distribution by operating source for heavy duty – high dynamics operation.

It must be remarked that the overall PEMFC degradation origin distribution by operating state is not equal to the time distribution of the cell operation under these states. The reason is simple, each of them, as has been deeply discussed in chapter 1.4.2, generates different amounts of degradation to the cell, and with different origins (membrane or catalyst, for example). Therefore, what is being shown in figure 43 is the share for which each operating state is responsible of the overall performance decay generated in the PEMFC, which is the key application input for the developed model by this master's thesis.

Once this has been properly defined and after applying the fully presented methodology, the simulation is launched, and the following results are obtained (figures 45-47):

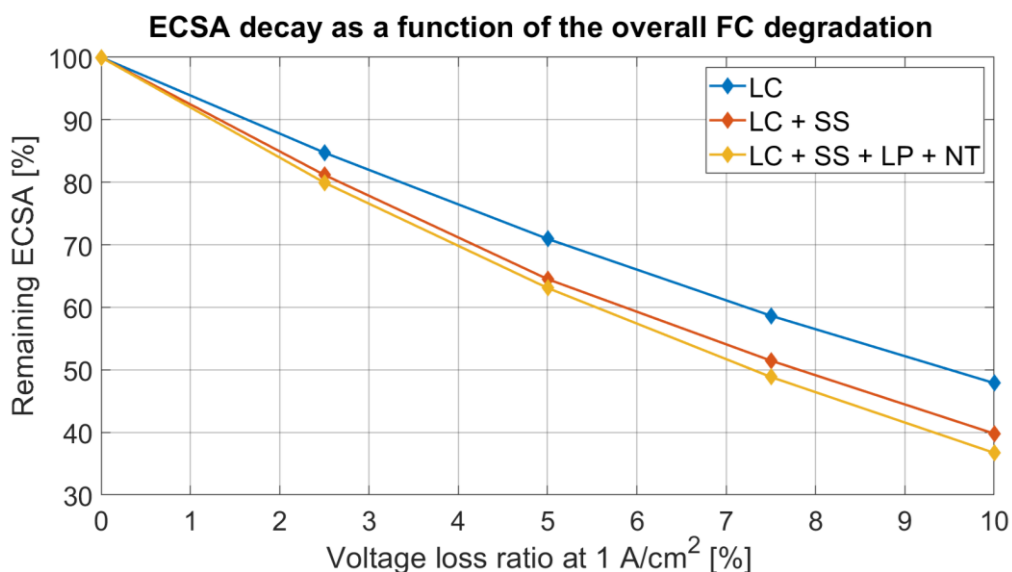


Figure 45. FC degradation model predictive result for the ECSA loss.

Starting by the electrochemical active surface area decay at an overall 10% performance loss, it can be observed (figure 45) that the main degradation of this catalyst “health” indicator has its origin on the load-cycling operating state, breaking the 50% *ECSA* loss barrier just by itself. By comparison, a more moderate loss is promoted by the start-up and shutdown from the absolute point of view (less than a 10%). However, the relative impact of this latter is considerably higher as the cycle time under this condition compared to load cycling is very low, as only half start up-shutdown cycle occurs for a complete HDDT driving cycle against dozens of load changes (see figure 44, high dynamics). Finally, the combination of natural and low-power condition promotes a further *ECSA* loss of less than a 4%, being the less harmful to the catalyst degradation of the three previous conditions.

Influence over catalyst degradation at 10% FC performance loss			
Operating state	Overall Degradation share	Initial <i>ECSA</i>	Final <i>ECSA</i>
LC	~68 %	100 %	47.8 %
LC + SS	~89 %	47.8 %	39.8 %
LC + SS + LP + NT	~100 %	39.8 %	36.7 %
Remaining <i>ECSA</i>			36.7 %

Table 23. Catalyst degradation for a 10% overall PEMFC performance loss.

The *ECSA* state is the most reliable indicator to evaluate the catalyst health at a PEMFC, each percentage loss implies directly a percentage unit loss in the catalyst activity, therefore seriously affecting the PEMFC performance. It has been observed that nearly two thirds of the total *ECSA* has been lost, being a dramatic catalyst degradation, which, along with the other two degradation sources (R_{Ω} and i_{H_2}), will be analyzed in the following chapter (5.1 Industry recommendations).

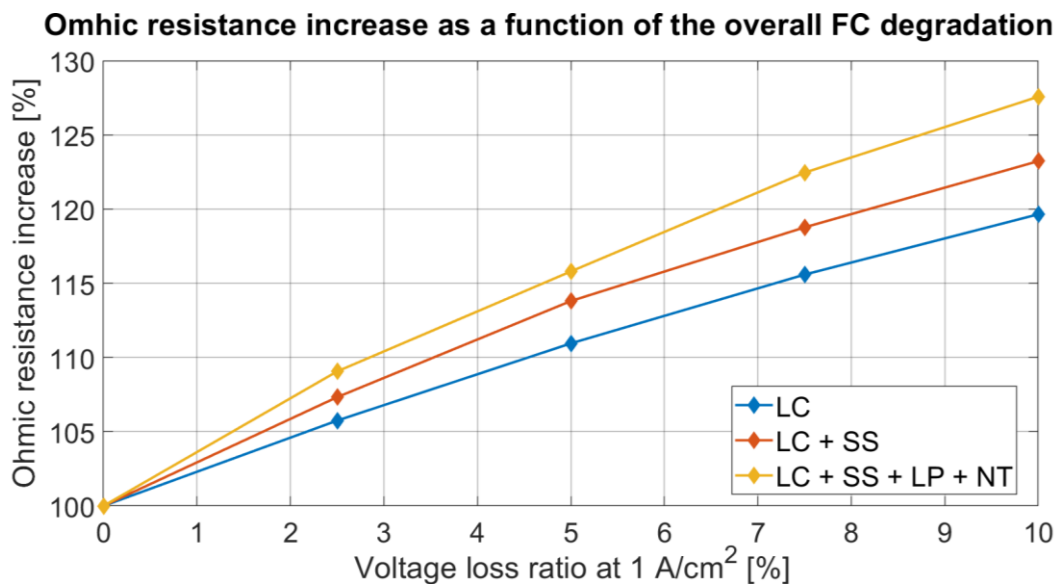


Figure 46. FC degradation model predictive result for the ohmic resistance increase.

The next set of results given by the model show the ohmic resistance (R_{Ω}) evolution, which mainly accounts for the PEMFC membrane chemical degradation (figure 46). Here, the load cycling state still dominates but at a lower relative share than for the catalyst degradation, with a generated resistance increase of less than the 20%, from a total of 27%. Conversely, the low-power state summed up to the natural state generate more than a 4 % resistance increase, surpassing in this case the start-stop degradation (3%). This fact, despite the lower overall degradation share against start-stop, is probably due to the high membrane resistance which the low-power state promotes, as analysed in 1.4.2.

Influence over membrane chemical degradation at 10% FC performance loss			
Operating state	Overall Degradation share	Initial R_{Ω}	Final R_{Ω}
LC	~68 %	100 %	119.6 %
LC + SS	~89 %	119.6 %	123.2 %
LC + SS + LP + NT	~100 %	123.2 %	127.5 %
R_{Ω} increase			127.5 %

Table 24. Membrane ohmic resistance increase for a 10% overall PEMFC performance loss.

The ohmic resistance increase (R_{Ω}) mainly implies a worse membrane performance regarding the hydrogen protons transport in the reaction increasing therefore the resistance voltage losses as has been already analysed in this text. This decay, in not as critical as the previously found for the $ECSA$ loss from the catalyst, first because the R_{Ω} increase has been lower than the $ECSA$ decay. Second because an $ECSA$ decay of the 63% implies that the remaining active catalyst area is just the 37%, and the cell would stop working if losing the 100% of the $ECSA$, probably, even before. On the other hand, the ohmic resistance has increased a 27%, implying a loss in the proton conductive efficiency, however with a 100% or bigger ohmic resistance increase, the cell would probably continue to work, but just with a bigger ohmic voltage loss.

Hydrogen crossover increase as a function of the overall FC degradation

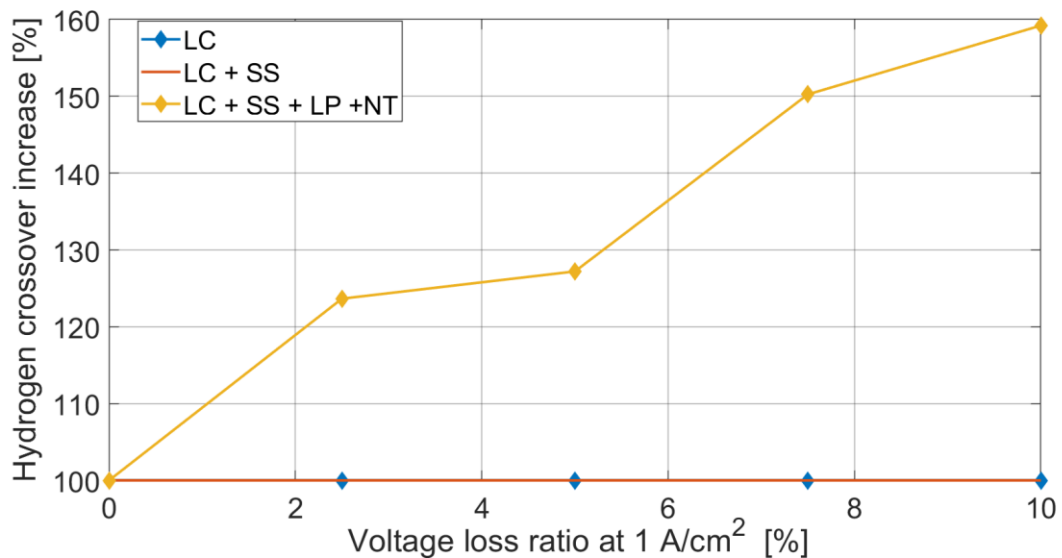


Figure 47. FC degradation model predictive result for the Hydrogen crossover current.

Finally, the hydrogen crossover current (i_{H_2}) predicted increase is given by the PEMFC degradation model. This crossover current is one of the most extended measures to evaluate the membrane mechanical degradation. Due to several factors analysed in 1.4.1 and 1.4.2 the mechanical decay in the membrane leads to thinning, pinhole formation, cracks formation and other mechanical stress consequences. All these factors lead to an undesired migration of hydrogen from anode to cathode and it is relatively easy to measure (chapter 1.4.3). The relevance of this degradation indicator could be at the same level that the catalyst ECSA loss, because high increases in this membrane parameter not only led to worse cell performance, but also to the membrane failure.

Influence over membrane mechanical degradation at 10% FC performance loss			
Operating state	Overall Degradation share	Initial i_{H_2}	Final i_{H_2}
LC	~68 %	100 %	100 %
LC + SS	~89 %	100 %	100 %
LC + SS + LP + NT	~100 %	100 %	159.2 %
i_{H_2} increase			159.2%

Table 25. Membrane hydrogen crossover increase for a 10% overall PEMFC performance loss.

As can be observed in figure 47 and table 26, the hydrogen crossover generated by the load cycling and start-stop states is neglectable, by contrast, the low power state is extremely harmful to the membrane from the mechanical point of view. This latter, only by accounting a 5% in the overall cell degradation, generates, on its own, a dramatic 60% of hydrogen crossover current increase. This result might be surprising, compared to its low overall share and taking into account the neglectable hydrogen crossover increase for load-change and start-stop. However, several studies conclude that the low-power condition, due to the addition of intensified oxygen permeation and high cathode potentials, generate high rates of free radicals, promoting extreme chemical degradation which also end ups leading to mechanical degradation to its severity [33]. The other 6% of overall cell degradation belongs to natural state, which at the same time is composed by the load cycling and start stop states observed both to be harmless regarding this degradation indicator.

Final PEMFC degradation source predictive model results					
Operating state	Overall Degradation	ECSA	i_{H_2}	R_{Ω}	\overline{RMSD}
LC	~68 %	47.8 %	100 %	119.6 %	0.01599 V
LC + SS	~89 %	39.8 %	100 %	123.2 %	0.02248 V
LC + SS + LP + NT	~100 %	36.7 %	159.2 %	127.5 %	0.02610 V
Final	100 %	36.7 %	159.2%	127.5%	0.02610 V

Table 26. Final results from the PEMFC predictive degradation model.

Finally, a resume table is given above, displaying the degradation source predicted results along with the \overline{RMSD} value of the simulation, which indicates and average voltage deviation between the degraded model predicted curves and the reference degraded curve [23] of 26.1 mV as a guarantee of model calibration.

5.1. Industry recommendations

The influence of this FC load profile whose origin is a high FC – battery dynamics FCEx heavy-duty road transport vehicle is being further analysed in the present section, with the objective of proposing countermeasures for the heavy-duty vehicles and PEMFC industry in order to develop more durable fuel cells for this type of applications. Therefore, basing on the predicted degradation source results and also taking into account the theoretical and experimental basis detailed in 1.4.2 some recommendations are going to be exposed for the catalyst and membrane durability and with a focus on the PEMFC manufacturing and design industry and on the vehicle manufacturers.

With this, the fourth and final partial objective of this master's thesis will be fulfilled, with the purpose of bringing some light regarding the PEMFC degradation origin which is of high interest to both industries, which are strongly related. From the point of view of the PEMFC manufacturers industry, having detailed feedback of how their products' structure is being affected by a certain application which may become a high potential customer in near future is a new opportunity to develop new generations of PEMFC with higher lifespan expectancy. In fact, this type of information would even allow them to develop specific variants of PEMFC per each application further than just offering a variety of sizes and power outputs.

From the heavy-duty industry, the market option of having available specific PEMFC's types for their own application regarding an extended lifespan expectancy makes, indeed, their whole product considerably more competitive as degradation is one of the biggest concerns regarding the FCV industry [24]. Besides, identifying the harshest trends for the PEMFC components in their energy management strategy (EMS) when designing FCEx powertrains also allow them to adapt it and push their durability to a more competitive level.

Therefore, it could be said that the most potentially-benefited industry from developments like the predictive degradation source model made for this master's thesis would be the heavy-duty road vehicles industry in this case. However, it must be noted that this model is not only applicable to these vehicles as will be stated in the future work chapter (chapter 6).

Before giving the industry recommendations, it must be noted that the following are high level proposals based on the model predictive results, and further research and validation is needed to define more specific and reliable ones. The following countermeasures are going to be divided in catalyst and membrane durability recommendations, which at the same time will be divided into FC structure recommendations, for the PEMFC manufacturers, and dynamics recommendations for the FCV manufacturers.

5.1.1. Catalyst durability recommendations

It has been demonstrated that the load change, through the dynamic water demand, gas demand, humidity state and voltage state, among others, promotes many mechanisms for catalyst degradation like catalyst ionomer redistribution, Pt migration, Pt agglomeration, Pt oxidation, Pt washing away or catalyst layer delamination. Alongside, the start-up and shutdown state generates extremely high cathode potentials and therefore dramatic carbon support corrosion with the subsequent consequences to the catalyst layer health state. Finally, but at a lower level, low potentials also enhance high cathode voltage levels with the same consequence as the latter mentioned. Taking all of this into account alongside with the predicted results the following counter measures are recommended.

PEMFC design recommendations (PEMFC manufacturers)

1. Smaller platinum particles. The key factor for a high amount of ECSA is high surface to weight ratio, therefore reducing its size increases the specific electrochemical active surface area and also lowers the need of increasing the platinum content for higher performance and durability, as this would rise the ratio between active surface and platinum weight.
2. Graphitized carbon as catalyst support. The latest's trends in the PEMFC research field are leading to new anti-corrosion carbon substrates developed for catalyst supports which bring higher resistance against corrosion through graphitization processes [91, 92]. These materials are good candidates to be incorporated in the catalyst carbon support which when reaching high potentials tend to get corroded, affecting the platinum active particles.

FC dynamic strategy (Vehicle manufacturers)

1. Smoother voltage changes (lower dynamics). High FC dynamics or load changes promote rapid changes in the humidity state and gasses distribution generating serious imbalances which affect the catalyst durability, being the first cause for its degradation.
2. Avoid unnecessary start-up and shutdown cycles. These cycles generate extremely high cathode potentials producing severe carbon corrosion and the consequent catalyst decay.
3. Avoid idling or very low power states. Extremes are typically bad for everything; however, a very low power usage may appear an innocent operation for PEMFC degradation. The reality is that this state also generates high cathode potentials with the previously commented carbon support deterioration and, consequently, catalyst degradation.

5.1.2. Membrane durability recommendations

Besides the catalyst degradation, the other critical PEMFC element prone to degrade and therefore promoting overall performance loss is the proton exchange or polymer electrolyte membrane. This element has been studied through two indicators, the membrane ohmic resistance and the hydrogen crossover current. Even though a stronger linkage can be associated between the first and the membrane chemical degradation, and between the second and the membrane mechanical degradation, both reliably reflect the deterioration of this element, which depends on a complex interaction of chemical, thermal, and mechanical phenomena.

As the scientific literature establishes and as has been afterwards verified through the model prediction, the load change state through the constant dynamics in gas supply and humidity generate chemical and thermal degradation affecting this element. Furthermore, the start-stop condition and low-power condition promote high cathode potentials which, through the deformation of the carbon support due to corrosion, affect the interfacial connection between catalyst and membrane, therefore deteriorating it. Finally, the low-power state also generates high oxygen permeation which brings out the worst consequence for the membrane, enhancing both chemical and mechanical degradation leading to severe increase of the hydrogen crossover which can end up in a permanent membrane mechanical failure.

PEMFC Structural recommendations (PEMFC manufacturers)

1. Lower thickness. The complex discussion of the membrane thickness has its origin in a constant trade-off between cell performance and membrane durability. While a thin PEMFC membrane brings better ionic conductivity and therefore reduced ohmic losses it also decreases the membrane lifespan, as it also reduces its mechanical strength, and the creation of pinholes and cracks is more likely to happen. However, the aim of this thesis is to study the specific degradation for an overall cell performance loss of a 10%. This overall loss is far from the membrane mechanical failure, as “only” a 60% of hydrogen crossover increase has been predicted at this point, while there are experimental studies reporting increases of more than a 1000% with the membrane still being functional [72]. Therefore, the decision is to recommend thinner membranes for overall performance decay targets of 10%.
2. Reinforced membranes. Besides the previous recommendation, an additional membrane reinforcement which does not imply increasing its thickness is proposed. As reliability is always an essential topic in the powertrain industry, in combination with the thinning of the membrane, a mechanical reinforcement is recommended to avoid unexpected failures. This proposal may imply exploring alternative membrane materials or structures other than the classical Nafion[®], which is also a hot topic in the PEMFC latest research lines [93].

FC dynamic strategy (Vehicle manufacturers)

Even though the priority level may change for each recommendation when comparing dynamic countermeasures to avoid catalyst degradation than for membrane degradation, they end up being the same:

1. Smoother voltage changes/ lower dynamics. Aggressive cycling leads to going from one cell set of conditions to the opposite in a matter of seconds, this has been demonstrated to be fatal for the catalyst degradation, but furthermore, it also worsens the membrane performance therefore high dynamics should be avoided.
2. Avoid unnecessary start-up and shutdown cycles. Start-stop leads to high carbon support corrosion which may affect structurally the membrane; therefore, it is recommended to reduce its frequency as much as possible.
3. Avoid idling or very low power states. Despite the two previous, idling is by far the harshest condition for membrane performance loss and durability, being able to lead on its own the membrane to the total failure, therefore it is recommended to avoid pure FC idling situations (OCV).

Each of the previous recommendations have been based on the scientific literature, after reviewing dozens of literature references and developing a predictive degradation source PEMFC model with a methodology strongly based on experimental degradation studies. However, the recommendations and the simulation result haven't been validated and may not be fully precise, although they represent faithfully the tendencies of the main components of the MEA to degrade with the operating conditions, based on the experimental results retrieved from the scientific literature

6. Conclusion and Future Work

To conclude with this master's thesis, the main and partial objectives initially established are analysed along with the final results. The main purpose of this work was to develop a PEMFC – literature based predictive degradation model capable of identifying the most relevant degradation trends within the FC physical structure, applied in this case to the heavy-duty road transport sector. This objective, along with the partial ones, have been accomplished and are being reviewed individually in the following points.

- After its calibration and validation, it can be concluded that the objective of developing a mathematical polarization curve model with good sensitivity to different operating conditions has been successfully achieved. The first has been demonstrated through the low \overline{RMSD} achieved (5 mV, table 18) when comparing the model curve and the experimental curves, showing a consistent sensitivity against pressure variations (1.3/2.5 bar) at the operating LT-PEMFC temperature (80°C). On the other hand, a successful validation has been also achieved, showing an accurate response when comparing experimental and model voltage outputs for the same input conditions (figure 42).
- The degradation source limits identification (ECSA, ohmic resistance and hydrogen crossover) as a function of the voltage degradation rate has been a challenging task. The literature studies focused on this matter do not usually show this specific relationship, therefore the available experimental data is very limited, but has been enough to develop a methodology capable of defining upper and lower limits for each indicator and for the main PEMFC operating states.
- Thanks to the two prior points, a literature - based PEMFC degradation predictive model has been successfully developed and has been applied to a heavy-duty road transport application. The predicted degradation given by the model has been aligned with the expected degradation for each operating condition and to each element (membrane and catalyst) as the literature establishes. Furthermore, the predicted degradation origin trends (ECSA, ohmic resistance and hydrogen crossover) have kept the degraded polarization model curve close to the experimental ones with an \overline{RMSD} of 26 mV, therefore guarantying reliability in the given degradation results.
- Finally, in order to contribute to the PEMFC and FCV industry, a set of industry recommendations have been proposed to each, regarding the studied application (high-dynamics heavy-duty FCREx). On one side, recommendations for a more durable cell design regarding the membrane and catalyst degradation to the PEMFC manufacturers industry. Conversely, several proposals have been made to the FCV manufacturers in order to avoid the harshest FC dynamic states which promote the major part of the FC performance loss.

Future work

The following points are the proposed future work lines:

1. Model validation. This model is based on the segregation into the different PEMFC operating states' degradation trends. Therefore, to achieve the best validation possible, experimental ASTs under each of the studied conditions should be performed with a strong focus on the overall degradation rate. For this, it is furtherly proposed to increase the overall cell degradation checkpoints, performing frequent CV, EIS and LSV tests to define a solid report of the ECSA, ohmic resistance and hydrogen crossover evolution alongside with the voltage degradation rate.
2. Model application. Different dynamic conditions and applications should generate different degradation trends by applying this model and methodology. Therefore, to test the model sensitivity against different PEMFC operating conditions it is recommended to extend its usage to lower-dynamics heavy-duty applications and to the complete dynamic range for medium and light-duty applications. Eventually, other types of applications like PEMFC drones might be of interest.
3. Model calibration. The weakest current density range of this model is demonstrated to be the high current range. The concentration or mass transport losses are the predominant cause for voltage loss under high FC load, therefore it is proposed to furtherly research the mathematical definition and calibration of this term.
4. Degradation source indicators. Aligned with the previous, it is proposed to put additional efforts on researching about the evolution of the mass transfer resistance under degradation conditions, which is directly associated to the previously mentioned concentration losses.
5. Degraded PEMFC elements. Up to this point the focus has laid exclusively on the membrane and catalyst, which are scientifically proved to be the main responsible for the PEMFC performance decay. However, there are other elements which suffer from serious degradation and also affect the FC performance. For this reason, it is proposed to seek for degradation indicators which could represent the catalyst carbon support and the gas diffusion layer degradation.
6. Degradation source limits identification. The literature review is a critical basis for this PEMFC predictive degradation model; therefore, a further and deeper literature research is proposed to get further model consistency.
7. Methodology. The applied methodology for this study is aligned and based on the latest experimental PEMFC degradation studies. However, there might be steps which probably have to be refined as the definition of the degradation coefficients, which have been based on an interrelation of the ECSA, ohmic resistance and hydrogen crossover current, and ideally should be independent.

7. Budget

At this chapter a cost analysis of this master's thesis will be presented.

Labour Costs

This master's thesis started on the 13th of September of 2022 and is finishing on the 12th of January 2023. The different phases in which it has been divided is shown in the following table, along with the working load by phase measured in days (table 27). Furthermore, an average of 6 hours of work per day has been estimated, including weekends, on which the thesis work has not been paused.

Master's thesis calendar						
	September (Days)	October (Days)	November (Days)	December (Days)	January (Days)	Total (Days)
Literature Research	18	21	0	0	0	39
Model development	0	10	30	4	0	44
Model application	0	0	0	7	0	7
Thesis writing	0	0	0	20	12	32
Total days						122
Total hours (6 hours per day)						732

Table 27. Time distribution along the master's thesis development.

By summing the total amount of days per master's thesis phase and then taking into account the average working time per day (6 hours), 732 hours of author working time results. Besides, the PhD professor R. Novella and the PhD researcher M. López Juárez have also taken part of this thesis in matter of supervision, guiding and meetings. The average hour salary for the three mentioned participants is the following:

- PhD professor: 16.74 €/h.
- PhD researcher: 14.61 €/h.
- Graduated engineer: results in 4.15 €/h.

With this salary, the total labour costs are being calculated in the following table (table 28):

Employee	Time (hours)	€/ hour	Total cost €
PhD professor	10	16.74	167.4
PhD researcher	50	14.61	730.5
Graduated engineer	732	4.15	3,037.8
Total			3,935.7 €

Table 28. Labour costs.

Equipment costs

The equipment costs section is based on the usage of a computer device and the cost of the software's licenses which have been needed for the development of this master's thesis. For the development of this master's thesis the Microsoft Office package and MATLAB have been necessary, therefore both licenses' cost will be included. Alongside, the laptop cost will be estimated as the project duration over the average amortization time.

Item	Unitary price (€)	Units (-)	Amortisation period (years)	Usage period (years)	Total (€)
Microsoft office license	69	1	1	0.33	22.77
MATLAB license	860	1	1	0.33	283.8
Asus Laptop	959	1	6	0.33	52.75
Total					359.32 €

Table 29. Equipment and software costs.

Total costs

To calculate the overall budget, each of the previous costs are summed. To this value a 15% must be considered regarding the general costs, and a further 7% for industrial benefits. To the remaining amount the taxes must be also added (Spanish IVA), bringing therefore the final project cost.

Item	Subtotal (€)	Total (€)
Labour costs	3,935.7	
Equipment and software costs	359.32	
Execution Budget		4,295.02
General costs (15%)	644.25	
Industrial Benefit (7%)	300.65	
Overall investment budget		5,239.92
Taxes (IVA) (21%)	1078.94	
Total project cost		6,340.30

Table 30. Budget calculation table.

The total Project cost (taxes included) is **6,340.30 €**.

References

- [1]: consilium.europa.eu. (2022). Objetivo 55 - El plan de la UE para la transición ecológica - Consilium. Retrieved December 12, 2022, from <https://www.consilium.europa.eu/es/policies/green-deal/fit-for-55-the-eu-plan-for-a-green-transition/>
- [2]: cdecomunidaddemadrid.wordpress.com. (2022). La neutralidad del carbono como objetivo 2050 para la Unión Europea – Eurobitácora. Retrieved December 12, 2022, from <https://cdecomunidaddemadrid.wordpress.com/2022/09/12/la-neutralidad-del-carbono-como-objetivo-2050-para-la-union-europea/>
- [3]: eea.europa.eu. (2022). High time to shift gear in transport sector — European Environment Agency. Retrieved December 12, 2022, from <https://www.eea.europa.eu/signals/signals-2022/articles/high-time-to-shift-gear>
- [4]: PEM & MMP. (2021). Electric Drives and Storage Systems. Production Engineering of E-Mobility Components & Mechatronics for Mobile Propulsion, RWTH Aachen University.
- [5]: Uwe Sauer, D. (2021). Battery Storage Systems. Institute for Power Electronics and Electrical Drives, RWTH Aachen University.
- [6]: cnh2.es. (n.d.). Hidrógeno - Centro Nacional de Hidrógeno. Retrieved December 13, 2022, from <https://www.cnh2.es/el-hidrogeno/>
- [7]: fgcsic.es. (2011). El hidrógeno: metodologías de producción. Retrieved December 13, 2022, from https://fgcsic.es/lychnos/es_es/articulos/hidrogeno_metodologias_de_produccion
- [8]: cicenergigune.com. (n.d.). Métodos de producción de hidrógeno y sus colores | CIC energiGUNE. Retrieved December 13, 2022, from <https://cicenergigune.com/es/blog/metodos-produccion-hidrogeno-colores>
- [9]: azocleantech.com. (2021). Oman and the World’s Largest Green Hydrogen Plant. Retrieved December 14, 2022, from <https://www.azocleantech.com/article.aspx?ArticleID=1257>
- [10]: elperiodicodelaenergia.com. (2022). Bruselas creará un Banco Europeo de Hidrógeno para invertir 3.000 millones - El Periódico de la Energía. Retrieved December 14, 2022, from <https://elperiodicodelaenergia.com/bruselas-creara-un-banco-europeo-de-hidrogeno-para-invertir-3-000-millones/>
- [11]: futuredrive.es. (n.d.). ¿Cuánto tarda en cargar un Tesla? Retrieved December 14, 2022, from <https://futuredrive.es/es/blog/cuanto-tarda-cargar-un-tesla>
- [12]: www.motorpasion.com. (2021). Recorrido pieza a pieza a través de un vehículo de pila de combustible de hidrógeno. Retrieved December 14, 2022, from <https://www.motorpasion.com/espaciotoyota/recorrido-pieza-a-pieza-a-traves-vehiculo-pila-combustible-hidrogeno>
- [13]: Pischinger, S. (2021). Mobile Propulsion Fundamentals. Chair of Thermodynamics of Mobile Energy Conversion Systems (TME), RWTH Aachen University.
- [14]: hydrogeneurope.eu. (2022). Another big day for European hydrogen. Retrieved January 11, 2023, from <https://hydrogeneurope.eu/another-big-day-for-european-hydrogen/>

- [15]: elperiodicodelaenergia.com. (2022). Así será el nuevo “boom” del hidrógeno verde en los próximos años: se producirán 25 millones de toneladas para 2030 - El Periódico de la Energía. Retrieved December 15, 2022, from <https://elperiodicodelaenergia.com/asi-sera-el-nuevo-boom-del-hidrogeno-verde-en-los-proximos-anos-se-produciran-25-millones-de-toneladas-para-2030/>
- [16]: motor.elpais.com. (2022). Estos son los coches de hidrógeno que se venden en España. Retrieved December 15, 2022, from <https://motor.elpais.com/coches-electricos/estos-son-los-coches-de-hidrogeno-que-se-venden-en-espana/>
- [17]: wikipedia.org. (2022). Fuel cell vehicle - Wikipedia. Retrieved December 16, 2022, from https://en.wikipedia.org/wiki/Fuel_cell_vehicle
- [18]: prensa.toyota.es. (2020). Toyota y el hidrógeno: una historia de pasado, presente y (mucho) futuro. Retrieved December 15, 2022, from <https://prensa.toyota.es/toyota-y-el-hidrogeno-una-historia-de-pasado-presente-y-mucho-futuro/>
- [19]: Curran, S. J., Wagner, R. M., Graves, R. L., Keller, M., & Green, J. B. (2014). Well-to-wheel analysis of direct and indirect use of natural gas in passenger vehicles. *Energy*, 75, 194–203. <https://doi.org/10.1016/j.energy.2014.07.035>
- [20]: Molina, S., Novella, R., Pla, B., & Lopez-Juarez, M. (2021). Optimization and sizing of a fuel cell range extender vehicle for passenger car applications in driving cycle conditions. *Applied Energy*, 285, 116469. <https://doi.org/10.1016/J.APENERGY.2021.116469>
- [21]: Desantes, J. M., Novella, R., Pla, B., & Lopez-Juarez, M. (2022). A modeling framework for predicting the effect of the operating conditions and component sizing on fuel cell degradation and performance for automotive applications. *Applied Energy*, 317, 119137. <https://doi.org/10.1016/J.APENERGY.2022.119137>
- [22]: Desantes, J. M., Novella, R., Pla, B., & Lopez-Juarez, M. (2022). Effect of dynamic and operational restrictions in the energy management strategy on fuel cell range extender electric vehicle performance and durability in driving conditions. *Energy Conversion and Management*, 266, 115821. <https://doi.org/10.1016/J.ENCONMAN.2022.115821>
- [23]: Lopez-Juarez, M. (2022). Analysis of hydrogen fuel cell powerplant architectures for future transport applications, Ph.D. Thesis. Departamento de máquinas y motores térmicos. Universitat Politècnica de València.
- [24]: energy.gov. (2017). Hydrogen Storage Technologies Roadmap Fuel Cell Technical Team Roadmap. Retrieved December 18, 2022, from https://www.energy.gov/sites/prod/files/2017/11/f46/FCTT_Roadmap_Nov_2017_FINAL.pdf
- [25]: NEMA Standard, Publ. No. CV 1-1968, National Electrical Mfgs. Assoc., New York (1968).
- [26]: wikipedia.org. (2022). Fuel cell - Wikipedia. Retrieved December 18, 2022, from https://en.wikipedia.org/wiki/Fuel_cell#History
- [27]: fuelcellsworks.com. (n.d.). PEMFC - FuelCellsWorks. Retrieved December 18, 2022, from <https://fuelcellsworks.com/knowledge/technologies/pemfc/>
- [28]: Pischinger, S. (2021). Alternative and electrified vehicle propulsion systems. Chair of Thermodynamics of Mobile Energy Conversion Systems (TME), RWTH Aachen University.

- [29]: wikipedia.org. (2022). Proton-exchange membrane fuel cell - Wikipedia. Retrieved December 19, 2022, from https://en.wikipedia.org/wiki/Proton-exchange_membrane_fuel_cell
- [30]: Djilali, N., & Sui, P. C. (2008). Transport phenomena in fuel cells: From microscale to macroscale. *International Journal of Computational Fluid Dynamics*, 22(1–2), 115–133. <https://doi.org/10.1080/10618560701740017>
- [31]: Abderezzak, B. (2018). Introduction to Hydrogen Technology. Introduction to Transfer Phenomena in PEM Fuel Cell, 1–51. <https://doi.org/10.1016/B978-1-78548-291-5.50001-9>
- [32]: Litster, S., & McLean, G. (2004). PEM fuel cell electrodes. *Journal of Power Sources*, 130(1–2), 61–76. <https://doi.org/10.1016/J.JPOWSOUR.2003.12.055>
- [33]: Ren, P., Pei, P., Li, Y., Wu, Z., Chen, D., & Huang, S. (2020). Degradation mechanisms of proton exchange membrane fuel cell under typical automotive operating conditions. *Progress in Energy and Combustion Science*, 80, 100859. <https://doi.org/10.1016/J.PECS.2020.100859>
- [34]: Atifi, A., Mounir, H., & el Marjani, A. (2014). Effect of internal current, fuel crossover, and membrane thickness on a PEMFC performance. *Proceedings of 2014 International Renewable and Sustainable Energy Conference, IRSEC 2014*, 907–912. <https://doi.org/10.1109/IRSEC.2014.7059860>
- [35]: Zhu, L. Y., Li, Y. C., Liu, J., He, J., Wang, L. Y., & Lei, J. du. (2022). Recent developments in high-performance Nafion membranes for hydrogen fuel cells applications. *Petroleum Science*, 19(3), 1371–1381. <https://doi.org/10.1016/J.PETSCI.2021.11.004>
- [36]: Bhattacharya, P. K. (n.d.). Water flooding in the proton exchange membrane fuel cell.
- [37]: Stolten, Detlef. (2021). Fundamentals and technology of hydrogen fuel cells. Chair of Fuel Cells. RWTH Aachen University.
- [38]: Dicks, A. L., & Rand, D. A. J. (2018). Fuel Cell Systems Explained. Fuel Cell Systems Explained. <https://doi.org/10.1002/9781118706992>
- [39]: wikipedia.org. (2022). Tafel equation - Wikipedia. (n.d.). Retrieved December 22, 2022, from https://en.wikipedia.org/wiki/Tafel_equation
- [40]: Khan, S. S., Shareef, H., Wahyudie, A., & Khalid, S. N. (2018). Novel dynamic semiempirical proton exchange membrane fuel cell model incorporating component voltages. *International Journal of Energy Research*, 42(8), 2615–2630. <https://doi.org/10.1002/ER.4038>
- [41]: Shao, Y., Yin, G., & Gao, Y. (2007). Understanding and approaches for the durability issues of Pt-based catalysts for PEM fuel cell. *Journal of Power Sources*, 171(2), 558–566. <https://doi.org/10.1016/J.JPOWSOUR.2007.07.004>
- [42]: Liu, D.-J., Yang, J., & Gosztola, D. J. (2007). Investigation of Aligned Carbon Nanotubes as a Novel Catalytic Electrodes for PEM Fuel Cells. *ECS Transactions*, 5(1), 147–154. <https://doi.org/10.1149/1.2728997>
- [43]: Knights, S. (2012). Operation and durability of low temperature fuel cells. *Polymer Electrolyte Membrane and Direct Methanol Fuel Cell Technology*, 137–177. <https://doi.org/10.1533/9780857095473.2.137>

- [44]: Lim, C., Ghassemzadeh, L., van Hove, F., Lauritzen, M., Kolodziej, J., Wang, G. G., Holdcroft, S., & Kjeang, E. (2014). Membrane degradation during combined chemical and mechanical accelerated stress testing of polymer electrolyte fuel cells. *Journal of Power Sources*, 257, 102–110. <https://doi.org/10.1016/J.JPOWSOUR.2014.01.106>
- [45]: Shah, A. A., Ralph, T. R., & Walsh, F. C. (2009). Modeling and Simulation of the Degradation of Perfluorinated Ion-Exchange Membranes in PEM Fuel Cells. *Journal of The Electrochemical Society*, 156(4), B465. <https://doi.org/10.1149/1.3077573/XML>
- [46]: Zatoń, M., Rozière, J., & Jones, D. J. (2017). Current understanding of chemical degradation mechanisms of perfluorosulfonic acid membranes and their mitigation strategies: a review. *Sustainable Energy & Fuels*, 1(3), 409–438. <https://doi.org/10.1039/C7SE00038C>
- [47]: Pei, P., Chang, Q., & Tang, T. (2008). A quick evaluating method for automotive fuel cell lifetime. *International Journal of Hydrogen Energy*, 33(14), 3829–3836. <https://doi.org/10.1016/J.IJHYDENE.2008.04.048>
- [48]: Bezmalinovic, D., Simic, B., & Barbir, F. (2015). Characterization of PEM fuel cell degradation by polarization change curves. *Journal of Power Sources*, 294, 82–87. <https://doi.org/10.1016/J.JPOWSOUR.2015.06.047>
- [49]: Lai, Y. H., & Fly, G. W. (2015). In-situ diagnostics and degradation mapping of a mixed-mode accelerated stress test for proton exchange membranes. *Journal of Power Sources*, 274, 1162–1172. <https://doi.org/10.1016/J.JPOWSOUR.2014.10.116>
- [50]: Pivac, I., Bezmalinović, D., & Barbir, F. (2018). Catalyst degradation diagnostics of proton exchange membrane fuel cells using electrochemical impedance spectroscopy. *International Journal of Hydrogen Energy*, 43(29), 13512–13520. <https://doi.org/10.1016/J.IJHYDENE.2018.05.095>
- [51]: Urchaga, P., Kadyk, T., Rinaldo, S. G., Pistono, A. O., Hu, J., Lee, W., Richards, C., Eikerling, M. H., & Rice, C. A. (2015). Catalyst Degradation in Fuel Cell Electrodes: Accelerated Stress Tests and Model-based Analysis. *Electrochimica Acta*, 176, 1500–1510. <https://doi.org/10.1016/J.ELECTACTA.2015.03.152>
- [52]: Harzer, G. S., Schwämmlein, J. N., Damjanović, A. M., Ghosh, S., & Gasteiger, H. A. (2018). Cathode Loading Impact on Voltage Cycling Induced PEMFC Degradation: A Voltage Loss Analysis. *Journal of The Electrochemical Society*, 165(6), F3118–F3131. <https://doi.org/10.1149/2.0161806JES/XML>
- [53]: Wang, G., Huang, F., Yu, Y., Wen, S., & Tu, Z. (2018). Degradation behavior of a proton exchange membrane fuel cell stack under dynamic cycles between idling and rated condition. *International Journal of Hydrogen Energy*, 43(9), 4471–4481. <https://doi.org/10.1016/J.IJHYDENE.2018.01.020>
- [54]: Venkatesan, S. V., Dutta, M., & Kjeang, E. (2016). Mesoscopic degradation effects of voltage cycled cathode catalyst layers in polymer electrolyte fuel cells. *Electrochemistry Communications*, 72, 15–18. <https://doi.org/10.1016/J.ELECOM.2016.08.018>
- [55]: Liu, M., Wang, C., Zhang, J., Wang, J., Hou, Z., & Mao, Z. (2014). Diagnosis of membrane electrode assembly degradation with drive cycle test technique. *International Journal of Hydrogen Energy*, 39(26), 14370–14375. <https://doi.org/10.1016/J.IJHYDENE.2014.02.161>

- [56]: Shan, J., Lin, R., Xia, S., Liu, D., & Zhang, Q. (2016). Local resolved investigation of PEMFC performance degradation mechanism during dynamic driving cycle. *International Journal of Hydrogen Energy*, 41(7), 4239–4250. <https://doi.org/10.1016/J.IJHYDENE.2016.01.048>
- [57]: Liu, D., & Case, S. (2006). Durability study of proton exchange membrane fuel cells under dynamic testing conditions with cyclic current profile. *Journal of Power Sources*, 162(1), 521–531. <https://doi.org/10.1016/J.JPOWSOUR.2006.07.007>
- [58]: Lin, R., Cui, X., Shan, J., Técher, L., Xiong, F., & Zhang, Q. (2015). Investigating the effect of start-up and shut-down cycles on the performance of the proton exchange membrane fuel cell by segmented cell technology. *International Journal of Hydrogen Energy*, 40(43), 14952–14962. <https://doi.org/10.1016/J.IJHYDENE.2015.09.042>
- [59]: Ettingshausen, F., Kleemann, J., Marcu, A., Toth, G., Fuess, H., & Roth, C. (2011). Dissolution and Migration of Platinum in PEMFCs Investigated for Start/Stop Cycling and High Potential Degradation. *Fuel Cells*, 11(2), 238–245. <https://doi.org/10.1002/FUCE.201000051>
- [60]: Jo, Y. Y., Cho, E. A., Kim, J. H., Lim, T. H., Oh, I. H., Jang, J. H., & Kim, H. J. (2010). Effects of a hydrogen and air supply procedure on the performance degradation of PEMFCs. *International Journal of Hydrogen Energy*, 35(23), 13118–13124. <https://doi.org/10.1016/J.IJHYDENE.2010.04.072>
- [61]: Zakrisson, E. (n.d.). The Effect of Start/Stop Strategy on PEM Fuel Cell Degradation Characteristics.
- [62]: Eom, K., Kim, G., Cho, E., Jang, J. H., Kim, H. J., Yoo, S. J., Kim, S. K., & Hong, B. K. (2012). Effects of Pt loading in the anode on the durability of a membrane–electrode assembly for polymer electrolyte membrane fuel cells during startup/shutdown cycling. *International Journal of Hydrogen Energy*, 37(23), 18455–18462. <https://doi.org/10.1016/J.IJHYDENE.2012.09.077>
- [63]: Kim, J. H., Cho, E. A., Jang, J. H., Kim, H. J., Lim, T.-H., Oh, I.-H., Ko, J. J., & Oh, S. C. (2009). Development of a Durable PEMFC Startup Process by Applying a Dummy Load: I. Electrochemical Study. *Journal of The Electrochemical Society*, 156(8), B955. <https://doi.org/10.1149/1.3148222>
- [64]: Durst, J., Lamibrac, A., Charlot, F., Dillet, J., Castanheira, L. F., Maranzana, G., Dubau, L., Maillard, F., Chatenet, M., & Lottin, O. (2013). Degradation heterogeneities induced by repetitive start/stop events in proton exchange membrane fuel cell: Inlet vs. outlet and channel vs. land. *Applied Catalysis B: Environmental*, 138–139, 416–426. <https://doi.org/10.1016/J.APCATB.2013.03.021>
- [65]: Kim, J. H., Cho, E. A., Jang, J. H., Kim, H. J., Lim, T. H., Oh, I. H., Ko, J. J., & Oh, S. C. (2009). Effects of Cathode Inlet Relative Humidity on PEMFC Durability during Startup–Shutdown Cycling: I. Electrochemical Study. *Journal of The Electrochemical Society*, 157(1), B104. <https://doi.org/10.1149/1.3254170>
- [66]: Franck-Lacaze, L., Bonnet, C., Choi, E., Moss, J., Pontvianne, S., Poirot, H., Datta, R., & Lopicque, F. (2010). Ageing of PEMFC's due to operation at low current density: Investigation of oxidative degradation. *International Journal of Hydrogen Energy*, 35(19), 10472–10481. <https://doi.org/10.1016/J.IJHYDENE.2010.07.180>

- [67]: Han, M., Shul, Y. G., Lee, H., Shin, D., & Bae, B. (2017). Accelerated testing of polymer electrolyte membranes under open-circuit voltage conditions for durable proton exchange membrane fuel cells. *International Journal of Hydrogen Energy*, 42(52), 30787–30791. <https://doi.org/10.1016/J.IJHYDENE.2017.10.160>
- [68]: Gaumont, T., Maranzana, G., Lottin, O., Dillet, J., Didierjean, S., Pauchet, J., & Guétaz, L. (2017). Measurement of protonic resistance of catalyst layers as a tool for degradation monitoring. *International Journal of Hydrogen Energy*, 42(3), 1800–1812. <https://doi.org/10.1016/J.IJHYDENE.2016.10.035>
- [69]: Wang, Z. B., Zuo, P. J., Chu, Y. Y., Shao, Y. Y., & Yin, G. P. (2009). Durability studies on performance degradation of Pt/C catalysts of proton exchange membrane fuel cell. *International Journal of Hydrogen Energy*, 34(10), 4387–4394. <https://doi.org/10.1016/J.IJHYDENE.2009.03.045>
- [70]: Yu, J., Matsuura, T., Yoshikawa, Y., Islam, M. N., & Hori, M. (2005). In situ analysis of performance degradation of a PEMFC under nonsaturated humidification. *Electrochemical and Solid-State Letters*, 8(3), A156. <https://doi.org/10.1149/1.1854781/XML>
- [71]: Yuan, X. Z., Zhang, S., Wang, H., Wu, J., Sun, J. C., Hiesgen, R., Friedrich, K. A., Schulze, M., & Haug, A. (2010). Degradation of a polymer exchange membrane fuel cell stack with Nafion® membranes of different thicknesses: Part I. In situ diagnosis. *Journal of Power Sources*, 195(22), 7594–7599. <https://doi.org/10.1016/J.JPOWSOUR.2010.06.023>
- [72]: Chandesris, M., Vincent, R., Guetaz, L., Roch, J. S., Thoby, D., & Quinaud, M. (2017). Membrane degradation in PEM fuel cells: From experimental results to semi-empirical degradation laws. *International Journal of Hydrogen Energy*, 42(12), 8139–8149. <https://doi.org/10.1016/J.IJHYDENE.2017.02.116>
- [73]: Liu, D., & Case, S. (2006). Durability study of proton exchange membrane fuel cells under dynamic testing conditions with cyclic current profile. *Journal of Power Sources*, 162(1), 521–531. <https://doi.org/10.1016/J.JPOWSOUR.2006.07.007>
- [74]: Xie, J., Wood, D. L., Wayne, D. M., Zawodzinski, T. A., Atanassov, P., & Borup, R. L. (2005). Durability of PEFCs at High Humidity Conditions. *Journal of The Electrochemical Society*, 152(1), A104. <https://doi.org/10.1149/1.1830355/XML>
- [75]: In Situ PEM FC Electrochemical Surface Area And Catalyst Utilization Measurement - Scribner Associates. (n.d.). Retrieved January 11, 2023, from <https://www.scribner.com/faq/1-in-situ-pem-fc-electrochemical-surface-area-and-catalyst-utilization-measurement/>
- [76]: Lindström, R. W., Kortsdottir, K., Wesselmark, M., Oyarce, A., Lagergren, C., & Lindbergh, G. (2010). Active Area Determination of Porous Pt Electrodes Used in Polymer Electrolyte Fuel Cells: Temperature and Humidity Effects. *Journal of The Electrochemical Society*, 157(12), B1795. <https://doi.org/10.1149/1.3494220/XML>
- [77]: Barbir, F. (2005). PEM fuel cells: Theory and prac. *PEM Fuel Cells: Theory and Prac*, 1–433. <https://doi.org/10.1016/B978-0-12-078142-3.X5000-9>
- [78]: ossila.com. (n.d.). Linear Sweep Voltammetry: Intro & Applications | Ossila. Retrieved December 29, 2022, from <https://www.ossila.com/en-eu/pages/linear-sweep-voltammetry>

- [79]: Murschenhofer, D., Kuzdas, D., Braun, S., & Jakubek, S. (2018). A real-time capable quasi-2D proton exchange membrane fuel cell model. *Energy Conversion and Management*, 162, 159–175. <https://doi.org/10.1016/J.ENCONMAN.2018.02.028>
- [80]: Jouin, M., Gouriveau, R., Hissel, D., Péra, M. C., & Zerhouni, N. (2016). Degradations analysis and aging modeling for health assessment and prognostics of PEMFC. *Reliability Engineering & System Safety*, 148, 78–95. <https://doi.org/10.1016/J.RESS.2015.12.003>
- [81]: Barbir, F. (2005). Fuel Cell Electrochemistry. *PEM Fuel Cells*, 33–72. <https://doi.org/10.1016/B978-012078142-3/50004-5>
- [82]: Burlatsky, S. F., Gummalla, M., O'Neill, J., Atrazhev, V. v., Varyukhin, A. N., Dmitriev, D. v., & Erikhman, N. S. (2012). A mathematical model for predicting the life of polymer electrolyte fuel cell membranes subjected to hydration cycling. *Journal of Power Sources*, 215, 135–144. <https://doi.org/10.1016/J.JPOWSOUR.2012.05.005>
- [83]: Kakaç, S. (Sadık), Pramuanjaroenkij, A., & Vasil'ev, L. L. (Leonard L. (2008). *Mini-micro fuel cells : fundamentals and applications*. 422.
- [84]: Thampan, T., Malhotra, S., Zhang, J., & Datta, R. (2001). PEM fuel cell as a membrane reactor. *Catalysis Today*, 67(1–3), 15–32. [https://doi.org/10.1016/S0920-5861\(01\)00278-4](https://doi.org/10.1016/S0920-5861(01)00278-4)
- [85]: Corbo, P., Migliardini, F., & Veneri, O. (2007). Experimental analysis and management issues of a hydrogen fuel cell system for stationary and mobile application. *Energy Conversion and Management*, 48(8), 2365–2374. <https://doi.org/10.1016/J.ENCONMAN.2007.03.009>
- [86]: Corbo, P., Migliardini, F., & Veneri, O. (2008). Experimental analysis of a 20 kWe PEM fuel cell system in dynamic conditions representative of automotive applications. *Energy Conversion and Management*, 49(10), 2688–2697. <https://doi.org/10.1016/J.ENCONMAN.2008.04.001>
- [87]: mathworks.com. (n.d.). Genetic Algorithm - MATLAB & Simulink. Retrieved January 2, 2023, from <https://uk.mathworks.com/discovery/genetic-algorithm.html>
- [88]: athworks.com. (n.d.). What Is the Genetic Algorithm? - MATLAB & Simulink - MathWorks United Kingdom. Retrieved January 2, 2023, from <https://uk.mathworks.com/help/gads/what-is-the-genetic-algorithm.html>
- [89]: wikipedia.org. (n.d.). Genetic algorithm - Wikipedia. Retrieved January 2, 2023, from https://en.wikipedia.org/wiki/Genetic_algorithm
- [90]: apps.automeris.io. (n.d.). WebPlotDigitizer - Copyright 2010-2022 Ankit Rohatgi. (n.d.). Retrieved January 5, 2023, from <https://apps.automeris.io/wpd/>
- [91]: Xue, Q., Huang, J. B., Yang, D. J., Li, B., & Zhang, C. M. (2021). Enhanced PEMFC durability with graphitized carbon black cathode catalyst supports under accelerated stress testing. *RSC Advances*, 11(32), 19417–19425. <https://doi.org/10.1039/D1RA01468D>
- [92]: Jung, W. S. (2018). Study on durability of Pt supported on graphitized carbon under simulated start-up/shut-down conditions for polymer electrolyte membrane fuel cells. *Journal of Energy Chemistry*, 27(1), 326–334. <https://doi.org/10.1016/J.JECHEM.2017.05.012>
- [93]: Applications of Membrane Technology in the Dairy Industry. (2015). *Handbook of Membrane Separations*, 524–557. <https://doi.org/10.1201/B18319-24>